

**MEMORY REACTIVATION IN RAT MEDIAL PREFRONTAL CORTEX
HAPPENS DOMINANTLY IN A SUB-STATE OF CORTICAL
UP STATE DURING SLOW WAVE SLEEP**

SOROUSH MALEK

Master of Science, Institute for Advanced Studies in Basic Sciences, 2016

A thesis submitted
in partial fulfilment of the requirements for the degree of

MASTER OF SCIENCE

in

NEUROSCIENCE

Department of Neuroscience
University of Lethbridge
LETHBRIDGE, ALBERTA, CANADA

© Soroush Malek, 2020

MEMORY REACTIVATION IN RAT MEDIAL PREFRONTAL CORTEX
HAPPENS DOMINANTLY IN A SUB-STATE OF CORTICAL
UP STATE DURING SLOW WAVE SLEEP

SOROUSH MALEK

Date of Defence: April 3, 2020

Dr. Masami Tatsuno	Associate Professor	Ph.D.
Dr. Bruce McNaughton	Professor	Ph.D.
Thesis Co-Supervisor		

Dr. David Euston	Associate Professor	Ph.D.
Thesis Examination Committee Member		

Dr. Artur Luczak	Professor	Ph.D.
Thesis Examination Committee Member		

Dr. Andrew Iwaniuk	Associate Professor	Ph.D.
Chair, Thesis Examination Committee		

DEDICATION

To my parents.

ABSTRACT

Sleep has been conjectured to play an essential role in memory consolidation. The interaction between the cortex and the hippocampus is believed to be crucial in consolidation of episodic memory during slow-wave sleep. Here, I analyzed the neural activity of medial prefrontal cortex of rats that ran the sequence-memory task. Applying a three-state hidden Markov model revealed that UP-DOWN oscillation can be divided into DOWN states and two UP subtypes. DOWN states were separated from UP states by low firing rates and the two UP subtypes were distinguished by the differences in the decaying rate of population vector and the duration. Interestingly, the faster decorrelating sub-state contains memory reactivation predominantly. Next, by analyzing the hippocampal local field potentials in relation to the UP sub-states, we found that the power of sharp-wave ripples was stronger during the reactivating UP sub-state. Our results provide further support to the theory of memory consolidation.

PREFACE

This MSc project has been a long journey, which was started and continued by many people before I start working on it. I would never have been able to complete it without people who have been involved in it. I would like to express my deepest appreciation to all of them.

The experimental part of the project was performed by Dr. David Euston and his colleagues. Subsequently, Dr. Adrian Ponce-Alvarez and Dr. Sonja Gruen performed the initial HMM model to implement it on neural data. Afterward, LeAnna Kalvi performed subsequent HMM analysis and reactivation analysis.

I am also grateful to Karim Ali who readily provided assistance in data analysis alongside us.

ACKNOWLEDGMENT

First and foremost, I would like to express my sincere gratitude to my dear supervisors, Prof. Masami Tatsuno and Prof. Bruce McNaughton, for their great help and supports during my MSc studies and research. It has been a great pleasure working with them. They inspired me all the time by their patience, enthusiasm, motivation, and immense knowledge.

I would also like to thank the members of my committee, Prof. David Euston and Prof. Artur Luczak. I offer my sincere appreciation for the learning opportunities and the insightful feedback provided by them.

Nobody has been more important to me in the pursuit of this project than the members of my family. I would like to thank my family, whose love, support, and guidance are with me in whatever I pursue.

I must express my very profound gratitude to my friends for providing me with unfailing support and continuous encouragement throughout my years of study and through the process of researching and writing this thesis. This accomplishment would not have been possible without them.

TABLE OF CONTENTS

DEDICATION	i
ABSTRACT	iv
PREFACE.....	v
ACKNOWLEDGMENT	vi
LIST OF TABLES	xi
LIST OF FIGURES	xii
1. Introduction	1
1.1. Sleep role on learning and memory	1
1.2. Memory consolidation theories	3
1.3. REM sleep.....	6
1.4. NREM sleep.....	7
1.5. Slow-wave sleep	7
1.6. UP and DOWN	8
1.7. UP and DOWN in the cortex	9
1.7.1. DOWN State in the cortex	9
1.7.2. UP state in the cortex.....	9
1.7.3. Dynamic balance of excitation and inhibition	10
1.8. UP and DOWN detection.....	11

1.9.	Sharp Wave-Ripple.....	11
1.10.	Bayesian deconstruction.....	13
1.10.1.	Replay detection	15
1.11.	Explained variance measure of reactivation strength.....	16
1.12.	Template matching	17
1.13.	Computation of template matches	19
1.14.	Hidden Markov model.....	20
1.15.	State-space model	22
2.	Methods.....	26
2.1.	Recording procedures	26
2.2.	Detection of UP-DOWN oscillation epochs	27
2.3.	Hidden Markov model.....	28
2.4.	Template matching analysis.....	37
2.5.	Population vector decorrelation	38
2.6.	Principal Component Analysis (PCA)	39
2.7.	Cross-correlation between SWRs and UP transitions	40
2.8.	Cross-correlation between MUA's of mPFC and HPC.....	40
3.	Results	41
3.1.	Epochs detection	41
3.2.	DOWN state and two UP sub-states can be separated by a three-state HMM	42

3.3.	Two subtypes of UP states	44
3.4.	Using state vector decorrelation to characterize two UP sub-types	50
3.5.	UP-1 and UP-2 proportions.....	55
3.6.	Memory reactivation	56
3.7.	Memory reactivation mostly occurs in the UP-2.....	57
3.8.	Memory reactivation distribution in UP state and UP sub-states	61
3.9.	Average firing rate of UP states within the UP state.....	68
3.10.	Which type of sub-states, UP states tend to start and end with	70
3.11.	Which type of sub-states, reactivating UP states tend to start and end with.....	72
3.12.	UP sub-states were clustered distinctively by PCA and tSNE	78
3.13.	Pre-task sleep analysis in comparison to post-task sleep	81
3.14.	Obtaining more than two UP sub-states with higher states of HMM.....	87
3.15.	Correlation of UP sub-states to themselves and to each other	104
3.16.	SWRs correlation with DOWN-to-UP transition and UP-1 to UP-2 transition ...	106
3.17.	Using two HMM two-states	110
3.18.	The hippocampus LFP analysis	111
3.19.	The cortex LFP analysis	113
4.	Discussion.....	118
4.1.	Future work	121
4.2.	Conclusion.....	122

Reference	125
Appendix.....	135

LIST OF TABLES

Table 1. The number of neurons recorded in each data set.	27
Table 2. The exponential time constant, τ , for UP-1 and UP-2, for pre-task sleep.	83

LIST OF FIGURES

Figure 1. Detection of epochs of UP and DOWN.....	42
Figure 2. A sample of three detected states using a three-state HMM for one epoch	43
Figure 3. Example of the raster plot of another epoch and the three states detected by HMM.....	44
Figure 4. The firing rate distribution for the three states detected by HMM	46
Figure 5. Mean firing rates for DOWN state and two UP sub-states.....	47
Figure 6. Distribution of duration for the three states detected by HMM.	49
Figure 7. Durations for DOWN state and two UP sub-states.....	49
Figure 8. State vector decorrelation for UP-1 and UP-2, for three data sets	53
Figure 9. State vector decorrelation for UP-1 and UP-2	54
Figure 10. The average decay rates for UP-1 and UP-2, for all 10 data sets	54
Figure 11. The proportion of happening for UP-1 and UP-2	55
Figure 12. An example of the template matching method.....	58
Figure 13. The number of reactivation occurs during UP-1 and UP-2.....	59
Figure 14. The average number of reactivation happens during the UP-1 and UP-2, across all data sets.....	60
Figure 15. Distribution of reactivation for UP-1 and UP-2.....	63
Figure 16. UP state, UP-1, UP-2 and reactivation ($Z=5$).....	64
Figure 17. UP state, UP-1, UP-2 and reactivation ($Z=6$).....	65
Figure 18. The representation of how reactivation happening during UP-1, sorted by duration	66
Figure 19. The representation of how reactivation happening during UP-2, sorted by duration	66
Figure 20. The representation of how reactivation happening during UP-1, sorted chronologically.....	67
Figure 21. The representation of how reactivation happening during UP-2, sorted chronologically	67
Figure 22. Average firing rates for the ten binned UP states	69
Figure 23. The comparison between the distribution of reactivation and firing rates during the ten binned UP states.....	70

Figure 24. Which UP sub-state, UP states start and end with?	71
Figure 25. The representation of reactivating UP states with z-score 5	73
Figure 26. The representation of reactivating UP states with z-score 6	74
Figure 27. How short reactivating UP states start and end.....	75
Figure 28. How long reactivating UP states start and end.....	76
Figure 29. How short non-reactivating UP states start and end	77
Figure 30. How long non-reactivating UP states start and end	77
Figure 31. PCA analysis for UP sub-states, UP-1 and UP-2, for post-task sleep	80
Figure 32. tSNE firing rate analysis for UP sub-states, UP-1 and UP-2, for post-task sleep	80
Figure 33. Firing rates distribution of DOWN, UP-1, and UP-2, for pre-task sleep	81
Figure 34. Duration distribution of DOWN, UP-1, and UP-2, for pre-task sleep.....	82
Figure 35. State vector decorrelation of UP-1 and UP-2, for pre-task sleep.....	83
Figure 36. Comparison of PCA analysis for pre-task and post-task sleep	84
Figure 37. Another example of a comparison of PCA analysis for pre-task and post-task sleep.	85
Figure 38. Another example of a comparison of PCA analysis for pre-task and post-task sleep.	86
Figure 39. Cluster strength comparison for pre-task and post-task sleep.....	87
Figure 40. Distribution of firing rates for the four detected states by four-state HMM....	89
Figure 41. Distribution of duration for the four detected states by four-state HMM	89
Figure 42. State vector decorrelation for the three detected UP states	90
Figure 43. The distribution of reactivation in three UP sub-types.....	92
Figure 44. The firing rate distributions for all states detected by a six-state HMM.....	94
Figure 45. Distribution of duration for the six detected states by six-state HMM.....	94
Figure 46. State vector decorrelations for all UP sub-states separated by a five-state HMM.....	95
Figure 47. Reactivation distribution for five-state HMM.....	98
Figure 48. PCA analysis for normalized firing rate for four, five, six-state, and ten-state HMMs (7165-11p)	100

Figure 49. PCA analysis for normalized firing rate for four, five, six-state, and ten-state HMMs (7165-31p)	102
Figure 50. Cluster strength comparison for different states of HMM	104
Figure 51. The pair-wise correlation coefficient between each UP sub-state	106
Figure 52. The Cross-correlation of transition between DOWN to UP and Ripple	108
Figure 53. The Cross-correlation of transition between UP-1 to UP-2 and Ripple	109
Figure 54. The similarity between states detected by two-state and three-state HMMs	111
Figure 55. Log power comparison between UP-1 and UP-2 for hippocampus LFP	112
Figure 56. UP-1 and UP-2 power frequency bands comparison (Hippocampus LFP)....	115
Figure 57. Log power comparison between UP-1 and UP-2 for cortex LFP	116
Figure 58. UP-1 and UP-2 power frequency bands comparison (Cortex LFP)	117

List of abbreviation

EEG	Electroencephalogram
HMM	Hidden Markov Model
HPC	Hippocampus
LIA	Large-irregular activity
mPFC	medial Prefrontal Cortex
NREM	Non-rapid Eye Movement
PFC	Prefrontal Cortex
REM	Rapid Eye Movement
SO	Slow Oscillation
SWP-r	Sharp Wave-Ripple
SWS	Slow Wave Sleep

1. Introduction

1.1. Sleep role on learning and memory

Humans and animal studies suggest that the quantity and quality of sleep have an essential impact on learning and memory (Jenkins & Dallenbach, 1924; Barrett & Ekstrand, 1972; Plihal & Born, 1997; Stickgold et al., 2000; Korman et al., 2007). Sleep is a natural and recurring state during which the responsiveness to sensory stimuli reduces, and it distinguishes by a loss of consciousness. Sleep in mammals split into two major sleep stages, non-rapid eye movement sleep (NREM) and rapid eye movement sleep (REM) (Rasch & Born, 2013).

The researches on sleep started a century ago, and it has demonstrated that sleep has a variety of functions; however, sleep's exact functions are still debatable. From an evolutionary perspective, loss of consciousness and reduction of sensory awareness to potential dangers threaten survival; but sleep is a phenomenon that exists in almost all animals. Sleep has been suggested to have a role in saving and restoration of energy resources, brain detoxication from free radicals, most importantly, memory and synaptic plasticity (Rasch & Born, 2013). It has been suggested that sleep is an integral part of consolidation for the newly acquired memories (Karni et al., 1944; Fishebin, 1971; Pearlman & Becker, 1974; Smith & Butler, 1982; Smith & Kelly, 1988; Marr et al., 1991; Stickgold et al., 2000; Laureys et al., 2002; Fenn et al., 2003). The finding of neuronal reactivation during the post-experience task (Pavlides & Winson, 1989), has supported the idea that after encoding happened successfully, the novel memory traces, should be replayed in the related neuronal networks as far as trace consolidation getting

accomplished by synaptic plasticity (Hebb, 1949; Gutwein et al., 1980; Winson, 1985; Ribeiro et al., 1999; Ribeiro et al., 2004). It has been found that post-acquisition reactivation during sleep maintains the temporal relationship of alert, exploratory in the hippocampus (Wilson & McNaughton, 1994; Skaggs & McNaughton, 1996; Nadasdy et al., 1999; Poe et al., 2000; Louie & Wilson, 2001; Lee & Wilson, 2002; Ribeiro et al., 2004) and in the cerebral cortex (Hoffman and McNaughton 2002; Ribeiro et al., 2004; Euston et al., 2007; Ji & Wilson, 2007; Lansink et al., 2008; Johnson et al., 2010), making a correlated replay of activity pattern across two neurons (Wilson & McNaughton, 1994) or multi neuron ensemble (Louie & Wilson, 2001).

Thus far, experience related reactivation during sleep have observed in rodents (Pavlides & Winson, 1989; Wilson & McNaughton, 1994; Skaggs & McNaughton, 1996; Qin et al., 1997; Kudrimoti et al., 1999; Nadasdy et al., 1999; Louie & Wilson, 2001; Lee & Wilson, 2002; Foster & Wilson., 2006; Euston et al., 2007; Giri et al., 2019), nonhuman primates (Hoffman & McNaughton, 2002), songbirds (Dave & Margoliash, 2000), and human (Maquet et al., 2000). These findings strongly indicate that reactivation during sleep is a general biological phenomenon.

A growing body of studies has been done on memory reactivation in the hippocampus in the last couple of decades. Initially, during the subsequent sleep, a selective increase in the firing rate of rat place cells, which had been allowed to be active in their place field, was observed (Pavlides & Wilson, 1989). This observation suggested that the upraised activity of a single neuron can preserve during subsequent sleep.

Hebb's postulate states that any two neurons or network of neurons which are persistently active at the same time would tend to become associated in the way that

activity of one of them facilitate the activity in the other. We can summarize the theory as follows “Cells that fire together wire together” (Hebb, 1949). According to his theory, it is essential to investigate whether the correlation between neuron-pair which formed during waking, preserve during subsequent sleep. Wilson and McNaughton exhibited the correlations had increased during the task were preserved during subsequent sleep. (Wilson & McNaughton, 1994). Further studies indicate that these enhanced correlations are more noticeable during the subsequent sharp-wave ripples (Kudrimoti et al., 1999; Nadasdy et al., 1999; Louie & Wilson, 2001).

Most recent memory and learning theories suggest that the interaction between a hippocampal, as a fast learning network where episodic memory establishes, and neocortical, a slow learning network where statistical regularities of the world extracts, underlie memory encoding process (Marr, 1971; Buzsaki, 1989; McClelland et al., 1995; Skelin et al., 2019).

Studies have shown that the hippocampus has been involved in rapid memory encoding and also the retrieval of recent memories. On the other hand, the neocortex seems to be involved in a gradual and long term part in memory consolidating process.

1.2. Memory consolidation theories

Memory consolidation defines as a category of a process during which memory traces stabilize after its initial acquisition (Dudai, 2004). Consolidation distinguishes into two specific processes, synaptic consolidation and system consolidation. Synaptic consolidation defines as the late-phase long-term potentiation (Bramham & Messaoudi, 2005) and happens during the first few hours after learning. On the other hand, systems

consolidation refers to the process during which hippocampus-dependent memories gradually, in a period of weeks to years, become independent of the hippocampus.

Hippocampus hub-like anatomical configuration allows it to organize an enormous range of cortical networks and thus can initiate the reactivation of neocortical patterns and then lead to the retrieval of the memory in a way that all the different aspects of the memory coherently recalled (Battaglia et al., 2011; Teyler & DiScenna, 1986; Skelin et al., 2019).

Finding the evidence of hippocampal-cortical interaction during sleep and rest periods, when the brain is significantly secluded from external sensory inputs, can be a key support to the shift in the hippocampal-dependence of memory (Buzsaki, 1989; Marr, 1971; McNaughton 2010; Skelin et al., 2019).

The memory consolidation phase is assumed to be distinguished by these three key patterns in LFP: hippocampal sharp-wave ripples, cortical slow oscillations, and neocortical sleep spindles (Amzica & Steriade, 1997; Siapas & Wilson, 1998; Sirota et al., 2003; Isomura et al., 2006; Staresina et al., 2015; Skelin et al., 2019). The consolidation phase also can be characterized by the compressed, within the range of 4-10, reactivation of the neural activity patterns that were presented previously during behaviour (Wilson & McNaughton, 1994; Skaggs & McNaughton, 1996; Nadasdy et al., 1999; Euston et al., 2007; Skelin et al., 2019).

Here some memory consolidation theories have been discussed; the standard memory consolidation theory, the multi-trace memory consolidation theory, newer multiple storage site theory, and memory indexing theory.

According to the standard memory consolidation theory, the hippocampus is essential for the retrieval of recent memory. On the other hand, for remote memories, the neocortex is sufficient for recall. The transfer of memory during non-rapid eye movement (NREM), which is the stage of sleep distinguished by the slow and high-amplitude activity in the cortical EEG and noticeable reduction of muscle tone, from hippocampal to neocortical is widely believed to involve replay of the neural patterns which represent the memory (Squire & Alvarez, 1995; Frankland & Bontempi, 2005). Consistent with the standard memory consolidation theory, it has been shown that patterns of brain activity during a task tend to be repeated during subsequent sleep in the rat's medial prefrontal cortex (Euston et al., 2007).

Based on the multi-trace memory consolidation theory, which structures on the difference between semantic memory and episodic memory, it is assumed that the hippocampus is always involved in the process of retrieval and storage of episodic memories. On the other hand, semantic memories, which include the basic information encoded during the storage of episodic memories, is then built in the other brain areas such as neo-cortex apart from the hippocampus, in the process of consolidation (Nadel & Moscovitch, 1997).

Enough unambiguous shreds of evidence suggesting long-term memory finally and over a long time period, become independent of the hippocampus (Frankland & Bontempi, 2005; Squire, 1992), have not been found yet. As a result, an alternative memory consolidation has been proposed; a more straightforward multiple storage site theory (Sutherland & Lehmann, 2011). Based on this hypothesize, with event

recapitulations, different memory representations are formed independently in multiple networks (Sutherland & Lehmann, 2011).

According to memory indexing theory, it is postulated that an index to the pattern of neocortical activity, which represents a special memory episode, can be store on the hippocampus. As a result, when a particular hippocampal activity pattern reactivates, it sequentially will reactivate the indexed neocortical sequence and, it conducts the memory retrieval (Teyler & DiScenna, 1986; Skelin et al., 2019).

In summary, despite the decades of studies regarding memory consolidation, there is still an ongoing debate on memory consolidation theory, and the factors initiating and regulating the process are still indefinite; this needs further investigation yet.

1.3. REM sleep

REM sleep can be characterized by the physiological resemblance of the brain to waking states, also it includes fast and low-amplitude desynchronized oscillatory activity in cortical EEG. As a result, it is also known as paradoxical sleep and occasionally desynchronized sleep. In the hippocampus, theta activity, which is characterized by a high amplitude synchronous train of sinusoidal waves and the approximate frequency range of 4 to 12 Hz (Stewart & Fox, 1990), is the hallmark of REM sleep in rodents (Robinson et al., 1977). Besides, REM sleep can also be characterized by rapid eye movement and is accompanied by the loss of muscle tone and the propensity of the sleeper to dream vividly; it is the part of sleep accompanied with vivid dreaming and sleepers would often remember a narrative description of what was experienced during the sleep (Hobson et al., 2000). During REM sleep, the cortex exercises a ‘’

desynchronized” state characterized by suppressed low-frequency fluctuations (Steriade & McCarley, 2005; Harris & Thiele, 2011).

1.4. NREM sleep

NREM sleep can be characterized by the occurrence of slow and high-amplitude activity in the EEG signal of cortical areas, and fast and large amplitude depolarizing event (40-100 msec) in the hippocampus, and also the noticeable reduction of muscle tone. Considering these features, it can be distinguished from waking and REM sleep. It is the dominant state of sleep at the beginning of human nocturnal sleep, which the density and duration of it reduce across the sleep. Additionally, NREM sleep has distinct physiological markers, which are a decrease in heart rate, respiration rate, blood pressure, and metabolic levels in comparison to wakefulness (Shore et al., 1985; Zemaityte et al., 1984; Siegel, 2009). NREM sleep is usually associated with three distinct electrical oscillations, which are slow-wave oscillation, sharp-wave ripples, and spindles.

1.5. Slow-wave sleep

NREM sleep is divided into three main stages (Brinkman & Sharma, 2019). The first and the second stages are the shallower stages of NREM, during which the sleeper can easily be awakened. Slow-wave sleep composes of the deepest state of NREM (stage three); as a result, it is usually referred to the deep sleep. Slow-wave sleep is generally characterized by slow and high-amplitude cortical EEG signals since the EEG activity is synchronized and producing slow-wave sleep with a frequency range of 0.5-2 H. The main distinct characteristics of slow-wave sleep are moderate muscle tone, the absence or

slowness of eye movement, and lack of genital activity (Carlson, 2012). In the neocortex slow-wave sleep consists of two distinguished phases of DOWN and UP states. During slow-wave sleep and in the neocortex, there is the inhibition or hyperpolarizing phase, which is called the DOWN state. During the DOWN state, the neocortical neurons are in the rest. Also, there is another stage, which is an exciting or depolarizing phase and is called the UP state, where the neurons fire at a high rate (Steriade et al., 1993; Steriade et al., 2001).

1.6. UP and DOWN

The UP and DOWN fluctuation is observable from the synaptic markers, neural ensemble firing rates and LFP. UP and DOWN states refer to the spontaneous transitions of membrane potential between two levels of generalized spiking and neuronal depolarizing called UP state and network quiescence called DOWN state (Steriade et al., 1993; Cowan & Wilson, 1994; Cossart et al., 2003; Shu et al., 2003). The principal UP and DOWN fluctuation in the sleep, which characterize Non REM sleep and also underlie the slow oscillation, is the alternation of UP and DOWN states, defined as the periods of intense neural activity and silence or very low neural activity, respectively (Steriade et al., 1993; Cowan & Wilson, 1994; Cossart et al., 2003; Shu et al., 2003; Irene Navaro-Lobato, 2018).

In general, it has claimed that the UP and DOWN combination leads to a “push-pull” action, in which “push” reflects potentiating essential memory trace, and “pull” reflects weakening irrelevant traces.

1.7. UP and DOWN in the cortex

In the cortex, many cortical pyramidal cells switch between UP and DOWN states; this spontaneous fluctuation is most apparent when the cortex is showing the synchronized slow-wave sleep (Cowan & Wilson, 1994; Timofeev et al., 1996).

1.7.1. DOWN State in the cortex

It has been shown that hyperpolarization, which is generated by decreasing synaptic excitation, is the responsible mechanism for spontaneous DOWN states during slow-wave in the cortex and also in DOWN state triggered by cortical stimulation (Shu et al., 2003; Sanchez-Vives & McCormick, 2000; Waters & Helmchen, 2006; Timofeev et al., 2000; Contreras et al., 1996). The majority of excitatory input to cortical pyramidal neurons comes from thalamocortical neurons or other pyramidal neurons; as a result, the effect which suppresses these inputs can be accountable for the DOWN state occurrence (Wilson, 2008, Scholarpedia).

1.7.2. UP state in the cortex

Although the somatodendritic membrane nonlinearity can be responsible for the UP state in cortical pyramidal neurons (Waters & Helmchen, 2006), the main efforts to explain the UP state has focused on the neural ensemble than cellular properties (Bazhenov et al., 2002; Compte et al., 2003; Yuste et al., 2005; Holcman & Tsodyks, 2006).

1.7.3. Dynamic balance of excitation and inhibition

Inhibition is ubiquitous in the cortex and is mediated by GABAergic interneurons. Any activation of pyramidal neurons always induces an inhibitory response (Destexhe et al. 2003; Haidner et al., 2006; Rigas and Castro-Alamancos, 2007; Rudolph et al., 2007). This balance characteristic suggests a simple mechanism in which the network of neurons could generate UP and DOWN states in the cortex, which does not necessarily need any specific cellular mechanism. Altogether, DOWN states are the mutually-enforced silent part of the network.

Each input to each ensemble of neurons brings about both mutual excitation and associated inhibition. By having enough excitation, the ensemble will be re-excited by itself repeatedly, leading the neurons toward the UP state. In addition to excitation, pyramidal neurons produce the inhibition, making the net conductance force to a more negative reversal potential. Consequently, if the net excitation balance stays high enough and preserves the self-sustained activity of the network, the effect on each neuron will be a synaptic conductance with a reversal potential set. Otherwise, the network will not preserve self-sustained activity, and UP state will cease. As some of the neurons are generally susceptible to be triggered by random fluctuations in membrane potential during the UP state, the UP state might support itself as a stable or a transiently stable state. However, due to some accumulating fatigue, UP state slowly lose stability and get back to the DOWN state. By being in the DOWN state for a while, the network would be recovered and prepared to transit to another UP state. (Destexhe & Sejnowski, 2003; Wilson, 2008, Scholarpedia).

1.8. UP and DOWN detection

For detecting the UP and DOWN states the most common method was borrowed from the study of single-channel currents and is called the all-points histogram (Cowan & Wilson, 1994; Wilson & Kawaguchi, 1996; Pare et al., 1998). According to this approach, cells usually switch between two preferred membrane potentials, which can be seen by plotting the frequency of occurrence of various values of membrane potentials. These two preferred potentials are a very hyperpolarized membrane potential and a more depolarized, which is associated with DOWN and UP states, respectively (Wilson, 2008; Scholarpedia). Membrane potential fluctuations usually have a higher amplitude around the UP state, while comparatively, the DOWN state is free of noise. Additionally, as cortical networks run into the oscillations of tonic firing (UP states) and quiescence (DOWN states) (Steriade et al., 1993a; Timofeev et al., 2001; Luczak et al., 2007), these two distinct states can be differentiated by their population activities.

1.9. Sharp Wave-Ripple

Using the extracellular local field potential (LFP), the brief deflections in the hippocampal were observed during periods of NREM sleep (Vanderwolf, 1969; O'Keefe & Nadel, 1978); this conspicuous LFP pattern is called Large-irregular activity (LIA). Sharp wave-ripples (SRWs) is the specific pattern that can be recorded during LIA in the hippocampus (Buzsaki et al., 1983).

The sharp wave component of SWR can be characterized as an event associated with fast and synchronous depolarization of large fractions of the neurons in CA1, the sub-region of the hippocampus (O'Keefe & Nadel, 1978; Buzsaki et al., 1983; Buzsaki,

1986; Sullivan et al., 2011, Suzuki & Smith, 1988). CA1 sharp wave activity can be driven by upstream CA3, sub-region of the hippocampus, which is independent of external input (Buzsaki et al., 1983; Ylinen, A. et al., 1995). In fact, the robust recurrent connectivity in CA3 is considered to let the increased activity of roughly few pyramidal neurons to propagate quickly through the region and bring about synchronized population bursts during the event of sharp wave (Traub & Wong, 1982; Shen & McNaughton, 1996; Buzsaki, 2015; Hannah & Loren, 2018). On the other hand, ripple is a faster short-lasting, high amplitude 150–250 Hz oscillatory event, which is usually co-incident sharp waves to form sharp-wave ripple. In addition to CA1 pyramidal neurons, the strong recurrent activity from CA3 excites interneurons, developing the event of oscillatory excitation and inhibition of ensembles of pyramidal and interneuron cells that demonstrate ripple (O’Keefe & Nadel, 1978; Suzuki & Smith, 1987; Suzuki & Smith, 1988; Buzsaki et al., 1992; English et al., 2014; Stark et al., 2014; Buzsaki, 2015).

It is worth mentioning that ripple has been considered to have a significant role in supporting synaptic plasticity and memory consolidation (Girardeau & Zugaro, 2011; Carr et al., 2011). Also, animal studies have shown that the formation of new memories in rats would be impaired by the depletion of ripple activity by using electrical stimulation (Ego-Stengel & Wilson, 2010; Girardeau et al., 2009).

By the recent study of simultaneous electrophysiological and imaging recording of monkeys, it has been shown that SWRs can be differentiated into several sub-states, which contributes to the different dynamical events in the brain (Ramirez-Villegas et al., 2015).

Below, some of the methods that are useful in the data analysis part of this project, especially regarding measuring the reactivation strength, are discussed.

1.10. Bayesian deconstruction

The Bayesian approach is a conditional probability which is used to refine the model parameters. This approach by bringing updated information and combine it with the existing information, and update it constantly, can thus change the probability distribution of data (Schetz, 2015; Manchala et al., 2017).

Considering two events of A and B , the conditional probability of A given that B is true can be computed via Bayes rule:

$$P(A|B) = \frac{P(B|A)P(A)}{P(B)} \quad (1.1)$$

where $P(B) \neq 0$. In the above equation, $P(A|B)$ is the posterior probability, the probability of the proposition A when the evidence B is taken into account. Also, $P(A)$ is the prior probability of A , which indicates the prediction about A before taking the evidence into account. This prior probability could also measure the prior information. In order to specify the likelihood of observing B given A , a probability distribution called the likelihood was defined; it tells us if A is known, what are the likely values of B . The likelihood measures the range where the evidence B supports the A .

Bayesian reconstruction has been used in different fields of neuroscience such as visual orientation tuning, motor directional tuning, place cells, and replay detection (Foldiak, 1993; Sanger, 1996; Gerrard et al., 1995; Brown et al., 1996; Zhang et al., 1998; Davidson et al., 2009; Wu & Foster, 2014; Ambrose et al., 2018). As an example, by

having the position dependence firing rates of an ensemble of place cells, the Bayes formula can answer the inverse situation: given the firing rates of the ensemble of these cells, what is the most probable situation? As a result, after having the population firing rates maps for an ensemble of neurons and also the animal position distribution during a period of time, the goal is to compute the probability distribution of the animal's position at the later time t , given the firing rates of the ensemble of neurons within the time interval $(t - \tau/2, t + \tau/2)$, where τ is the time window (Zhang et al., 1998). Here, rather than a single position, the distribution of animal's positions would be computed. Let us suppose the position of the animal and number of spikes fired by the N neurons, are defined by the vectors $\mathbf{x} = (x, y)$, and $\mathbf{n} = (n_1, n_2, \dots, n_N)$. So, based on the Bayes formal, the reconstruction can be written as follows:

$$P(\mathbf{x}|\mathbf{n}) = \frac{P(\mathbf{n}|\mathbf{x})P(\mathbf{x})}{P(\mathbf{n})} \quad (1.2)$$

where $P(\mathbf{x}|\mathbf{n})$ is the probability of being at the position \mathbf{x} given the number of spikes \mathbf{n} . $P(\mathbf{x})$ is the probability of being at position \mathbf{x} , which can be measured with the experiment. $P(\mathbf{n}|\mathbf{x})$ is the probability of the number the spike \mathbf{n} to happen given that it is known that the animal is at location \mathbf{x} . $P(\mathbf{n})$ is the probability of the number of spikes \mathbf{n} to happen, and can be measured by normalizing $P(\mathbf{x}|\mathbf{n})$ over \mathbf{x} .

By assuming that the spikes of place cells have Poisson distributions and different cells are statistically independent of each other, for the $P(\mathbf{n}|\mathbf{x})$, it can be written as follows:

$$P(\mathbf{n}|\mathbf{x}) = \prod_{i=1}^N P(n_i|\mathbf{x}) = \prod_{i=1}^N \frac{(\tau f_i(\mathbf{x}))^{n_i}}{n_i!} \exp(-\tau f_i(\mathbf{x})) \quad (1.3)$$

where $f_i(x)$ is the average firing rate of neuron i at the position \mathbf{x} , and τ is the length of the time window. So, for $P(\mathbf{x}|\mathbf{n})$ we have

$$P(\mathbf{x}|\mathbf{n}) = c(\tau, n)P(\mathbf{x}) \left(\prod_{i=1}^N f_i(\mathbf{x})^{n_i} \right) \exp \left(-\tau \sum_{i=1}^N f_i(\mathbf{x}) \right) \quad (1.4)$$

in which $c(\tau, n)$ is a normalization factor and can be determined by the normalization condition $\sum_{\mathbf{x}} P(\mathbf{x}|\mathbf{n}) = 1$ (Sanger 1996).

1.10.1. Replay detection

In order to find a candidate replay event, by detecting the constant-velocity trajectory to describe the series of position estimates in the best possible way, each trajectory can be defined by the velocity (V) and starting location (ρ) of it (Davidson et al., 2009). For a candidate that consists of n position estimates calculated at an interval of Δt , the average likelihood R that the rat is within distance d of a particular trajectory can be expressed as follows (Davidson et al., 2009):

$$R(V, \rho) = \frac{1}{n} \sum_{k=0}^{n-1} P(|pos - (\rho + V \cdot k \cdot \Delta t)| \leq d) \quad (1.5)$$

where the value of d is empirically set to some low values to allow for the detection of replays with small local variation in velocity.

In order to find the most likely replay trajectory, the parameters maximizing R should be found. R_{max} value can be a measure of the goodness of fit of the detected trajectory and can be reported as the replay score for the event candidate.

Finally, in order to check whether for a particular event the replay score is higher than the

amount expecting by chance, the shuffled versions of the position estimates are used to obtain the replay detection procedure with them (Davidson et al., 2009).

1.11. Explained variance measure of reactivation strength

Explained variance simply is a way to measure the variation of a given data set by a mathematical model. Using the explained variance, the proportion of the variability of a given data set can be measured. More specifically, by assessing the firing rate correlation matrix for all pair of recorded neurons (Kudrimoti et al., 1999), the proportion of variability in the neuron-pair firing rate correlation during the task can be considered by the correlation during the succeeding sleep, and regarding the correlation that occurred for the preceding-task sleep session (Euston et al., 2007). The higher percentage of explained variance indicates a stronger similarity between task and post-task sleep patterns. Based on previous reactivation studies, the average EV values of ~15% and ~11% have found in rat hippocampus and medial prefrontal cortex, respectively (Kudrimoti et al., 1999; Euston et al., 2007).

It has shown that in order to obtain the explained variance, for each period (pre-task rest, task, and post-task rest), the spike trains of recorded neurons in each data set can be binned into non-overlapping intervals to assess the sequence of spike counts. For each pair of spike rate sequence, a Pearson's correlation coefficient was defined to be computed using the following formula:

$$C_{ij} = \frac{1/T \sum_{i=1}^T f_i(t) \cdot f_j(t) - \mu_i \cdot \mu_j}{\sigma_i \cdot \sigma_j} \quad (1.6)$$

where μ is the mean and σ is the standard deviation of $f(t)$, respectively (Perkel et al., 1967; Gerstein & Perkel, 1969). By calculation C_{ij} for all neuron pairs, the $N \times N$ matrix of pairwise activity correlation obtains. Consequently, three sets of firing-rate correlations, relating to pre-task rest, task, and post-task sleep would be generated.

For measuring the strength of reactivation in post-task rest, the activity patterns which occurred during the task and reappeared during the post-task sleep should be considered. Subsequently, activity patterns that existed during the sleep before the task should discount, as they were not induced by the task period. Considering all of these points, the explained variance of the correlation pattern in the post-task sleep, which was induced by a task experience, can be defined by the square of partial correlation of task and post-task sleep neuron-pair correlation, while partialling out all the pre-existing correlations during pre-task rest. As a result, the explained variance (EV) is as follows:

$$EV = r_{Task,Post|Pre}^2 = \left(\frac{r_{Task,Post} - r_{Task,Pre} \cdot r_{Post,Pre}}{\sqrt{(1 - r_{Task,Pre}^2)(1 - r_{Post,Pre}^2)}} \right)^2, \quad (1.7)$$

where *Post* and *Pre* refer pre-task rest and post-task rest, respectively. In this equation, *EV*, or $r_{Task,Post|Pre}^2$, represents the effect of the task on the neurons activity correlation in the post-task rest by eliminating all of the pre-existing correlated activities that had observed in the pre-task rest.

1.12. Template matching

Generally speaking, template matching is a technique to find a similar pattern to be a match for the pattern previously presented in the data and distinguished as the

template, later in the data. It has been shown that during a behavioural task (Louie & Wilson, 2001), the combination of spatial receptive fields and structured spatial behaviour produce characteristic ensemble spiking pattern in the rat CA1 cells, which the temporal structure of this pattern is determined by the sequence during which the animal performs the task. As the task was a repetitive experience, the patterns of activity were continually repeated during a specific session, giving the ensemble pattern a unique signature regarding the task. Considering that these patterns were activated repeatedly during the task would suggest these patterns might be a good sample to be regenerated during the subsequent sleep session after the task (Louie & Wilson, 2001).

In the sequence task study (Euston et al., 2007), by averaging binned firing rates of a group of neurons across many repetitions of the sequences, depending on data sets, between six to eight templates were created for each of six to eight sequence segments. For measuring the similarity between a template and the succeeding sleep session, the correlation coefficient can be calculated between their multi-unit activity patterns. For this measurement, a subset of recorded neurons is selected, which were active during all phases of the experiment and showed firing rate changes during the task.

To demonstrate that the observed correlation between the templates and sleep patterns could not have emerged only by chance, the significance of the template correlation coefficient was measured relative to a sample distribution from the shuffled template (Louie & Wilson, 2001).

1.13. Computation of template matches

The spike activity for all of the neurons from a recording session is stored in an $N \times T$ spike matrix, where N is the number of recorded cells and T represents discrete bins (Tatsuno et al., 2006). Each bin content contains the number of spikes of each cell during the bin. The single template matrix, X , is an $N \times M$ matrix, in which M is the number of bins in the temple. The target matrix Y , which has the same bin number, is also chosen. As a result, the matrixes are defined as follows (Tatsuno et al., 2006):

$$X = \begin{bmatrix} x_{11} & x_{12} & \cdots & x_{1M} \\ x_{21} & x_{22} & \cdots & x_{2M} \\ \vdots & \vdots & \cdots & \vdots \\ x_{N1} & x_{N2} & \cdots & x_{NM} \end{bmatrix}, \quad Y = \begin{bmatrix} y_{11} & y_{12} & \cdots & y_{1M} \\ y_{21} & y_{22} & \cdots & y_{2M} \\ \vdots & \vdots & \cdots & \vdots \\ y_{N1} & y_{N2} & \cdots & y_{NM} \end{bmatrix}. \quad (1.8)$$

The template matching method investigates the similarity of these two matrices. One way to measure the similarity is the standardize Pearson correlation coefficient for data matrices (Tatsuno et al., 2006). In the suggested technique, each row of these two matrices, X & Y , by subtracting its row mean, \bar{x}_c and \bar{y}_c , and then divided by the standard deviation, $\sigma_{x,c}$ and $\sigma_{y,c}$, respectively, is standardized to zero-mean and unit-variance. These parameters are defined as follows:

$$\bar{x}_c = \frac{1}{M} \sum_{m=1}^M x_{cm}, \quad \bar{y}_c = \frac{1}{M} \sum_{m=1}^M y_{cm}, \quad (1.9)$$

$$\sigma_{x,c} = \sqrt{\frac{1}{M} \sum_{m=1}^M (x_{cm} - \bar{x}_c)^2}, \quad \sigma_{y,c} = \sqrt{\frac{1}{M} \sum_{m=1}^M (y_{cm} - \bar{y}_c)^2}. \quad (1.10)$$

The z-score variables w_{cm} and z_{cm} , which were transformed by applying the normalization on x_{cm} and y_{cm} , are defined as follows:

$$w_{cm} = \frac{x_{cm} - \bar{x}_c}{\sigma_{x,c}}, \quad z_{cm} = \frac{y_{cm} - \bar{y}_c}{\sigma_{y,c}}. \quad (1.11)$$

This normalization method entirely suppressed the mean firing rate differences between different rows. This technique is then sensitive to the firing order relationships among different neurons. Then, by using the two-dimensional Pearson correlation coefficient, COR , also the new normalized variables w and z , the standardized Pearson measure can be defined as follows:

$$COR = \frac{\sum_{c=1}^N \sum_{m=1}^M (w_{cm} - \bar{w})(z_{cm} - \bar{z})}{\sqrt{\sum_{c=1}^N \sum_{m=1}^M (w_{cm} - \bar{w})^2} \sqrt{\sum_{c=1}^N \sum_{m=1}^M (z_{cm} - \bar{z})^2}}. \quad (1.12)$$

1.14. Hidden Markov model

Hidden Markov Model (HMM) is a statistical model with which it is possible to model a system that is assumed to be a Markov process with unknown (hidden) states. It is a ubiquitous tool to model the time series data. Recently, it has widely used in many different fields from speech recognition, computational molecular biology, data compression, artificial intelligence pattern recognition, and also computer vision (Ghahramani, 2001).

The hidden Markov model has two key defining features, and the name of it comes from them. Firstly, it supposes that the observation at time t is generated by a process during which the state S_t of the model is “hidden” from the observer. Secondly, each state of this hidden process has to satisfy the Markov feature, which is, the current

state of S_t at time t , given the value of all the states, only depends on the S_{t-1} at time $t - 1$, and it is independent of other states happening at $t - 2$ or before (Ghahramani, 2001); this is a Markov property. Similarly, the outputs satisfy a Markov property regarding states, and so given S_t , the observed variable O_t only depends on the value of S_t , both at time t , and is independent of the states and observations at all other times.

Considering all of Markov model properties, for the joint distribution of a sequence of states and observations, it can be factored as follows:

$$P(S_{1:T}, O_{1:T}) = P(S_1)P(O_1|S_1) \prod_{t=2}^T P(S_t|S_{t-1})P(O_t|S_t). \quad (1.13)$$

In order to briefly introduce the Markov chain process where the observation is a probabilistic function of the state and the system being modelled has an underlying stochastic process which is hidden and only can be observed by another set of stochastic processes that generate the observation sequence (Rabiner, 1989), let's consider the Urn and Ball Model. By assuming that there are N urns, and in each of which there is a large number of coloured balls, where there are M distinct colours of the balls, there is a good scenario of how an HMM can explain a model. Here are the steps: Based on some random process, a person selects an initial urn. Then, from this urn, a ball randomly is chosen, and its colour considers as the observation. Afterward, the ball replaces in the same urn from which it was selected before. Subsequently, a new urn is chosen randomly and then the same random selection for the ball. In this way, a finite sequence of observations of colours produces, which can be modelled by HMM. Based on these observations, the HMM determines which urn the ball(s) were selected from.

In this study, HMM has been used to detect different states in the prefrontal cortex of a rat during sleep by using the activity of recorded neurons.

It is worth mentioning that in the run and ball scenario, each state corresponds to a specific urn similar to each detected state in our study. Besides, the number of distinct observations which in the urn and ball scenario are the colours of the balls selected from urns, but in this study are the distinct neurons firing rates.

HMM is fully explained in the method section of this thesis.

1.15. State-space model

The state-space model (SSM) offers a general framework to analyze the deterministic and stochastic dynamical systems that can be observed or measured with a stochastic process. The state-space model has been successfully used to tackle a broad range of dynamical system problems in different fields such as engineering, statistics, computer science, and neuroscience. In computational neuroscience, the important goal is to develop statistical techniques to distinguish the features of the dynamic in neural and behavioural responses of experimental subjects recorded during experiments (Chen & Brown, 2013, Scholarpedia).

In this model, by considering a sequence of observations which are real-valued and N-dimensional vectors $\{O_1, O_2, \dots, O_T\}$, and by assuming that at each time step O_T was produced from M-dimensional hidden state variable X_t , in which the sequence of X 's is defined as a first-order Markov process (Ghahramani, 2001):

$$P(X_{1:T}, O_{1:T}) = P(X_1)P(O_1|X_1) \prod_{t=2}^T P(X_t|X_{t-1})P(O_t|X_t). \quad (1.14)$$

This shows that the mathematical description for the state-space model is similar to the HMM. But, here, instead of the hidden S variables, the continuous hidden X variables, replaced.

By assuming that the state transition probability, $P(X_t|X_{t-1})$, has two stochastic and deterministic components, we can rewrite it as follows:

$$X_t = f_t(X_{t-1}) + \varepsilon_t \quad (1.15)$$

in which f_t is the deterministic transition function establishing the mean of X_t given X_{t-1} , and ε_t is a random noise vector with a mean of zero. Also, for the observation probability $P(Y_t|X_t)$ in a similar way, we have:

$$Y_t = g_t(X_t) + \delta_t. \quad (1.16)$$

By assuming that both transition and output functions are linear and time-invariant, and also supposing the distribution for the state and observation noise variables are Gaussian, we will have a linear-Gaussian state-space model:

$$\begin{aligned} X_t &= AX_{t-1} + \varepsilon_t \\ Y_t &= BX_t + \delta_t \end{aligned} \quad (1.17)$$

where A and B are the state transition matrix and the observation matrix, respectively.

Similar to the HMM model, which will be fully explained in the method section, this method also is useful to be used in neuroscience.

In this present study, we have mostly focused on cortical memory reactivation, which is not well-studied in comparison to hippocampal memory reactivation. We also

were interested to see whether the UP state can be clustered to different sub-states or not. In spite of efforts to distinguish the UP state (McFarland et al., 2011; Ghorbani et al., 2012) and in contrast to the finding in the hippocampal SWRs, for UP state there is no clear study showing whether UP state can be clustered to several sub-types or not. Now the main question is if UP state is composed of multiple sub-states, what are the different features of these sub-states in terms of some features such as firing rate, duration, and most importantly, how these sub-states of UP state are contributed to the memory reactivation. In order to tackle these questions, previously recorded data sets of three rats, which were trained to do a sequential task, were used in our analysis project. For all of these three rats, multi-unit activities in the medial prefrontal cortex were recorded; also, for one of the rats, the multi-unit activity of the hippocampus was recorded.

Using several data analysis methods, including template matching (Euston et al., 2007; Tatsuno et al., 2006) and hidden Markov model (Rabiner, 1989), we have tried to investigate are UP states separable to different sub-states with different dynamics, and if they are, find the feature(s) they can be distinguishable with it. Subsequently, start studying their relations in regard to cortical memory reactivation.

Afterward, the contributions of these sub-states to the memory reactivation were studied in detail. We surveyed how reactivation distributed during the UP state and UP sub-states and also their phase preferences during the UP state and UP sub-states. Additionally, we explored what the features of the sub-state(s) containing the reactivation are. We also tried to study how the presence of reactivation can change the dynamic of UP states. Measuring the cluster distance between different UP sub-states also was one of the goals of this research; by doing this, one can show whether the UP-1 and UP-2 sub-

states are distinguishably clustered.

Moreover, by using the hippocampus multi-unit activity and LFP, we explored the relationship between the hippocampus and the cortex during these two UP sub-states.

Besides, by finding the timestamps during which the ripples occurred, we have tried to find the correlation of ripple to the different transitions in the cortex, the transition from DOWN to UP and also from different UP sub-types to each other.

Also, we were interested in studying the impact of task experience on the sleep, and specifically on the UP sub-types characteristics. It is also a matter of interest how the proportion of UP sub-types would be changed by the effect of task and how the UP-1 and UP-2 of UP state of pre-task sleep might be clustered differently in comparison to post-task sleep.

Finally, by using the application of higher than three-state of HMM (four-state, five-state, six-state, and ten-state), we tried to explore is still a UP sub-state containing the majority of reactivation regardless of the number of UP sub-types generating by the different state of HMM. By measuring the cluster distances of different HMM states, we can also find what number of HMM state is the optimum number to generate the highest distance and the most separated clusters.

2. Methods

2.1. Recording procedures

Three male Brown Norway/Fisher 344 Hybrid rats were used for the recording, which consisted of two 50-60 min sequential task sessions and three 30-60 min rest sessions. The recording started with the first rest session (rest 1), followed by the first task session (task 1), the second rest session (rest 2), the second task session (task 2) and the third rest session (rest 3). Two rats were implanted with a hyperdrive containing 12 independently movable tetrodes (Gothard et al., 1996) in the medial prefrontal cortex (mPFC) and twisted-pair local field potential electrodes in the hippocampus. The third rat was implanted with a dual-bundle Hyperdrive in the mPFC and CA1 of the hippocampus. The Number of recorded neurons is between 70 to 125 neurons in mPFC for the first and second rats. For the third rat, recorded using a dual-bundle Hyperdrive, around 55 to 62 neurons in mPFC and around 45 to 60 neurons in the hippocampus were recorded. The number of recorded neurons in each data set is mentioned in Table 1. Detailed procedures are fully explained in the experimental protocol of (Euston et al., 2007) In this thesis, we used the data from rest one as the pre-task rest session, task two as the task session and rest three as the post-task rest session because memory reactivation signal was most clearly detected in this combination (Euston et al., 2007).

Table 1. The number of neurons recorded in each data set.

Data set	# of recorded neurons in mPFC	# of recorded neurons in HPC
7165_11	72	-
7165_16	119	-
7165_31	122	-
7165_36	120	-
8202_07	74	-
8202_08	78	-
8202_09	69	-
8482_14	55	61
8482_15	62	49
8482_16	57	44

2.2. Detection of UP-DOWN oscillation epochs

In order to assess the epochs which potentially contain clear UP and DOWN states within slow-wave sleep, the firing rates of multi-unit activity using a 20 ms bin size was calculated. Subsequently, by finding all of the bins where the multi-unit firing rate is equal to zero, indicating clear DOWN states, a binary vector was made, which marks the position of these bins. Then, this binary vector was convolved with multiple Gaussian kernels, each with a width of 30 seconds and with different standard deviations of 1.5, 2,

and 3 seconds. Reasonable bimodal distributions were found for all of the 10 data sets and threshold based on the valley in each of these bimodal distributions was used. Finally, for each data set, by averaging over the three points regarding the valleys of the three different distribution, we have a threshold based on which we can detect parts of sleep, which potentially have higher UP and DOWN fluctuations. Using video recording, the selected epochs were verified that whether they occurred when the animal was motionless or not and we only selected the parts occurring during motionless.

2.3. Hidden Markov model

A Hidden Markov Model (HMM) is a statistical Markov model in which the system which is modelled is presumed to be a Markov process with unobserved (hidden) states (Rabiner, 1989). So, In a Hidden Markov Model (HMM), the state is not directly visible, but the output, dependent on the state, is visible. Each detectable state by HMM has a probability distribution over the possible output tokens. For an N recorded neuron system, the system is considered to be in one of the predetermined hidden firing rate states. In the HMM, each state is defined by a vector consisting of the average firing rates of the N recorded neurons. For each state, neurons are assumed to be independent of the events before and can be fully described by the immediate firing probability, similar to a stationary Poisson process. The HMM can be fully described by two matrices, E and A . E_{ij} is an emission matrix that determines the probability of neuron j firing in the state S_i . A_{ij} is a transition matrix that gives the probability of transitioning from state S_i to state S_j . The probability of a transition between two hidden states only depends on the identities of the states. As a result, A_{ij} is independent of time. The HMM model predicts

a distinct hidden state at time t to represent all of the information preceding it. These matrices, E and A , are determined as a part of the training algorithm for HMMs. The HMM used in this study was a three-state model trained by binning the multi-unit activity with 1 ms bins.

Each bin was then set to the ID of the neuron that fired in that bin, and if no neuron fired, a value of 0 was given. In cases where multiple neurons fired within the same bin, which was on average 1.68% of the bins of our recording for all of the data sets, a randomly selected neuron ID, amongst the IDs of firing neurons, was used. Neuron IDs were provided in the recording procedure by the Neuralynx cheetah recording system, and these IDs do not necessarily carry specific information.

In order to understand how HMM works, the key point is to calculate, $P(O|\lambda)$, which is the probability of the observation sequence O , given the model λ , where $O = O_1 \cdot O_2 \dots O_T$ and $\lambda = \{E, A\}$ (Rabiner, 1989). The first and easiest way of solving it is considering all of the possible state sequences of length T , which T is the number of all observations. Let us suppose we have this sequence of states:

$$Q = q_1 \cdot q_2 \dots q_T \quad (2.1)$$

in which q_1 is the initial state and q_T is the final state. The probability of the observation sequence O for the state sequence Q is

$$P(O|Q, \lambda) = \prod_{t=1}^T P(O_t|q_t, \lambda) \quad (2.2)$$

in which by assuming the observations are statistically independent, we get the following expression:

$$P(O|Q, \lambda) = e_{q_1}(O_1) \cdot e_{q_2}(O_2) \dots e_{q_T}(O_T) \quad (2.3)$$

in which we define $E_{ij} = \{e_i(j)\}$ as the probability distribution for the firing of neuron j in the state S_i .

For the state sequence Q :

$$P(Q | \lambda) = \pi_{q_1} a_{q_1 q_2} a_{q_2 q_3} \dots a_{q_{T-1} q_T} \quad (2.4)$$

Where $A = \{a_{ij}\}$ is the state transition probability distribution and defines as

$$a_{ij} = P[q_{t+1} = S_j | q_t = S_i], \quad 1 \leq i, j \leq N. \quad (2.5)$$

Subsequently, the joint probability of O and Q can be defined as

$$P(O, Q | \lambda) = P(O|Q, \lambda) P(Q, \lambda). \quad (2.6)$$

Then, by calculating the sum of this joint probability across all possible state sequences q , the probability of O , given the model, can be calculated as follows:

$$\begin{aligned} P(O | \lambda) &= \sum_{\text{all } Q} P(O|Q, \lambda) P(Q|\lambda) \quad (2.7) \\ &= \sum_{q_1, q_2, \dots, q_T} \pi_{q_1} e_{q_1}(O_1) a_{q_1 q_2} e_{q_2}(O_2) \dots a_{q_{T-1} q_T} e_{q_T}(O_T). \quad (2.8) \end{aligned}$$

Based on the equation (8), in the beginning, time t ($t = 1$), the state is q_1 with possibility of π_{q_1} , which gives the observation of O_1 with probability $e_{q_1}(O_1)$.

Subsequently, by a transition to state q_2 , in time $t + 1$, with probability $a_{q_1 q_2}$, and giving observation O_2 with probability $e_{q_2}(O_2)$. The transition continues to the final state q_T with probability $a_{q_{T-1} q_T}$.

One can quickly realize that to solving the last equation, since, during each time step, there are N possible states to be transited to, also for each state sequence about $2T$ calculation are required, then, in total, it needs $2T \cdot N^T$ order of calculations. That makes the calculation computationally unattainable; as for example, for $N=3$ states and $T= 1000$, the order of needed computations would be $2 \cdot 1000 \cdot 3^{1000}$, which clearly explains why a more efficient way of calculation is needed to tackle the problem; this approach is the Forward-Backward procedure.

The best approach to make the calculations computationally feasible is the Forward-Backward procedure (Rabiner, 1989).

The forward probability, $\alpha_t(i)$, is defined as

$$\alpha_t(i) = P(O_1 O_2 \dots O_t, q_t = S_i | \lambda) \quad (2.9)$$

which is the probability of the partial observation sequence up to time t , $O_1 O_2 \dots O_t$, with state S_i at time t , given the model λ .

The equation can be solved as follows:

1) Initialization:

$$\alpha_1(i) = \pi_i e_i(O_1), \quad 1 \leq i \leq N. \quad (2.10)$$

By introducing the joint probability of state S_i and initial observation O_1 , the forward probabilities are initialized.

2) Induction:

$$\alpha_{t+1}(j) = \left[\sum_{i=1}^N \alpha_t(i) a_{ij} \right] e_j(O_{t+1}), \quad 1 \leq t \leq T-1, \quad 1 \leq j \leq N. \quad (2.11)$$

By completing the computation for all states j , and subsequently, iterating all t , the probability of the complete history of the observation from which the likelihood $P(O|\lambda)$ can be obtained is defined by the forward probability as follows:

$$P(O|\lambda) = \sum_{i=1}^N \alpha_T(i). \quad (2.12)$$

As a result, to find $P(O|\lambda)$ we only need to find the sum of $\alpha_T(i)$'s.

By a little thought, it can be convincing that the amount of involved computation in the calculation of the above equation is N^2T , instead of $2T \cdot N^T$, so for a similar situation of $N=3$ for the states and $T=1000$, around 9000 computations would be needed.

In the same manner, the backward probability β_t can be defined as

$$\beta_t(i) = P(O_{t+1} O_{t+2} \dots O_T | q_t = S_i, \lambda). \quad (2.13)$$

Which is the probability of partial observation sequence from time $t+1$ to the end, given that the state at time t is S_i and the model is λ .

Again, for the backward probability, we can solve it as follows:

1) Initialization

$$\beta_T(i) = 1, \quad 1 \leq i \leq N. \quad (2.14)$$

Here for the initialization step we arbitrary define $\beta_T(i)$ to be 1 for all i .

2) Induction:

$$\beta_t(i) = \sum_{j=1}^N a_{ij} e_j(O_{t+1}) \beta_{t+1}(j), \quad t = T-1, T-2, \dots, 1, \quad 1 \leq i \leq N. \quad (2.15)$$

Again, the computation of calculation required for $\beta_t(i)$ has the order of N^2T .

In order to explain how the HMM parameters re-estimate $\xi_t(i, j)$, the probability of being in state S_i at time t and state S_j at time $t + 1$ given the model and the observation, can be defined as follows:

$$\xi_t(i, j) = P(q_t = S_i, q_{t+1} = S_j | O, \lambda). \quad (2.16)$$

Using the definition of the forward and backward probabilities $\xi_t(i, j)$ can be easily described in the following form:

$$\xi_t(i, j) = \frac{\alpha_t(i) a_{ij} e_j(O_{t+1}) \beta_{t+1}(j)}{P(O | \lambda)} \quad (2.17)$$

$$= \frac{\alpha_t(i) a_{ij} e_j(O_{t+1}) \beta_{t+1}(j)}{\sum_{i=1}^N \sum_{j=1}^N \alpha_t(i) a_{ij} e_j(O_{t+1}) \beta_{t+1}(j)} \quad (2.18)$$

where we used $P(q_t = S_i, q_{t+1} = S_j | O, \lambda)$ for the numerator and used $P(O | \lambda)$ for the denominator to reach to the desired measure of probability.

Also, the variable $\gamma_t(i)$, can be defined as follows:

$$\gamma_t(i) = P(q_t = S_i | O, \lambda). \quad (2.19)$$

Where $\gamma_t(i)$ is the probability of being in state S_i at time t , given the observation sequence O and the model λ . This equation can be explained by using the forward and backward probabilities as follows:

$$\gamma_t(i) = \frac{\alpha_t(i)\beta_t(i)}{P(O|\lambda)} = \frac{\alpha_t(i)\beta_t(i)}{\sum_{i=1}^N \alpha_t(i)\beta_t(i)}. \quad (2.20)$$

Then the relation between $\gamma_t(i)$ and $\xi_t(i, j)$ after summing over j is

$$\gamma_t(i) = \sum_{j=1}^N \xi_t(i, j) = \frac{\alpha_t(i)\beta_t(i)}{\sum_{i=1}^N \alpha_t(i)\beta_t(i)}. \quad (2.21)$$

Now by summing $\gamma_t(i)$ over the time index, the obtained quantity can be interpreted as the expected number of times that state S_i is visited, or equally, the expected number of transitions from S_i . Similarly, by summing $\xi_t(i, j)$ over time index, the expected number of transitions from S_i to S_j would be obtained. By using the above formulas, the method for re-estimation of HMM parameters $\lambda = \{E, A\}$ can be achieved. Then, the re-estimation of the model parameters in the maximization step is defined as follows:

$$a_{ij}^{new} = \frac{\sum_{t=1}^{T-1} \xi_t(i, j)}{\sum_{t=1}^{T-1} \gamma_t(i)} \quad (2.22)$$

$$e_i^{new}(j) = \frac{\sum_{t=1}^{T-1} \xi_t(i, j)}{\sum_{t=1}^{T-1} \gamma_t(i)}. \quad (2.23)$$

In equation (22), $\sum_{t=1}^{T-1} \xi_t(i, j)$ is the expected number of transitions from S_i to S_j and $\sum_{t=1}^{T-1} \gamma_t(i)$ is the expected number of transitions from S_i to any state. Thus, the variable a_{ij}^{new} can be interpreted as the probability of transition from S_i to S_j which is

exactly what it was supposed to be. For equation (23), $\sum_{\substack{t=1 \\ O_t=j}}^{T-1} \xi_t(i, j)$ is the expected number of times in which the system is in the state S_i and with observation $O_t = j$, which in this study indicates the probability distribution for the firing of neuron j . The denominator again is the expected number of times the system is in state S_i . Consequently, variable $e_i^{new}(j)$ is the probability of observing neuron j firing while the system is in the state S_i .

It has been proven by (Dempster et al., 1977) that the re-estimated model is more likely than the initial model: $P(O|\lambda^{new}) > P(O|\lambda)$. As a result, we can find a new model by which the observation of sequence is more likely to be generated, as the model is led to a maximum-likelihood estimate.

Each detected UP-DOWN oscillation epoch was treated as a separate trial that was used to train the HMM for each data set. The most probable sequence of hidden states was generated using this HMM for each epoch. In this study, similar to (Ponce-Alvarez et al., 2012), the re-estimation stops at the point the increase in the log of the likelihood is less than a tolerance factor (10^{-6}), or it was not reached by the maximum number of iterations (500). We reran the re-estimation algorithm ten times, each time by using new initial parameters, to verify that the likelihood has reached the global maximum likelihood and not only a local maximum. For the emission matrix, the initial components were chosen randomly, while for the transition matrix components were initialized as diagonal elements D , in the range (0.99 to 0.999), and for non-diagonal elements equal to $(1 - D)/(N - 1)$.

By using three-state HMM, the three states were identified as the DOWN state, the UP-1 state, and the UP-2 state. The DOWN state was distinguished as a state with a very low mean firing rate. The UP-1 state was defined by having a slower population vector decorrelation time constant than UP-2.

In order to check how much the result given by HMM is consistent, and as it is technically impossible to use cross-validation for our method, we used two methods to measure the stability of the HMM result instead.

In the first method, after finding all DOWN states which were provided by the original HMM, the number of all DOWN states was divided into two halves. First, an HMM was trained using only the data from the first half of the DOWN states and the corresponding UP state that followed each DOWN state. All the methods are the same except here we only used approximately half of the data to feed to the HMM. Similarly, another HMM was created using the second half of the DOWN states and associated following UP states.

For the second method, the DOWN states from the original HMM were split into even and odd subsets. Once again, two new models were trained using these two subsets and their subsequent UP states.

Finally, these four (first half, second half, odd, and even) models generated using these subsets of the original data were compared against the initial HMM to check the consistency of the results. (These results can be found in the appendix, Supplementary Figure 3.)

To investigate how much the neuron dynamics affected the results of the states detected by the HMM, we performed two types of shuffling of the input data: the data within each sub-type found by the original HMM was shuffled, and the data within the entire UP state was shuffled. Subsequently, this was compared to the results of the original HMM model. Each shuffling method was performed 10 times. Additionally, neuron IDs were randomly shuffled. The ten shuffles were compared against the original HMM to determine how much the neuron IDs influenced the results. Finding the consistency would imply the fact that the neuron ID itself is not the feature HMM uses to distinguish the final states. (These results can be found in the appendix, Supplementary Figure 4.)

2.4. Template matching analysis

As we typically had eight segments as parts of the sequence task, eight templates were generated for each session. Each template starts when the animal departs from one reward point and ends when the animal arrives at the next one. For the template, each row consists of spike counts from each neuron binned along the duration of the segment with a bin size of 100 ms, averaged over all traversals of that segment (Euston et al., 2007). In template matching analysis, we used stable neurons that were active during all parts of the experiment and showed the task-related change in their firing rates. In order to measure the similarity of a target matrix which is selected with the same size and dimensions as a template, we used correlation coefficient measure as defined in (Louie & Wilson, 2001). After template matching was performed, the template was shuffled and the template matching procedure was performed again. This shuffling was repeated 500

times. The mean and standard deviation of the correlation values found for each time bin from these shuffled template matching results was used to z-score the original template matching result. For the purpose of investigating whether the reactivation happens faster than the speed of the patterns during behaviour, we performed template matching analysis with different ranges of compression factors between 1 to 10x (Euston et al., 2007). To assess which compression factor is the best for the specific data set, we counted the number of significant peaks of the template matching results (e.g., the peaks $> z\text{-score} = 5$) and selected the compression factor with the maximum number of the peaks.

2.5. Population vector decorrelation

Sequences of spike times for each neuron were binned using a bin size of 1 ms to obtain the number of spikes fired within each bin. A population vector, defined as a vector containing the number of spikes fired for each neuron within a bin, was created and compared against all other population vectors succeeding it within the specific subtype event by computing the Pearson correlation coefficient. These correlation coefficients were then averaged at each lag across the different UP-1 and UP-2 states. An exponential function, $y = a * \exp\left(-\frac{x}{\tau}\right) + b$, was fit using the data up to the point where the correlation slope, which was smoothed using a 25 ms moving average, changes from negative to positive after an initial delay. The de constant, τ , was found from the fit exponential.

2.6. Principal Component Analysis (PCA)

To estimate how UP-1 and UP-2 can be distinguishably clustered, each subtype event was represented by a vector of the mean firing rate for each neuron within the subtype event and normalized using Z-score. These vectors were then concatenated together to create a matrix in which the PCA was performed on. The data was then projected on to each principal component, and the resulting scores for the first and second principal components were plotted against each other to produce two clusters for each subtype. The quality of these clusters was measured using cluster distance (Fellous, et al., 2004). For each cluster, the centroid was found by computing

$$\vec{c}_k = \frac{\sum_{i=1}^{N_k} \vec{x}_{k_i}}{N_k} \quad (2.24)$$

where \vec{x}_{k_i} is the two-dimensional projection for the i -th subtype event in cluster k with a size of N_k . Cluster distance

$$D = \frac{\sum_k D_k}{K} \quad (2.25)$$

was then calculated for each data set where

$$D_k = \frac{\sum_{\vec{p} \notin Q_k} \|\vec{p} - \vec{c}_k\|}{\sum_{\vec{p} \in Q_k} \|\vec{p} - \vec{c}_k\|} \times \frac{N_k}{N - N_k} \quad (2.26)$$

and Q_k is the set of all \vec{x}_{k_i} . This compares the distances from all points within cluster k to its centroid to the distance of all other points to centroid k . Based on this cluster strength measuring study (Fellous, et al., 2004), suggesting a threshold of two for D , the clusters which have a value higher than two can be considered as valid clusters. In this thesis, we call this clustering method the Jean-Marc method.

2.7. Cross-correlation between SWRs and UP transitions

To investigate the relationship between UP transitions and SWRs, we constructed a cross-correlation histogram with UP transitions being the reference signal. A bin size of 20 ms was used for all calculations, and the histogram was normalized by the number of UP transition events.

2.8. Cross-correlation between MUAs of mPFC and HPC

In order to investigate the relationship between cortex and hippocampus, and more specifically for the time we have different UP sub-types in the cortex, the multi-unit activities of mPFC and HPC were used to construct the firing rates for both mPFC and HPC by a 20 ms bin size. Then, by using cross-correlation between these multi-unit firing rates, the relationship for the time we have UP-1 and UP-2 in the cortex were studied respectively to find is the relationship is changing for different UP subtypes or not.

3. Results

3.1. Epochs detection

In order to investigate how the UP and DOWN states occur during the post-task sleep, by using a 20 ms bin size, the population firing rate was obtained. The fluctuation in the multi-unit activity for one example is shown (Figure 1, A). The gray patches in this figure depict periods of motionless. To find the parts of sleep which have the clear UP and DOWN transitions, we firstly measured the density of DOWN state, and then only detected the parts with high densities of DOWN state transitions as it is fully described in the method section. Subsequently, a binary vector was made from bins where the population firing rate is equal zero, indicating the possible DOWN states, and thus the binary vector marks the bins where the possible DOWN states occur. Then this binary vector was convolved with three different Gaussian kernels with three standard deviations of 1.5, 2, and 3 seconds. It was then normalized and subsequently averaged together to get the density of DOWN state. Then, we made the average histogram of kernel density for the DOWN state (Figure 1, B, left histogram). According to this histogram, we can assert that there is a bimodal distribution for the histogram; as a result, it is possible to find the value on the valley of the histogram and use it as a threshold. Using this threshold, the epochs of potential UP-DOWN oscillations were found (the blue bars (Figure 2, bottom)). After checking whether these epochs happened during motionless periods of sleep, these epochs of UP-DOWN oscillation were used for further analysis.

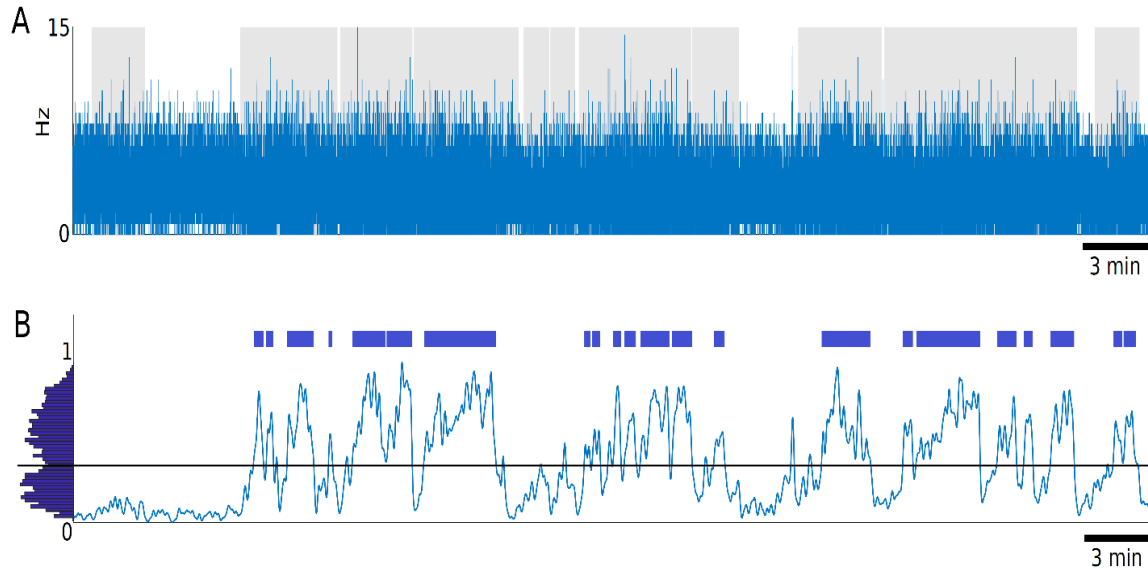


Figure 1. Detection of epochs of UP and DOWN. Top (A): This figure shows an example of the population firing rate using a 20 ms bin size for post-task sleep. The grey patches in the figure indicate periods of motionless. Bottom (B): Kernel density figure shows the average of three Gaussian kernels with standard deviations of 1.5, 2, and 3 seconds were used and then was averaged. In the left histogram, the distribution of values from the average kernel is shown. The threshold was found based on the position of the valley in this distribution and has been used to detect the epochs with high UP and DOWN fluctuations. Epochs are shown at the top of the figure with blue bars.

3.2. DOWN state and two UP sub-states can be separated by a three-state HMM

Using a three-state HMM, the epochs of UP-DOWN transitions were divided into three states, DOWN states and two UP sub-types. One of these states which was distinguished by a three-state HMM, had a significantly lower firing rate in comparison to other detected states. As the DOWN state is defined as a pretty much silent state, this detected state is called DOWN state. This indicates that HMM can successfully detect the DOWN state. The two other detected states by HMM have high firing rates, suggesting that they are the sub-states of UP states. For this analysis, I used 10 data sets from three

rats, and for all analyzed pre-task and post-task rests from these data sets, 275 samples out of 336 selected epochs of UP and DOWN were successfully separated into DOWN and two UP sub-types states and for other HMM was not able to detect the DOWN and two UP sub-types. Considering only post-task sleep epochs, all of 154 epochs were successfully separated into DOWN and two UP sub-states. Figure 2 and Figure 3 demonstrate how the detected states by HMM are.

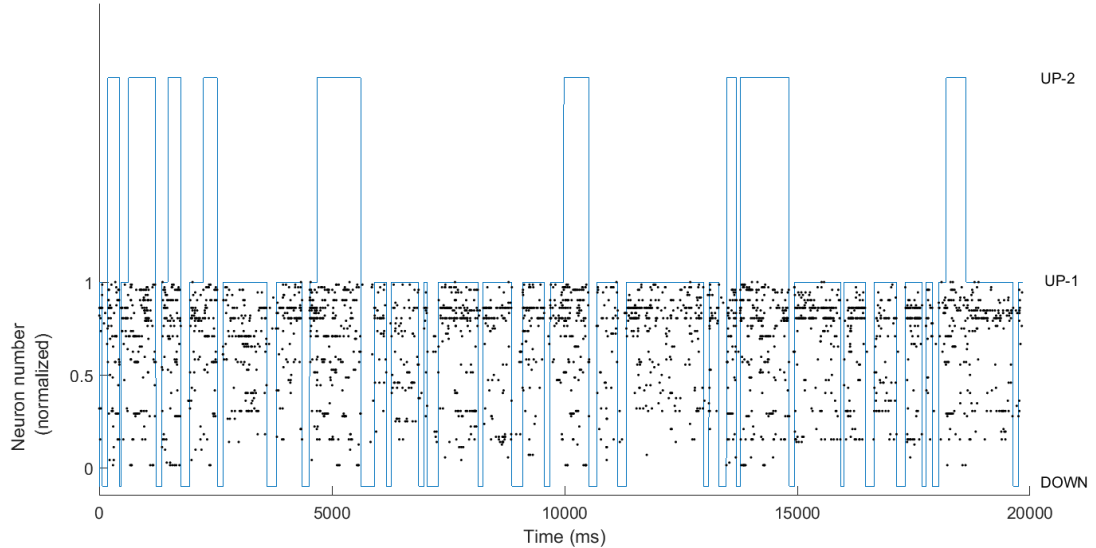


Figure 2. A sample of three detected states using a three-state HMM for one epoch. A raster plot depicting all the neurons firing during the selected epoch and the sequence of three different states, detected by HMM, is shown by the blue line.

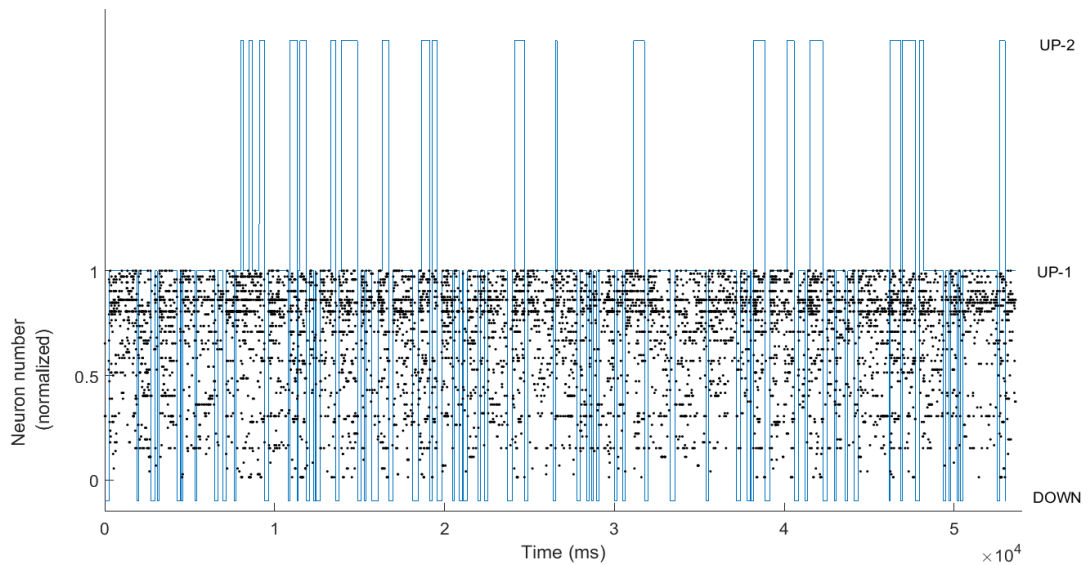


Figure 3. Example of the raster plot of another epoch and the three states detected by HMM.

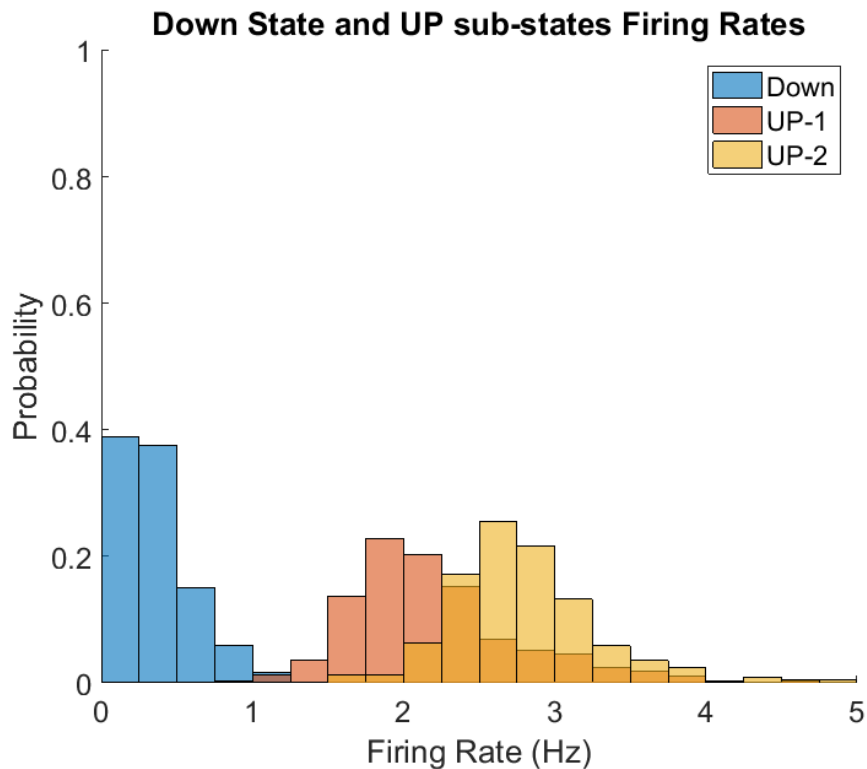
3.3. Two subtypes of UP states

As it was discussed, HMM detected DOWN state and two UP sub-states. Our study suggests these two detected UP sub-types have different features in terms of firing rate, duration, and, most importantly, state vector decorrelation.

In order to identify the two UP sub-states, we initially started by calculating the mean firing rate, which is defined as total spiking activities of all recording neurons during a specific sub-state event divided by the duration of sub-state. Our investigation demonstrates that it is entirely well-defined to use the mean firing rate to identify DOWN state as it is strongly skewed toward a very low firing rate (Figure 4, one example of one data set). This makes DOWN states finely distinguishable in terms of firing rate.

Although the mean firing rate for one of the two UP sub-types is always slightly higher

than the other one, the two UP sub-types have a similar distribution of firing rates (Figure 4, three examples of three data sets, from three rats). By performing the systematic analysis for all 10 data sets from all three animals, it has been confirmed that the firing rate distribution between DOWN state and two UP sub-states are significantly different while not significantly different between UP sub-states (multi-comparison test with Tukey-Kramer criterion: DOWN vs UP-1: $p = 6.34 \times 10^{-9}$, DOWN vs UP-2: $p = 1.12 \times 10^{-9}$, UP-1 vs UP-2: $p = 0.259$). Mean Firing rates for DOWN states and two UP sub-states were calculated for all of 10 data sets (Figure 5).



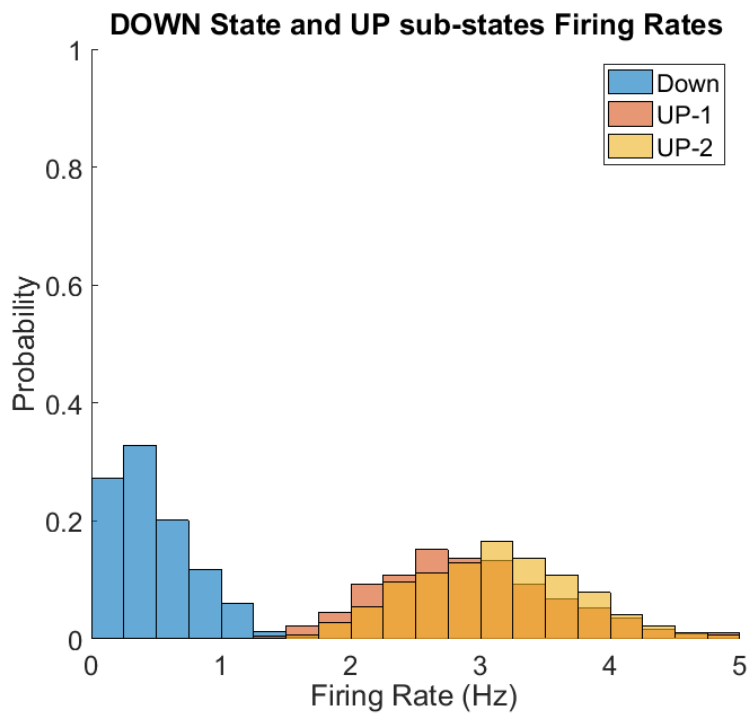
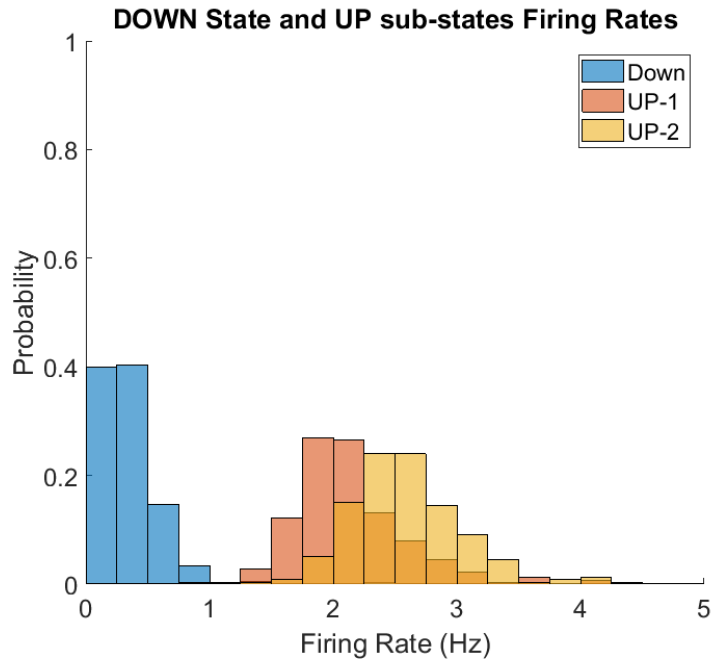


Figure 4. The firing rate distribution for the three states detected by HMM. (Three examples from three rats.) Different colours on histogram show the firing rate distributions for DOWN state and two UP sub-states detected by HMM, respectively. Although it denotes that the DOWN state has a clear lower firing rate in comparison to the other two states, there is not that much clear difference to distinguish the UP sub-states based on their firing rates.

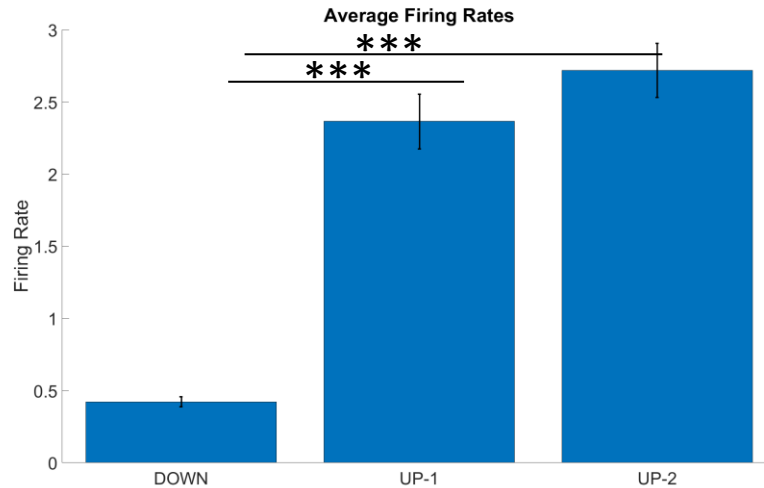
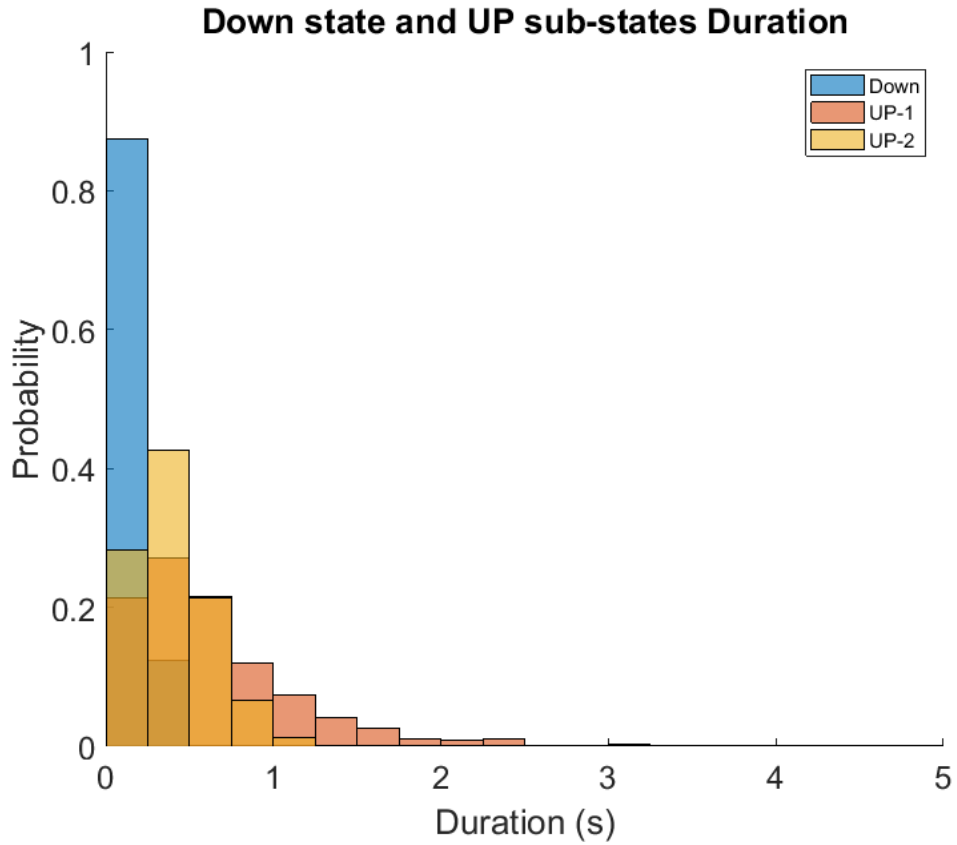
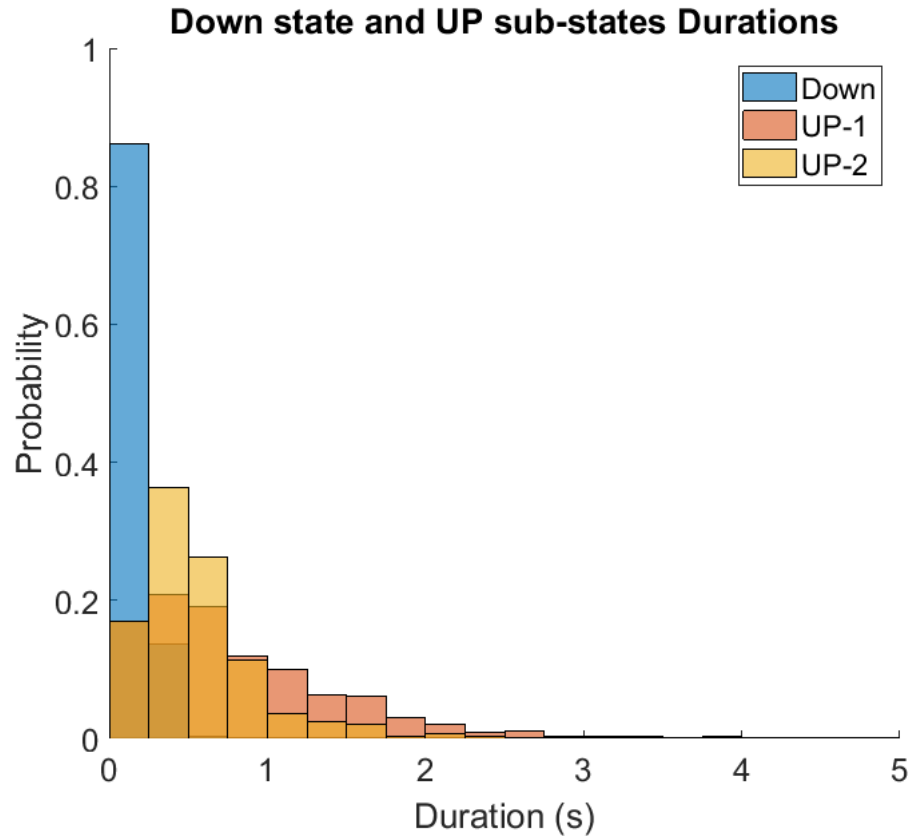


Figure 5. Mean firing rates for DOWN state and two UP sub-states. The bar plot shows SEM over data sets. It indicates that the DOWN state has a significantly lower firing rate than two UP sub-states. However, there is no significant difference between UP-1 and UP-2. (***= $p < 0.001$)

Secondly, by calculating the duration for all three states, we have tried to characterize these states based on the duration. According to the histogram of duration for three states, one can see that the DOWN duration is much shorter than the other two UP sub-states (Figure 6, three examples of three data sets, from three rats). Additionally, it suggests that UP-1 is significantly shorter than UP-2 (Figure 6, one example of one data set). By performing a statistical test on all of the data sets, the comparison of the medians of durations across all 10 data sets revealed that the DOWN state duration was significantly shorter than two UP sub-states. Also, it indicated that UP-2 duration was significantly shorter than UP-1 (multi-comparison test with Tukey-Kramer criterion: DOWN vs UP-1: $p = 3.41 \times 10^{-6}$, DOWN vs UP-2: $p = 0.0161$, UP-1 vs UP-2: $p = 0.0881$). Durations for DOWN states and two UP sub-states were calculated for all of the data sets (Figure 7).



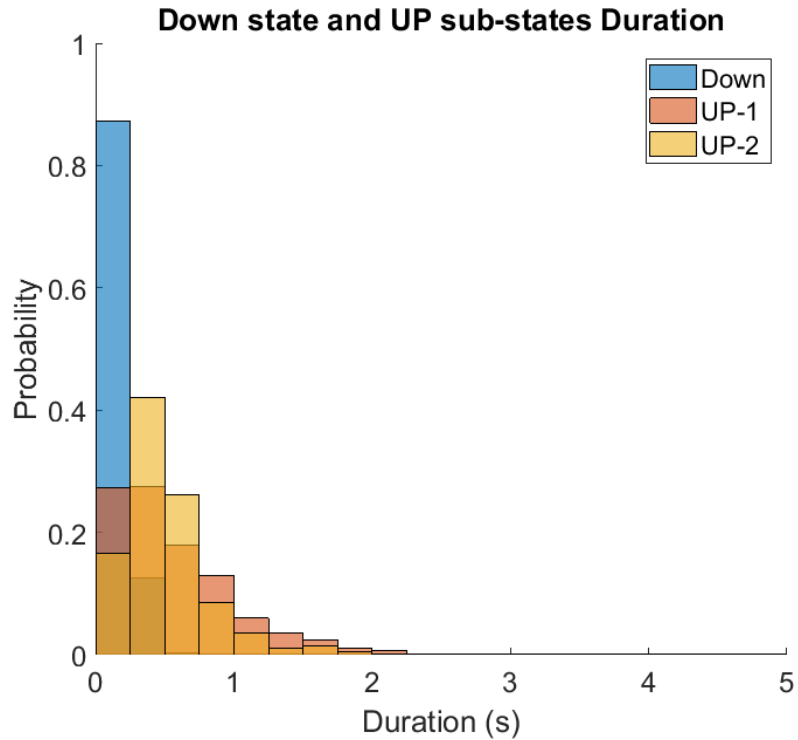


Figure 6. Distribution of duration for the three states detected by HMM. (Three examples from three rats.) It shows the distributions of duration for the DOWN states and two UP sub-states. Even though it demonstrates that the DOWN state has a much shorter duration in comparison to two UP sub-states, there is not a clear difference between the distribution of these two UP sub-states based on which we can distinguish the sub-states.

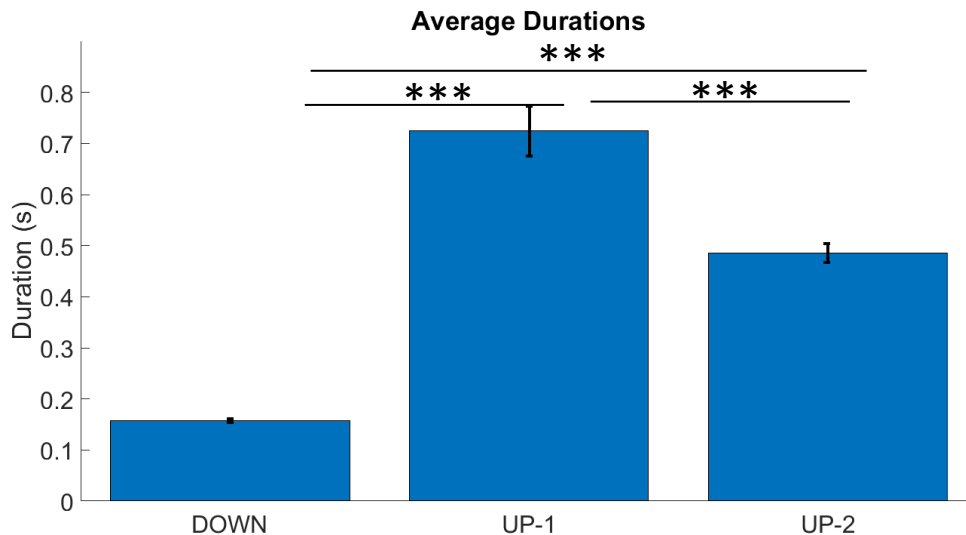


Figure 7. Durations for DOWN state and two UP sub-states. The bar plot shows SEM over data sets. It indicates that the DOWN state has a significantly lower firing rate than two UP sub-states. Additionally, UP-2 duration is significantly lower than UP-1. (***) = $p < 0.001$)

3.4. Using state vector decorrelation to characterize two UP sub-types

As with the firing rate, it was not possible to clearly distinguish the sub-states of UP, we have attempted to find another essential feature based on which we are able to characterize these states. As these sub-states could have different dynamics or different ways of changing the temporal activity, therefore, one important feature to distinguish them can be the state vector decorrelation. State vector decorrelation simply measures how fast the population vectors for these different sub-types decorrelate. In order to do that, first, for each event of UP-1, we made a population vector, where the firing rates of each individual neuron in each bin within the UP-1 event were calculated. Subsequently, we calculated the correlation coefficient between these population vectors to measure the temporal changes between them. More considerable changes in the adjacent population vector make vector decorrelation faster and vice versa. Then, to calculate state vector decorrelation for all of the UP-1 events, we averaged over all of the events of UP-1. Afterwards do the same process for UP-2.

As it is explained in detail in the method section, in order to reach the highest number of reactivation happening during motionless periods of sleep in each data set, we have tried different compression rates for template matching analysis, 1x to 10x. As a result, to be more consistent with the chosen compression rate in the template matching analysis, depending on the rate of it, we chose the associated bin size for this part of the analysis to make the population vector with the selected bin size. Different ranges of bin sizes between 10 ms-20 ms, for the range of compression rates between 5x-10x, have been used in the analysis. (For each data set, compression rates between 1x and 10x were explored and the one that had the most z-scored correlation peak values above 5 was

selected as the best compression rate.) Finally, we used the non-linear (exponential) function with a bias to fit the two averaged state vector decorrelation curve with it. The function we used is $y = a * \exp\left(-\frac{x}{\tau}\right) + c$, in which τ represents the rate of decorrelation.

Next after calculating the state-vector decorrelation for both of UP sub-states and for all of the data sets, we realized that there is always a considerable difference between their rates of decay. As an illustration, Figure 8 demonstrates that obviously one of the subtypes, UP-2, decorrelates much faster than the other, UP-1. Figure 9, which only includes the decorrelation rate for 1 second for both UP-1 and UP-2, shows the difference more clear. Here, one can see how much faster UP-2 is decorrelating than UP-2 for this data set.

Finding that it is also the same tendency for all of the other data sets indicates that there is always a clear difference between two UP sub-states decorrelation rates. To investigate whether there is a significant difference between the exponential time constants of UP-1 and UP-2 or not, the exponential time constants were averaged across all 10 data sets. This result is shown in Figure 10, which shows the average of τ for UP-1 is significantly higher than UP-2 (for UP-1 mean and sem are 153.3 ± 14.8 ms; and for UP-2 mean and sem are 87.7 ± 8.1 ms). Subsequently, by finding the state vector decorrelation, as the best parameter to distinguish the sub-states clearly, we call the sub-state with the slowly decay ‘UP-1’, and the one with fast decay ‘UP-2’.

By defining UP-1 as the state with slower vector decorrelation state and higher mean duration, and UP-2 as the faster vector decorrelation state and lower mean duration, we can associate the other features to these UP sub-states. Accordingly, in summary, UP-

2 has a relatively higher mean firing rate than UP-1 and has a lower variety in duration in comparison to the variability in UP-1 duration.

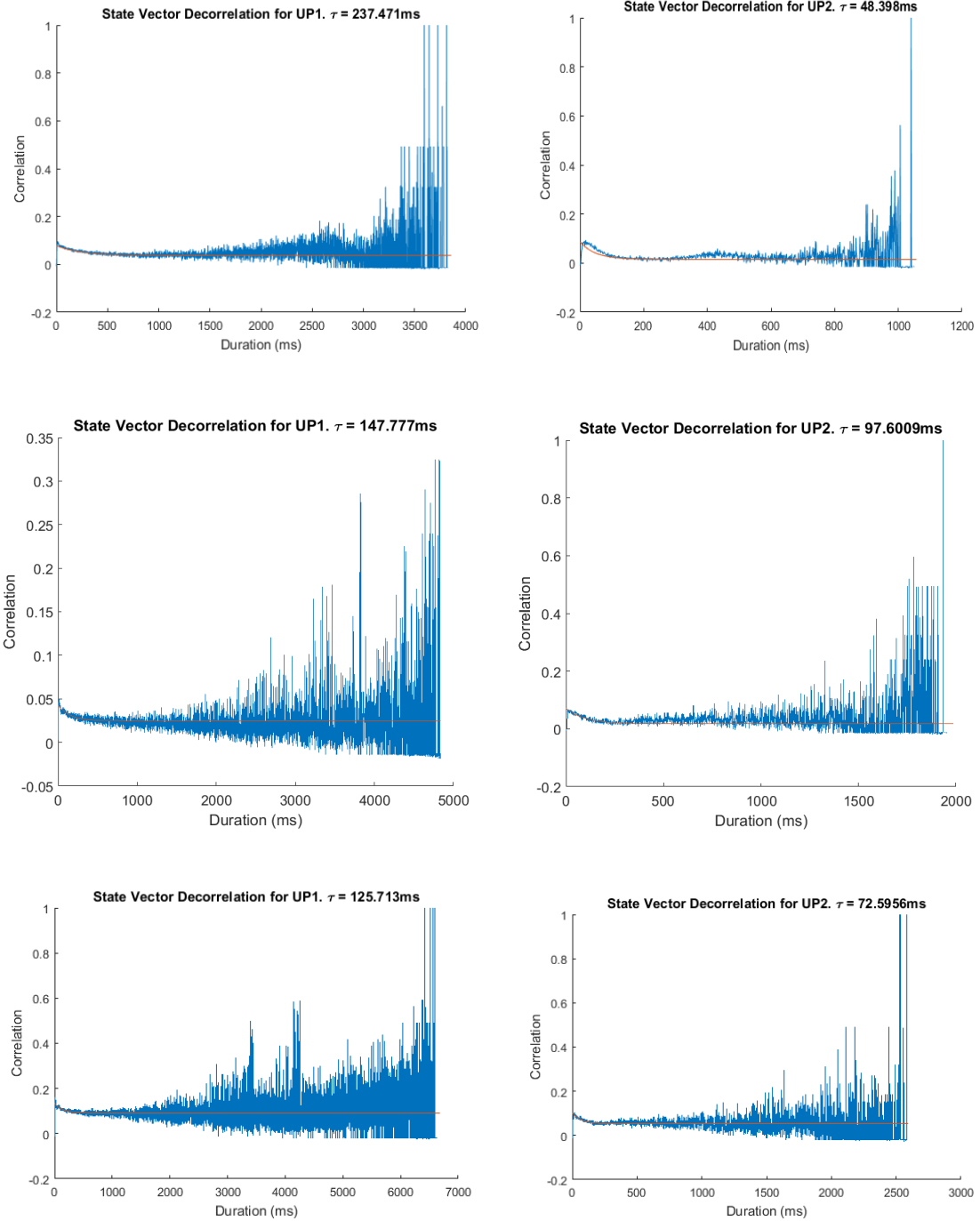


Figure 8. State vector decorrelation for UP-1 and UP-2, for three data sets (Three rats). The first data set on the top and the second in the middle and the third on the bottom. It demonstrates that these two state vectors have different rates and make it possible to characterize the UP sub-states based on them. The sub-state, which has a faster vector decorrelation, is called UP-2, and the one with slower decorrelation is called UP-1. Here, as the duration for different sub-states of UP are different, the scale of duration in the figures is different for them.

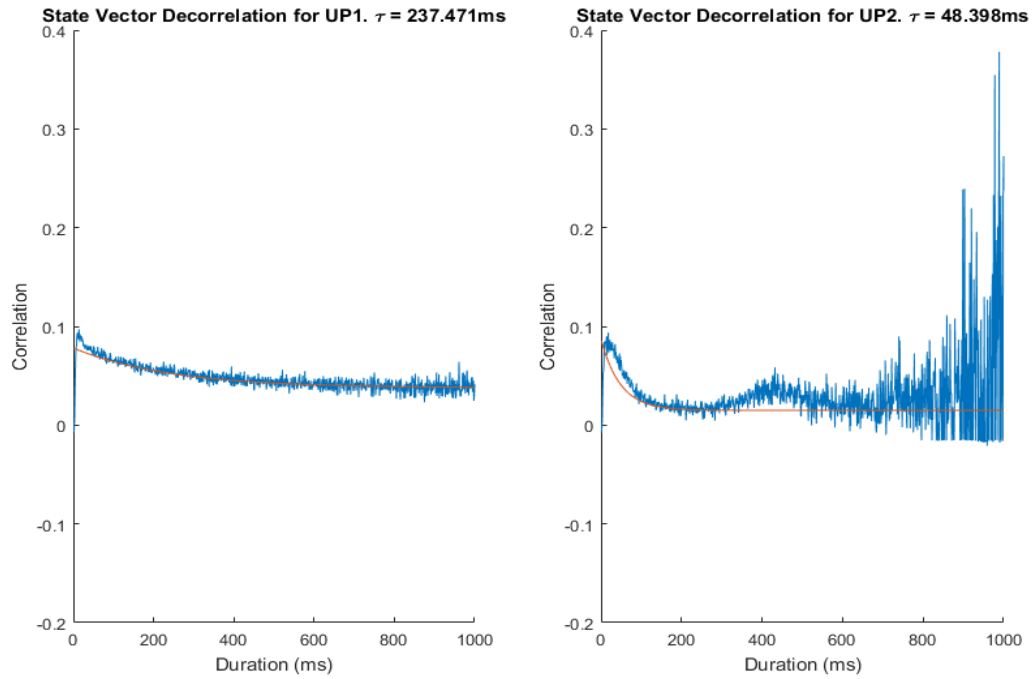


Figure 9. State vector decorrelation for UP-1 and UP-2. Here, we have the same example that was shown in the previous figure (top), using the same scale (1s).

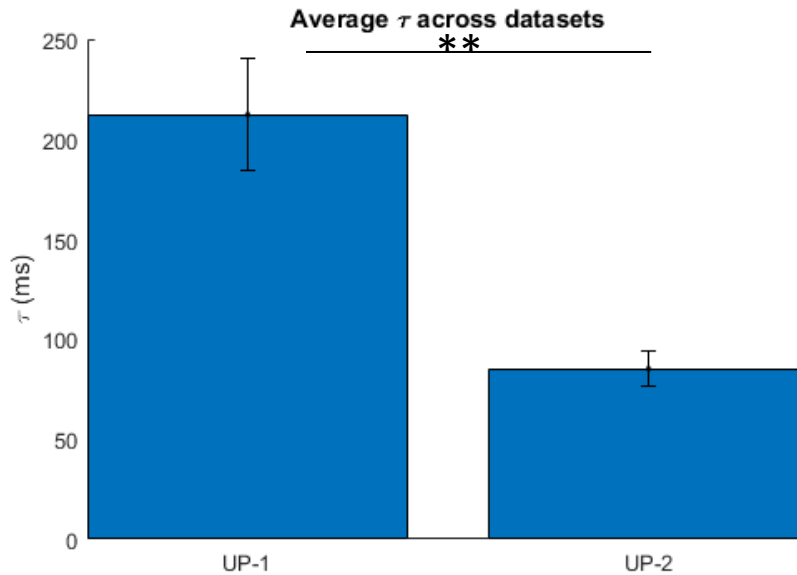


Figure 10. The average decay rates for UP-1 and UP-2, for all 10 data sets. This indicates that there is a significant difference in their decay rates, making the sub-states distinguishable by it. ($p = 0.002$)

3.5. UP-1 and UP-2 proportions

Our study suggests that one of the UP sub-states, UP-1, happens more frequently than the other sub-state, UP-2. So, in order to have a detailed view, initially the total time that UP state spent within each sub-state, UP-1 and UP-2, was measured, and finally the average for all data sets was found (Figure 11, left). The total duration of UP-1 was significantly longer than UP-2 (Mean and sem are 720.3 ± 88.9 sec ($78.1\% \pm 1.24\%$) for UP-1 vs. 201.5 ± 28.2 sec ($21.9\% \pm 1.24\%$) for UP-2, paired test t-test: $p = 4.1 \times 10^{-5}$). Also, we counted the total number of UP-1 and UP-2 in each data set and found the average for all data sets (Figure 11, right). Results indicate that UP-1 occurred significantly more than UP-2 (Mean and sem are $71.0 \pm 1.37\%$ for UP-1 vs. $29.0 \pm 1.37\%$ for UP-2, UP-1 and UP-2, paired t-test: $p = 1.2 \times 10^{-7}$).

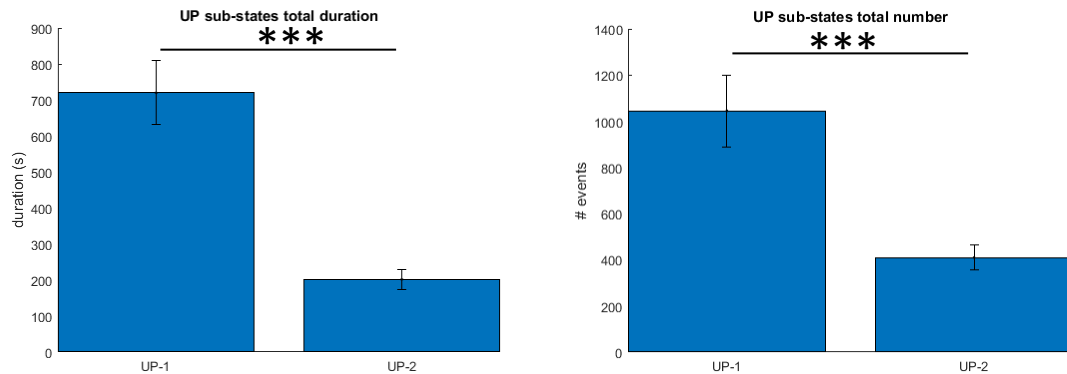


Figure 11. The proportion of happening for UP-1 and UP-2. Left: The proportion of happening for UP-1 and UP-2 in terms of their durations. Right: The proportion of the total event number for UP-1 and UP-2 happening in the UP states. (***) = $p < 0.001$)

3.6. Memory reactivation

Using template matching, we were able to find the reactivation number for different templates, as 6 to 8 templates regarding each segment of the sequence, and different compression factors regarding different compression rates, between 1 and 10, were generated. Thus, for each data set, different numbers of reactivation depending on template and compression rate, were assessed. Between these different templates and compression rates, the one which has the highest number of reactivation was selected. Consequently, based on the selected template and compression rate, all the timestamps where reactivation occurred were found. For our analysis, after finding the length of the reactivation, which depends on the bin size of the selected compression rate, we used the center of the template matching result for our further analysis. Also, the strength of reactivation was measured by the z-score method, in which a reactivation point with a z-score of 5 or higher can be considered as a strong reactivation, indicating a substantial similarity to the template. As a result, we used z-score of 5 and z-score of 6 for the following results, examples, and figures, etc. Figure 12 shows how reactivation points were detected. Firstly, the template for the specific data set during the task was made (fully described in the method section), and this template is shown in (Figure 12, top). The middle portion of this figure depicts one strong reactivation, in which the strength was measured by the z-score method. It is worth mentioning that this reactivation has a very high z-score and can be detected visually very well. However, as there are only a few z-score of 7 or higher, we used z-score 5 and 6 in our analysis to be able to contain more reactivation points in the analysis. There are not as strong as (Figure 12), but there are significant numbers of them, and they still can be detected visually. The bottom

portion in (Figure 12) shows the strong reactivation within the UP sub-state. The figure shows reactivation happens during the UP-2 sub-states, which is coloured by pink in the figure. The red line in the figure refers to z-score 7, indicating the detected reactivation is strong.

3.7. Memory reactivation mostly occurs in the UP-2

We discussed the features of UP sub-states and tried to characterize them based on these features. Furthermore, the other possible functional feature(s) of these two UP sub-states with which they can be distinguished from each other needs to be investigated. As a result, it is undoubtedly interesting to inquire whether the dynamics of these sub-states correlated with the occurrence of memory replay or not. Most interestingly, we found that memory reactivation occurring mostly in the fast decorrelated sub-type, UP-2, even though the UP-1 is the dominant UP sub-state and has a higher portion of UP states. Figure 13, left, shows the number of reactivation with z-score 5 happening during UP-1 and UP-2, respectively, for the data set 7165_11p. Figure 13, right, shows the same result but for z-score 6. It denotes that UP-2 is the sub-state containing the majority of reactivation for both z-score 5 and z-score 6, and interestingly the ratio of reactivation occurring in UP-2 is higher for z-score 6.

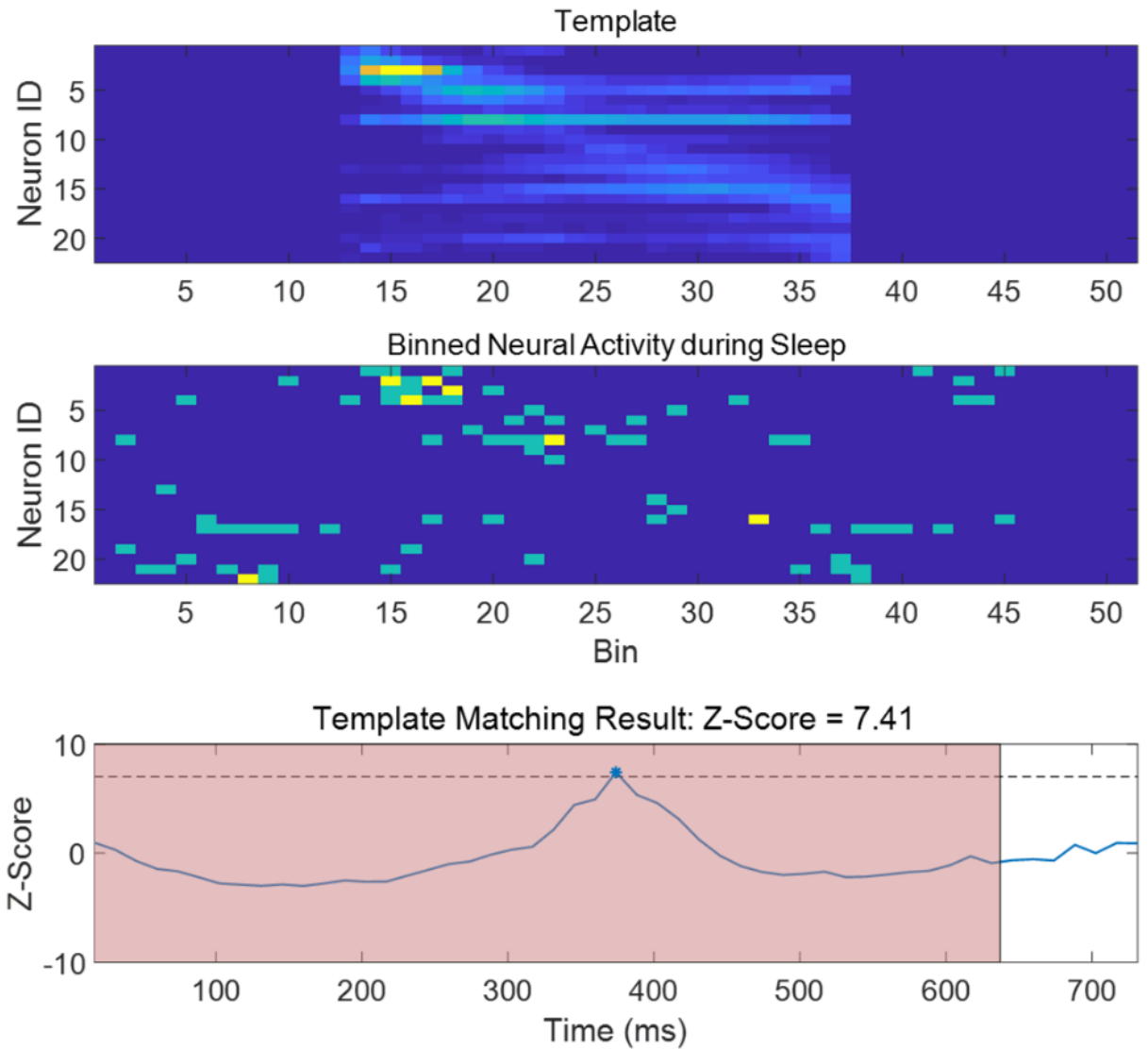


Figure 12. An example of the template matching method. The top figure shows the template, which was obtained by averaging across the activity from the task and for one segment of the sequence of one recording session. The middle figure shows one of the similar activities to the template, which happened during the post-task sleep. Here, by using a compression rate of seven, making the bin size seven times larger to be matched with the compression rate, a similar pattern to the template was found. The bottom figure is the corresponding z-score of the neural activity during sleep. The pink patch depicts UP-2, showing this pattern is occurring during the UP-2 and not UP-1.

The systematic investigation showed that it is the same tendency for all of the data sets regardless of the number of reactivation happening in the data set or the parameters

we used for template matching analysis such as compression factor and template number (Figure 14). The systematic investigation also indicated that by increasing template matching threshold, z-score, from 5 to 6, the ratio of replay happening in the UP-2 divided by the entire replay happening in the all UP states increases. More specifically, this ratio for the increase of z-score from 5 to 6 has increased from 91% to 94.5%. Considering the fact that the higher z-score replay is associated as a stronger reactivation of recent experience, we can conclude that UP-2 contains the more reliable replay more regularly. This makes this claim stronger that UP-2 has a particular dynamic, which basically correlated with the occurrence of replay and again suggests these sub-states are not spontaneously detected by HMM.

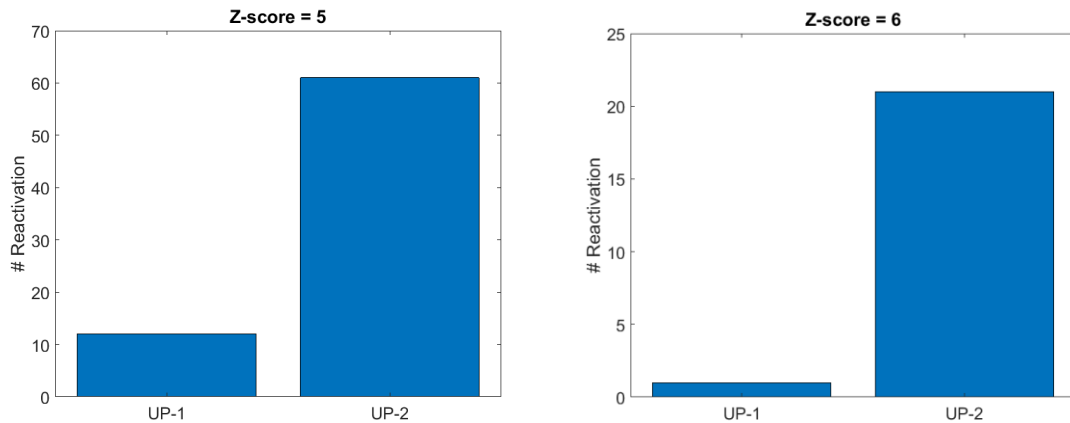


Figure 13. The number of reactivation occurs during UP-1 and UP-2. The left figure shows the number of memory reactivation, happening during UP-1 and UP-2, respectively, for z-score 5. It implies that the majority of reactivation points occur during UP-2 than Up-1. The right figure shows the same result but for z-score 6. It can clearly be seen that for z-score 6, UP-2 contains a higher percentage of reactivation in comparison to z-score 5.

It is worth mentioning that we also calculated the state vector decorrelation during tasks for all of the data sets in the very same way that we calculated it for the rest, except

this time we used the 100 ms bin size to calculate population vector decorrelation and obviously the compression rate of 1 was used. Then, we calculated the ratio between the exponential time constant for the task and for the UP-2 during the post-task sleep, τ_{task}/τ_{UP-2} . By averaging over all of the 10 data sets, we found that this ratio was between 4.1 and 12.7, with a mean of 7.5. These ratios suggest that the decorrelation rate during UP-2 is 7.5 times faster during the post-task sleep in comparison to the task. The ratio between the task and UP-1, τ_{task}/τ_{UP-1} , was between 1.8 and 7.1, with a mean of 4.5. These results confirmed that the compression rates we used for the template matching results are pretty similar to the ratio of exponential time constant between the task and UP-2, but not consistent with the task and UP-1. It again indicates that memory reactivation occurs predominantly in UP-2.

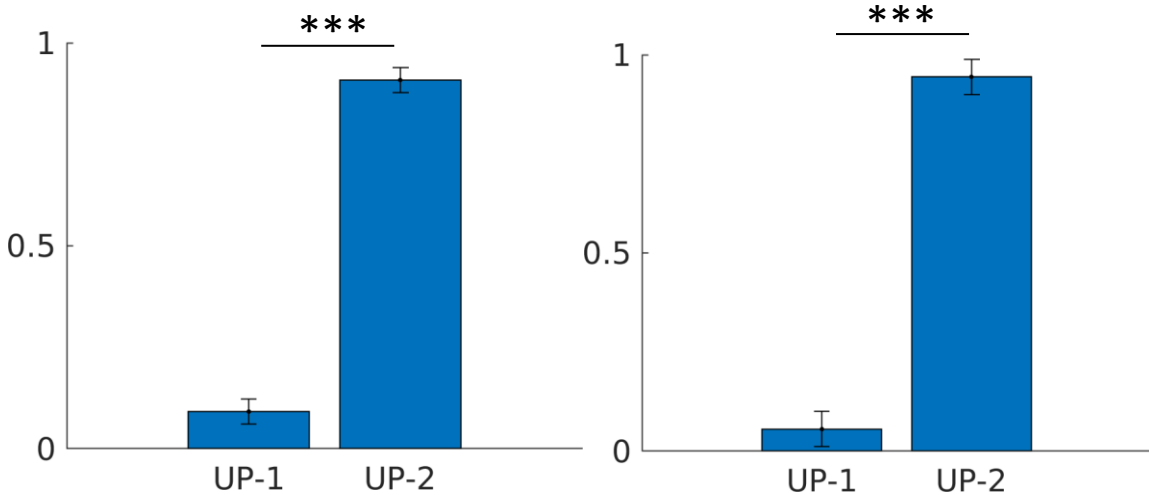


Figure 14. The average number of reactivation happens during the UP-1 and UP-2, across all data sets. The left figure shows the average number of reactivation of z-score 5 for all data sets. The right figure shows the same result but for z-score 6. It demonstrates that UP-2 contains the majority of reactivation for all data sets, and the proportion would be enhanced by increasing the z-score number from 5 to 6.

Also, for this experimental recording, previously, it has been shown (Euston et al., 2007) that replay in the post-task sleep was compressed 5-7 times in the medial prefrontal cortex (mPFC) of rat which is consistent with the decorrelation speed of the population vectors during UP-2.

3.8. Memory reactivation distribution in UP state and UP sub-states

In order to demonstrate how the reactivation points are distributed in UP state and, more importantly, in two sub-types of UP state, we used several approaches. For the first approach, firstly, we normalized all individual UP sub-state between 0 and 1 regardless of their durations and then divided each one to 10 bins (obviously the selected UP sub-state should be longer than 10 ms in this case). Subsequently, we tried to find during which of these ten bins the replay happened. Then, in the same manner, we calculated the total number of reactivation happening during these bins for all sub-types. Figure 15 shows how the memory reactivation distributed over the ten bins within each UP sub-state, UP-1 and UP-2, and then averaged across all data sets. As clearly can be seen (Figure 15), the majority of reactivation occurred during the UP-2; however, it is not clear that during which bin(s) of UP-2 reactivation tends to happen more. The main reason for showing reactivation distribution in this visualization was to find the phase preference(s) of them. Checking the results for all of the data sets indicates that reactivation tends to happen more during the first half of UP-2, and also more reactivation happens during the middle phases comparatively. In summary, we showed that memory reactivation tends to occur substantially more in UP-2, but it seems they do not have any specific preference within the UP-2 to occur at it the most.

The second approach that we used was sorting the UP state and also UP sub-states, UP-1 and UP-2, based on their duration. As it has shown in (Figure 16), we sorted all UP states based on their durations for one data set with stars showing the center of reactivation point with z-score 5. Also, the UP sub-types, UP-1 and UP-2, are shown in the figure with the blue and red colours, respectively. Based on this coloured figure, it is easy to understand that the UP-1, the blue colour in the figure, is the dominant UP sub-state. Figure 17 shows the same result for z-score 6. Using this method, we tried to investigate the relation between the duration of the UP state and the possibility of occurrence of reactivation in the UP state.

Also, with the same approach, we depicted the sorted UP-1, and UP-2 to investigate the sub-states correspondingly. Figure 18 and Figure 19 depict the sorted UP-1 and UP-2, respectively. Again, it indicates that UP-2 contains the majority of the replay. Also, it shows that UP-1 has more variety in terms of duration and a longer mean duration in comparison to UP-2.

In the last approach, we depicted the UP state and also UP sub-states based on their time of happening and in a chronological way. In this approach, we can investigate where reactivation tends to happen the most, at the early stage of rest, at the middle, or the end. Figure 20 and Figure 21 depict the chronological sorted UP-1 and UP-2, respectively. It seems there is no clear tendency based on this sorting to show which part of sleep reactivation tends to occur more.

In the following sections, we will use the term “reactivating” to reference any UP state event or sub-state event which contains the reactivation.

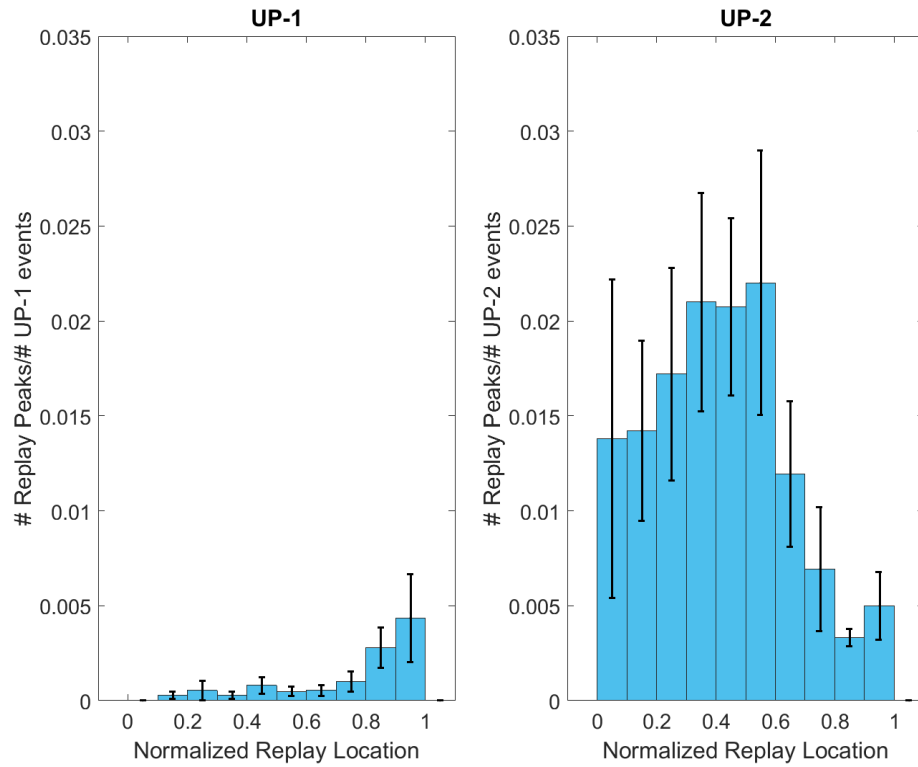


Figure 15. Distribution of reactivation for UP-1 and UP-2. Left figure: Here, firstly, each UP-1 event was divided into ten portions, and then for each bin, the number of reactivation happening within each bin across all UP-1 events was counted, and subsequently, it was divided by the total number of UP-1 event, and then averaged across all 10 data sets. Right figure: The same *procedure* was done for UP-2. Bar plots indicate the sem. These figures suggest that the majority of reactivation happens during UP-2. However, for this example, it seems reactivation tends to happen in the middle of UP-2 the most, suggesting there are no clear phase preferences in UP-2 for reactivation to happen at it mostly.

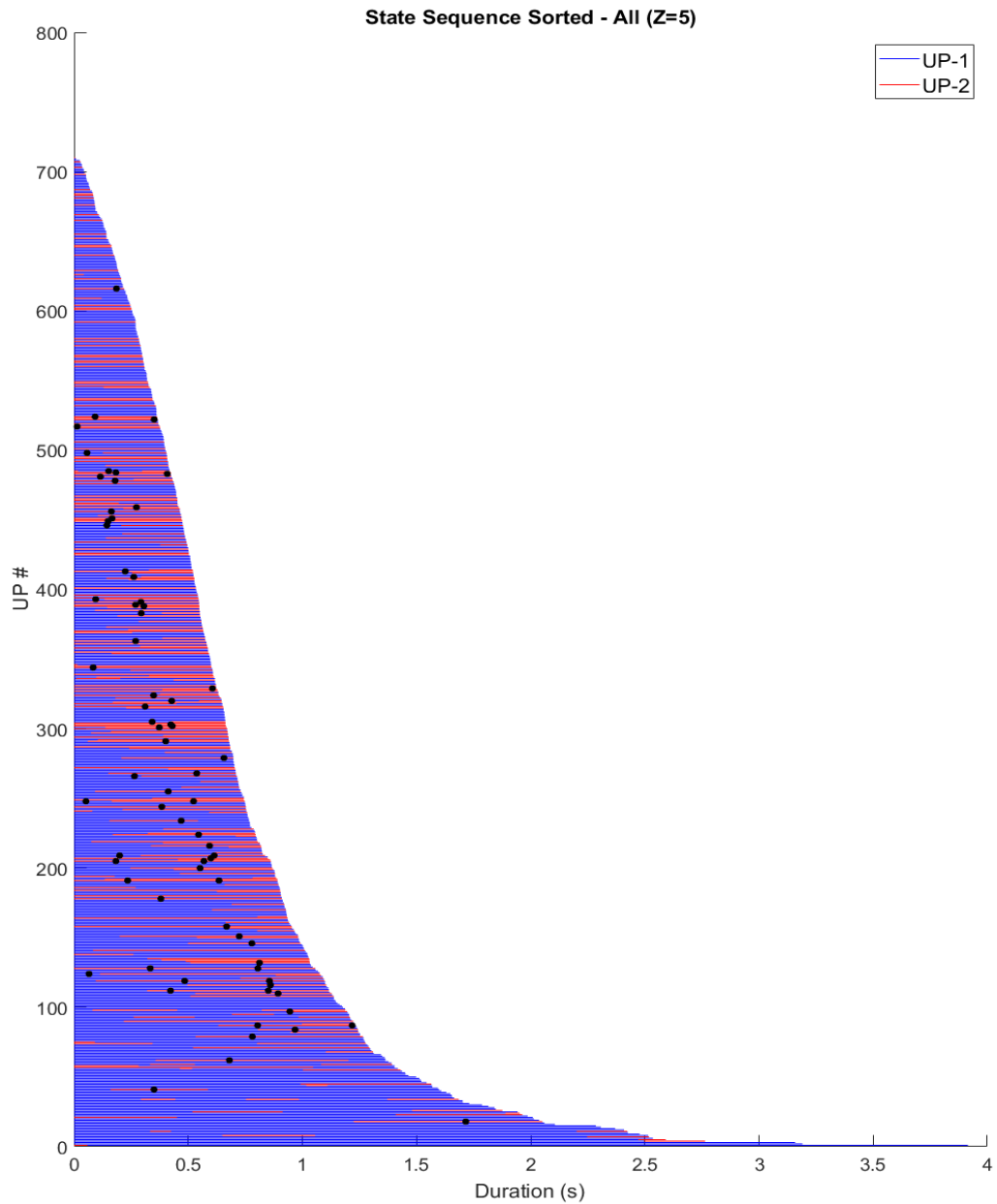


Figure 16. UP state, UP-1, UP-2 and reactivation ($Z=5$). Here, all UP states of one data set were sorted based on their duration, and then this figure was conducted. Also, different sub-state of UP, UP-1 and UP-2, has been shown in the figure by blue and red, respectively. Clearly, UP-1 is the dominant sub-state of UP, but UP-2 is the sub-state that contains the majority of reactivation. Here all reactivation of z-score 5 has been shown with the black dots.

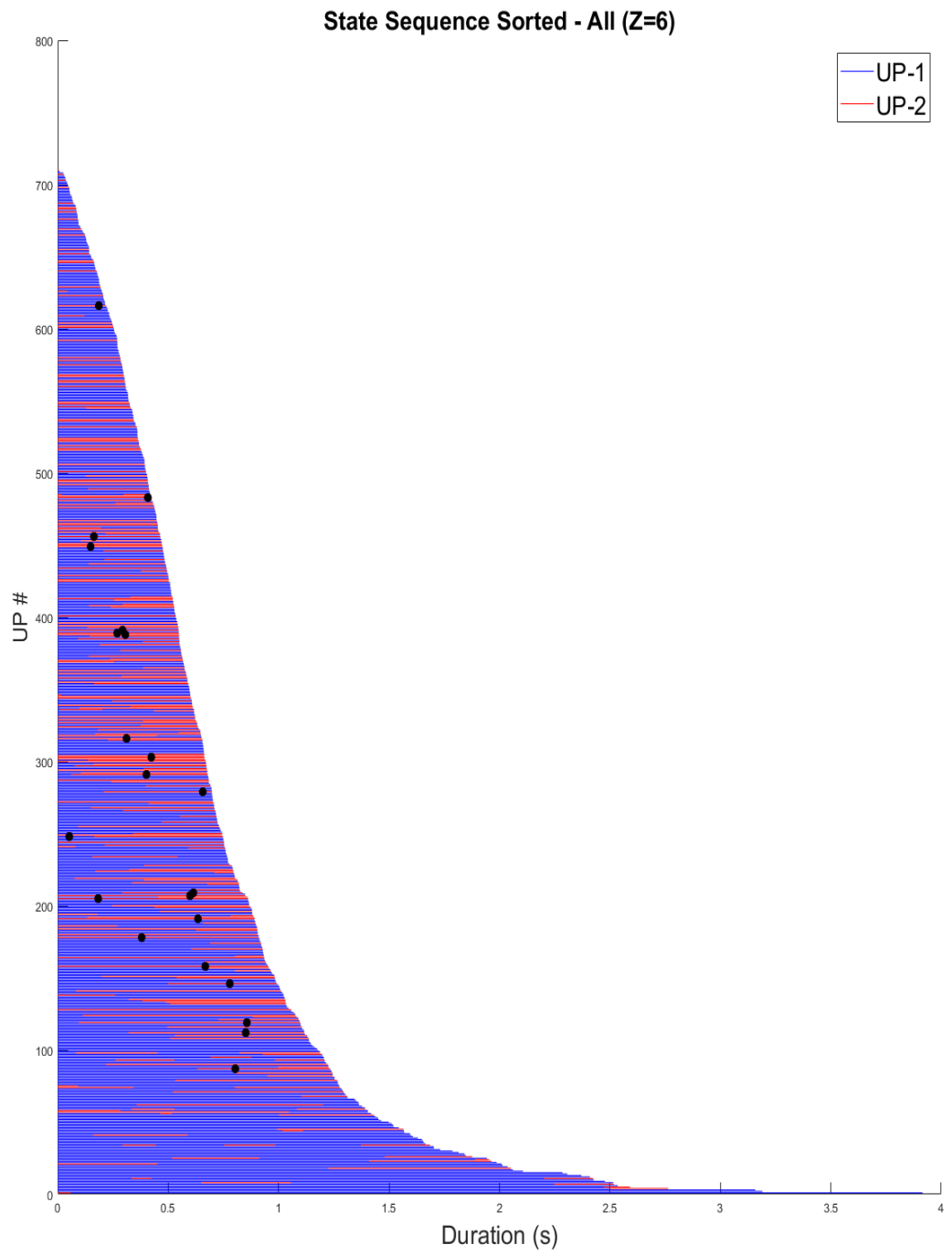


Figure 17. UP state, UP-1, UP-2 and reactivation ($Z=6$). Similar to (figure 14) but for reactivation with z-score 6.

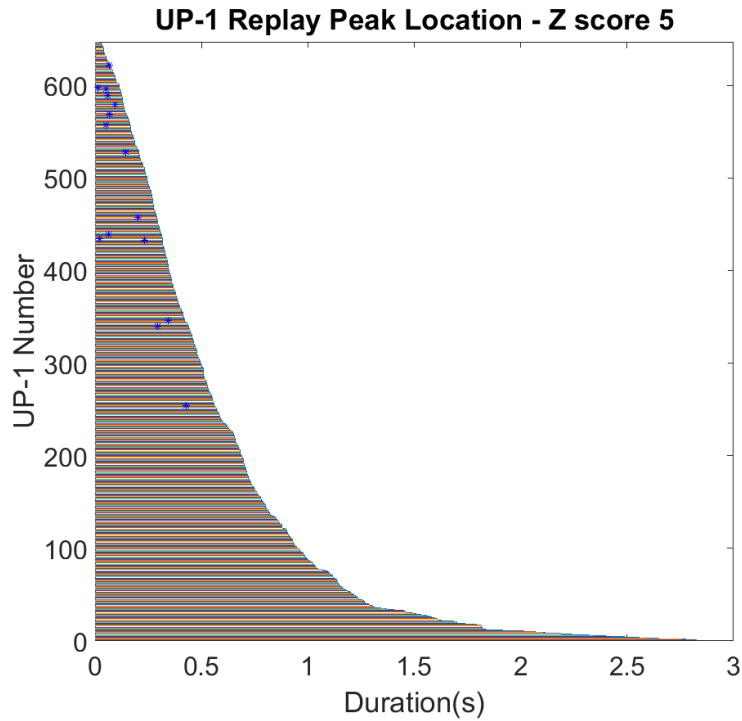


Figure 18. The representation of how reactivation happening during UP-1, sorted by duration. Here, all UP-1 sorted based on their durations. Blue stars indicate reactivation.

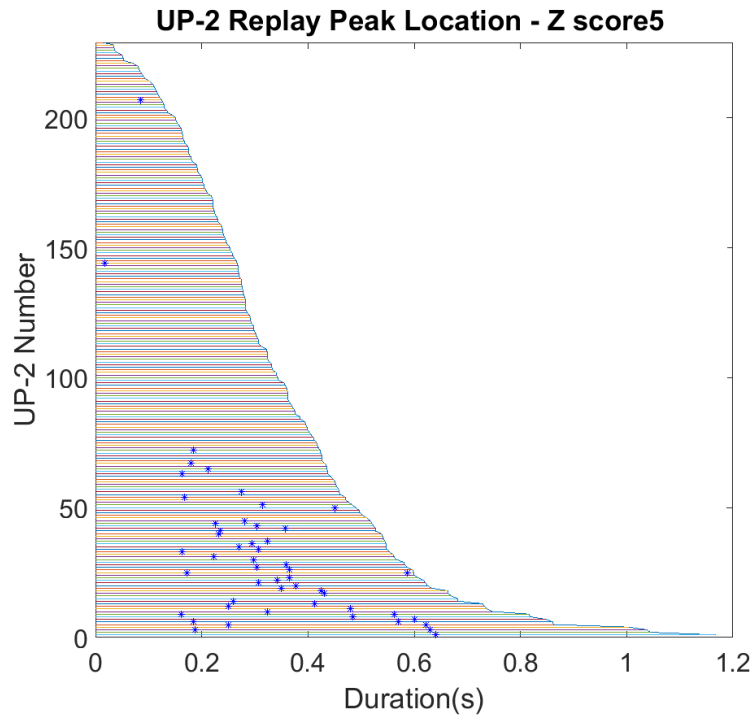


Figure 19. The representation of how reactivation happening during UP-2, sorted by duration. Here, all UP-2 sorted based on their durations. Blue stars indicate reactivation.

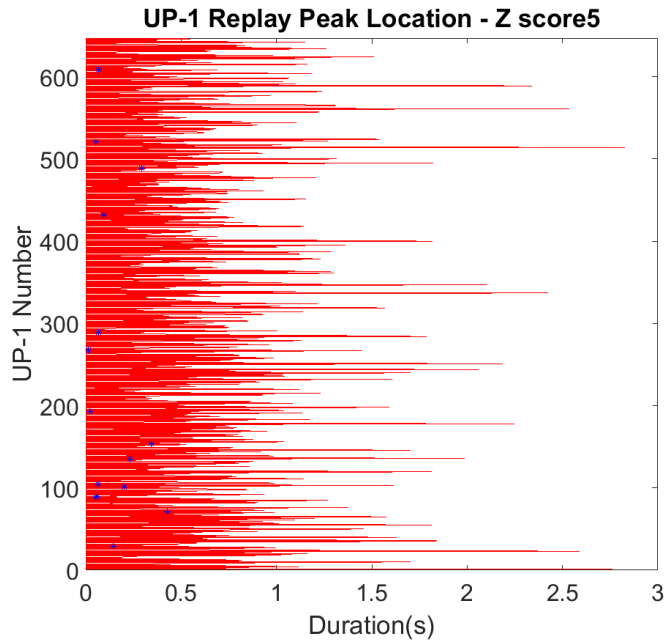


Figure 20. The representation of how reactivation happening during UP-1, sorted chronologically. Here, all UP-1 sorted by their time of happening. Blue stars indicate reactivation. In this way, one can study how reactivation distributed across the time of sleep.

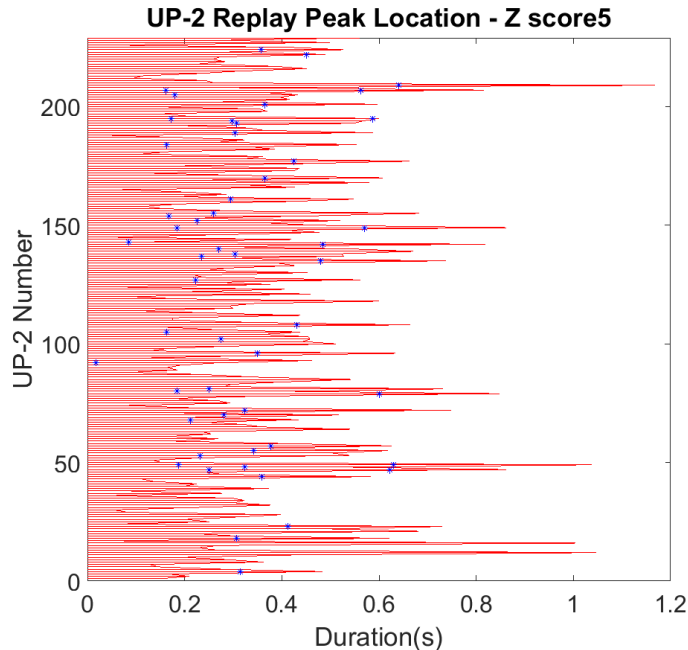


Figure 21. The representation of how reactivation happening during UP-2, sorted chronologically. Here, all UP-2 sorted by their time of happening. Blue stars indicate reactivation. In this way, one can study how reactivation distributed across the time of sleep.

3.9. Average firing rate of UP states within the UP state

It is also interesting to investigate the correspondence of firing rate within the UP state and the occurrence of memory reactivation in the UP state. To investigate it, initially, we divided all individual UP state event to 10 bin sizes, and then found the pertinent firing rates within the individual UP state event for each of these bins. Next, we averaged the result across all UP state events. Finally, we averaged the result across all 10 data sets. Figure 22, top, indicates that at the beginning and the end of UP states, the firing rate reaches the global and local maximum, respectively, and for the middle bins, the firing rate is lower in comparison. In Figure 22, the middle, we only calculated the firing rates for the reactivating UP states. Also, we calculated the firing rates within the only not-reactivating UP states (Figure 22, bottom). In general, these three figures show that firing rates within the UP states were influenced by the occurrence of reactivation. That influence is more apparent when it is compared with the occurrence of reactivation within the ten-binned UP states, which can be seen in (Figure 23). (Here, rather than considering the UP sub-states (Figure 15), we studied the UP state.) These two figures, Figure 22 & 23, suggest that the presence of reactivation within the ten-binned UP states can influence the firing rate of UP state in the same or adjacent bin(s), implying that the presence of reactivation can be mediated by an apparent increase in firing rates.

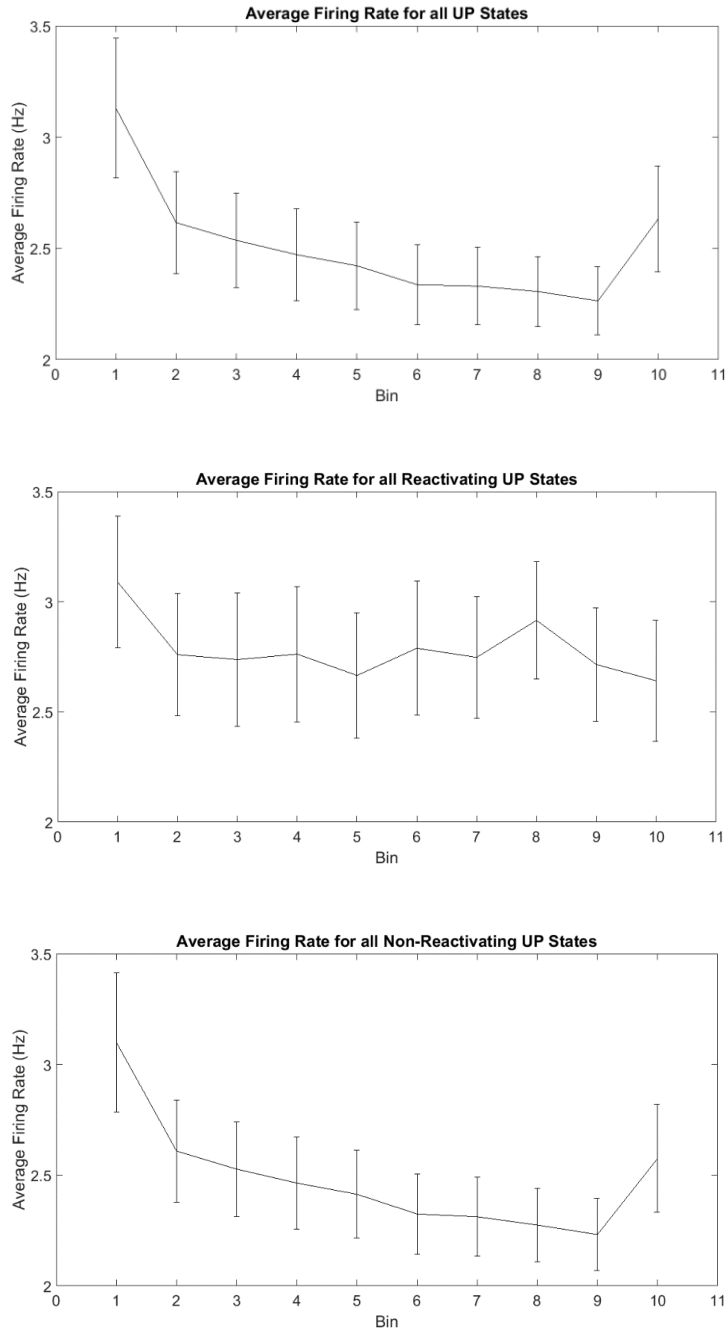


Figure 22. Average firing rates for the ten binned UP states. Top: All UP states were divided into ten bins, and the average firing rate for each portion (bin) was calculated then. Finally, it was averaged across all the data sets. This figure shows that there is a tendency in which the firing rate is higher at the start and end of each UP event. Middle: Here, only reactivating UP states were chosen, and the average firing rate for these selected UP states in each bin was calculated. Bottom: Here, only non-reactivating UP states were selected and the average firing rate was calculated across them. As a result, it suggests the presence of reactivation can affect the average firing rate within the UP state.

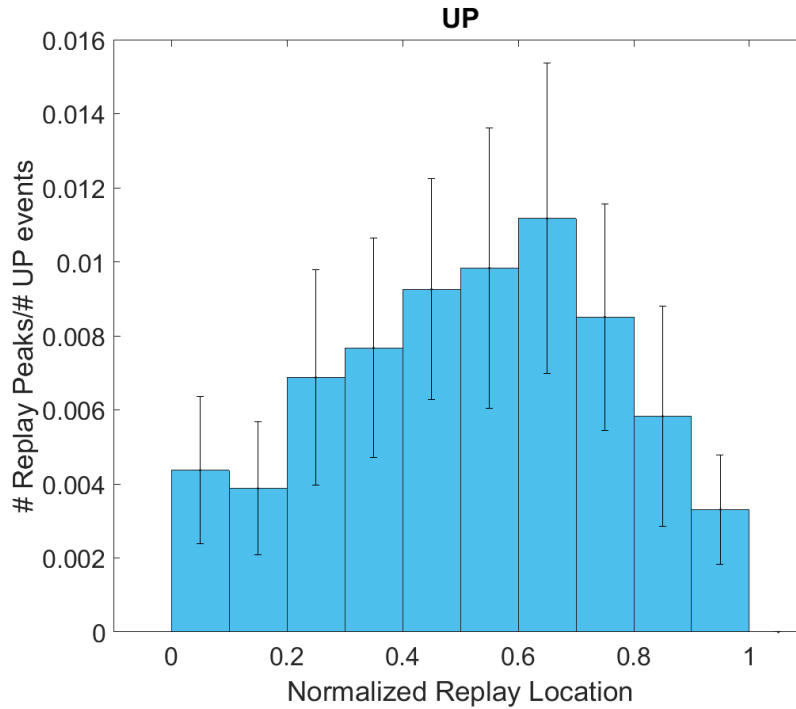


Figure 23. The comparison between the distribution of reactivation during the ten binned UP states. The figure shows the replay distribution for each bin within the UP state. By dividing each UP state to ten bins, and then finding the memory reactivation in each bin, subsequently averaging it across all UP states, and finally, by averaging across all 10 data sets, this figure is obtained. It can be observed that there is an increase in the firing rate in the middle bin sizes for reactivating UP states in comparison to all UP states, which is associated with the occurrence of reactivation distributed across different bins, especially middle bins, in the left figure.

3.10. Which type of sub-states, UP states tend to start and end with

As UP states are composed of UP-1 and UP-2, there are several cases that how UP states can be composed of these UP sub-states. For instance, it can be composed of only UP-1 or only UP-2 or start with one of them, then transit to another one and end with it. In order to investigate how the UP states are composed of sub-states, we used the approach of sorting UP state, then differentiated the UP-1 and UP-2 portion, which in (Figure 16) is coloured by blue and red lines within each UP state event, respectively.

Also, all of the reactivation has added to the figure and depicted by black dots. As the figure shows, by considering all UP states, the UP-1 is a dominant sub-state, and more importantly, the UP states tend to start and end with UP-1 than UP-2. Figure 24 shows the normalized result of starting and ending for UP sub-states for all data sets. More specifically, for each data set, we calculated the number of UP-1 and UP-2 with which the UP states start and end. Subsequently, as each data set has a very different number of UP state, we normalized the total number to 1 and then found the percentage of UP-1 and UP-2 the UP states start and end with. Finally, we averaged over all of the data sets.

In summary, Figure 24 depicts the average result for all 10 data sets when considering all UP states. According to the figure, UP states tend to start and end with UP-1 dominantly, which is reasonable as UP-1 is the dominant UP sub-state.

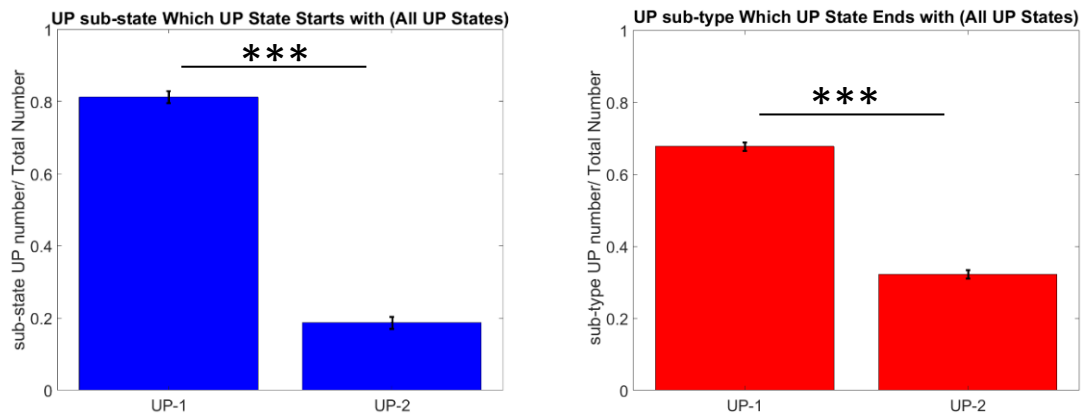


Figure 24. Which UP sub-state, UP states start and end with? Left: Considering all UP states, they tend to start with UP-1 than UP-2, which can be expected as the UP-1 is the dominant UP sub-state. Here all data sets were included, and the number of UP states in each data set was normalized to 1, and the proportion of UP-1 and UP-2, which UP states start with, were obtained. Right: Considering all UP states, they tend to end with UP-1 than UP-2. Here all data sets were included, and the number of UP states in each data set was normalized to 1, and the proportion of UP-1 and UP-2, which UP states end with, were obtained.

3.11. Which type of sub-states, reactivating UP states tend to start and end with

After surveying all UP states, we restricted the study to only reactivating UP states. Interestingly, our results suggest that the presence of reactivation changes the sequence of sub-types. In Figure 25, only the reactivating UP states with z-score 5 are included, and then they were sorted base on their duration. In general, this figure shows that even though reactivating UP state still has a tendency to start with UP-1, reactivating UP states tend to end with UP-2 than UP-1, despite the previous tendency for all UP states. Further investigations suggest that for the reactivating UP state, relatively short UP states are dominantly consist of UP-2. For the longer reactivating UP state, the UP state tends to start with UP-1 and then transit to UP-2 and end with it. This tendency is considerably different from the general UP state tendency, suggesting the presence of reactivation can affect the sequence of UP sub-states and also the dominance of the sub-state.

In Figure 26, only reactivating UP states with z-score 6 are used to investigate the sequence of sub-types for them. According to this figure, it can clearly be seen that the dominant sub-state is UP-2, which coloured as red. It is also clear that the majority of UP states start with UP-2, and all UP states end with UP-1. This figure suggests that for stronger reactivation, the influence of them on the sequence of UP sub-types is more considerable, and it makes the assumption that the sequence of sub-states is effected by reactivation more reliable.

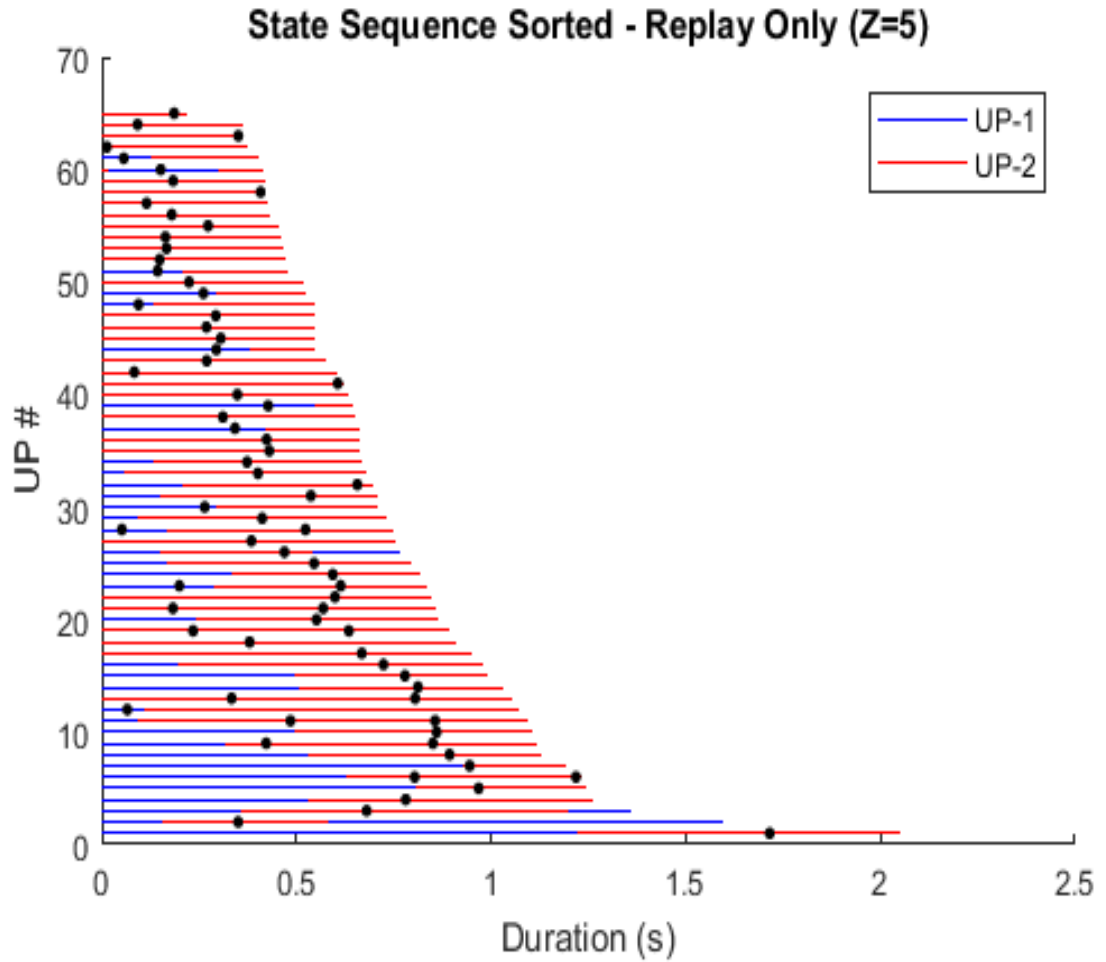


Figure 25. The representation of reactivating UP states with z-score 5. All the reactivating UP states were selected and then sorted based on their duration. Although for all UP states, UP-1 is the dominant UP sub-state, by considering reactivating UP states, UP-2 is the dominant UP sub-type. It demonstrates that with which sub-states, reactivating UP states start and end. This tendency seems to be different in comparison to all UP states.

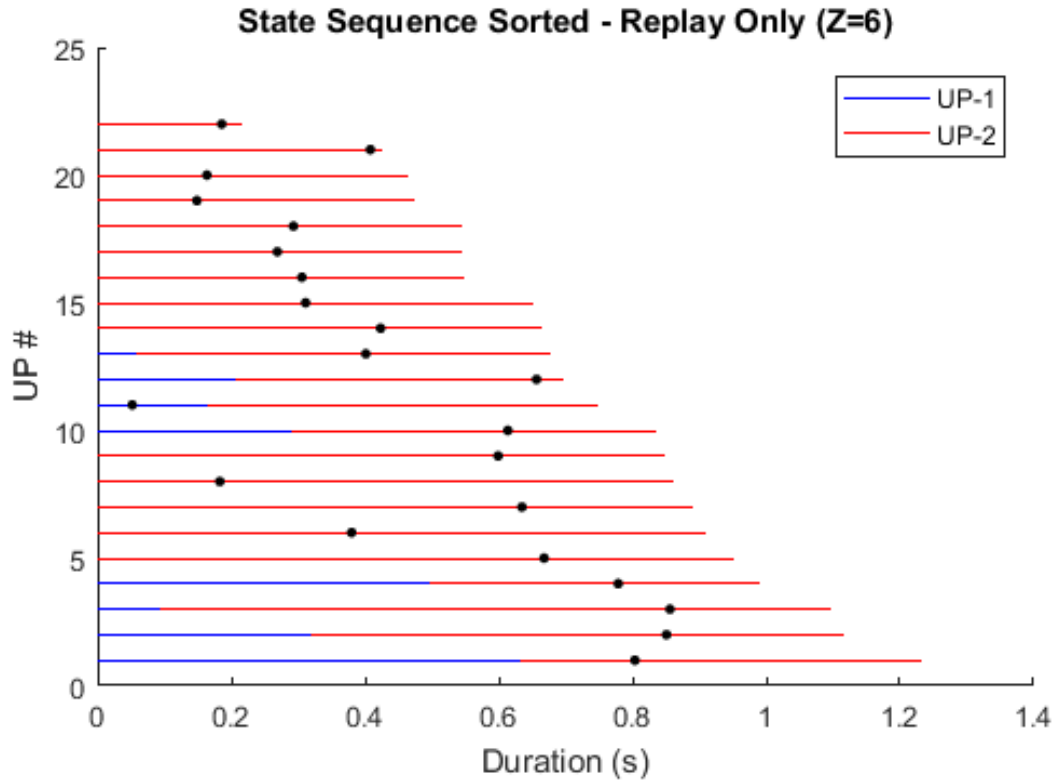


Figure 26. The representation of reactivating UP states with z-score 6. An example of reactivating UP states for z-score 6, which were sorted based on their duration. Clearly, now UP-2 is the dominant UP sub-state and UP states start and end with it dominantly.

To quantify it more systematically, we divided the reactivating UP states for each data set into two groups, so-called short and long UP states. In order to divide UP state into two short and long groups, because the average duration of reactivating UP state is different among different data sets, we used a range of thresholds of 580-1250 ms to have roughly the same number in both samples of short and long UP states. Consequently, we found that for short reactivating UP state as it is shown in Figure 27, they mostly start and end with UP-2 (Start (Figure 27, left): for UP-1 mean and sem are 0.3321 ± 0.0369 ; for UP-2 mean and sem are 0.6679 ± 0.0369 , End (Figure 27, right): for UP-1 mean and sem are 0.0520 ± 0.0186 ; for UP-2 mean and sem are 0.948 ± 0.0186). On the other hand, the

long reactivating UP states tend to start with UP-1 and predominantly end with UP-2, as can be seen in Figure 28 (Start (Figure 28, left): for UP-1 mean and sem are 0.682 ± 0.0366 ; for UP-2 mean and sem are 0.318 ± 0.0366 , End (Figure 28, right): for UP-1 mean and sem are 0.143 ± 0.0381 ; for UP-2 mean and sem are 0.857 ± 0.0381).

In summary, these results indicate that in general, UP state is composed of different sequences of UP sub-types, which can be affected by the duration of UP state itself and the presence of memory reactivation of recent experience.

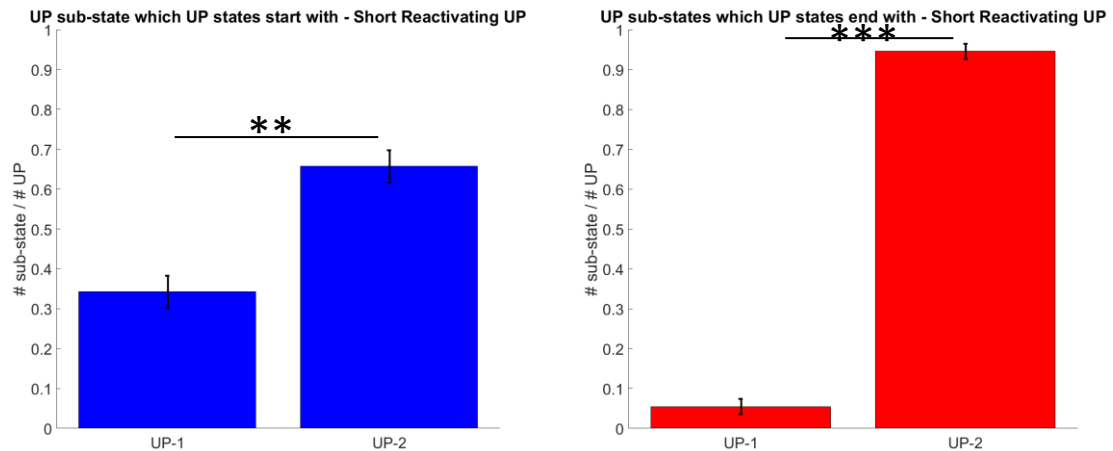


Figure 27. How short reactivating UP states start and end. Left: This figure shows the tendency for the short reactivated UP states, in which they tend to start with UP-2 than UP-1, which is in contrast with the general tendency for all UP states. Right: This figure indicates that short reactivated UP states strongly tend to end with UP-2 than UP-1, which again is not the case for all UP states.

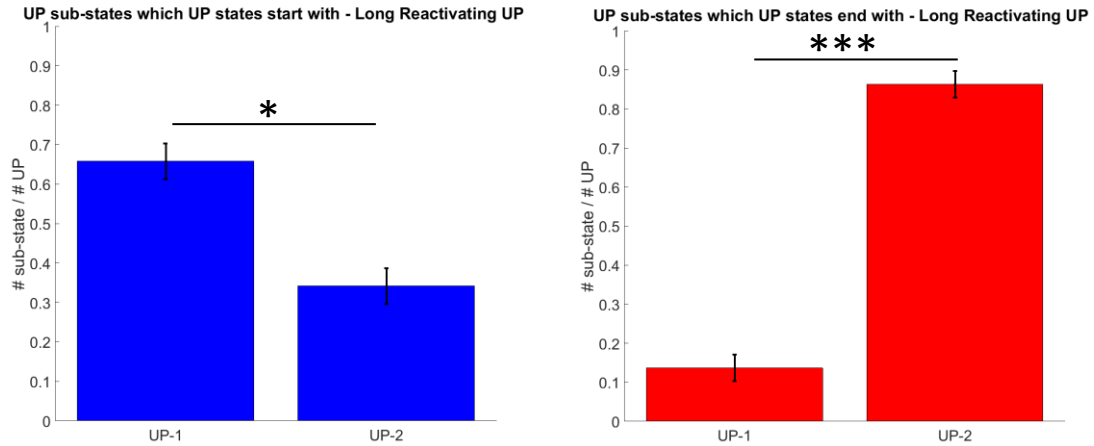


Figure 28. How long reactivating UP states start and end. Left: The figure shows that long reactivated UP states tend to start with UP-1 than UP-2, which is similar to the case for all UP states. Right: The figure indicates that long reactivating UP states still tend to end with UP-2 than UP-1, which is in contrast with the tendency for all UP states.

We also quantified this tendency more by dividing the Non-reactivating UP states into two groups, short and long UP states. Using the same duration threshold of 580-1250 ms, which were used previously for reactivating UP state, the non-reactivating UP states were categorized into short and long durations groups. Short non-reactivating UP states tend to start and end with UP-1, similar to the general tendency of UP states (Start (Figure 29, left): for UP-1 mean and sem are 0.798 ± 0.0134 ; for UP-2 mean and sem are 0.202 ± 0.0134 , End (Figure 29, right): for UP-1 mean and sem are 0.730 ± 0.0143 ; for UP-2 mean and sem are 0.271 ± 0.0143). Long non-reactivating UP states also tend to start and end with UP-1 than UP-2 (Start (Figure 30, left): for UP-1 mean and sem are 0.904 ± 0.0096 ; for UP-2 mean and sem are 0.096 ± 0.0096 , End (Figure 30, right): for UP-1 mean and sem are 0.741 ± 0.0244 ; for UP-2 mean and sem are 0.259 ± 0.0244). These results also indicate that the presence of reactivation can change the dynamic of UP states and how it consists of sub-states considerably.

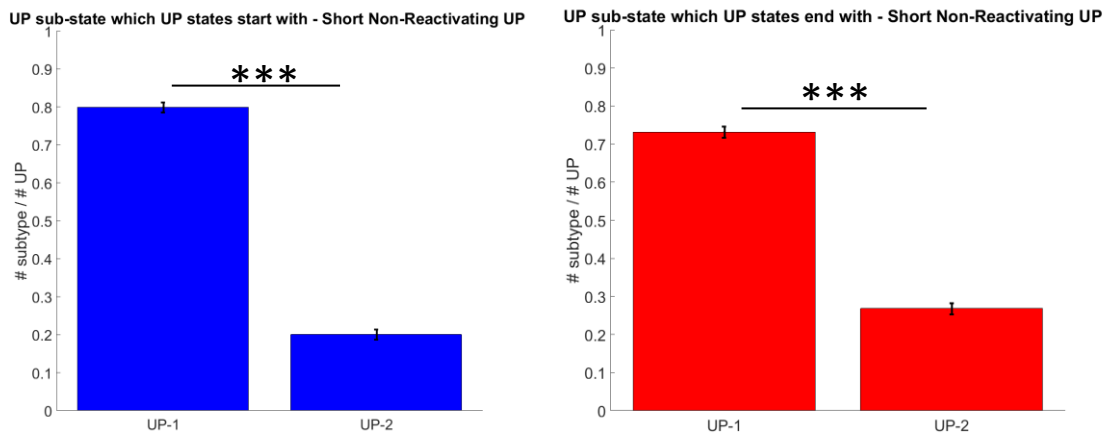


Figure 29. How short non-reactivating UP states start and end. Left: This figure shows the tendency for the short non-reactivated UP states, in which they tend to start with UP-1 than UP-2, similar to the general tendency for all UP states. Right: This figure indicates that short reactivated UP states strongly tend to end with UP-1 than UP-2, which again is similar to all UP states.

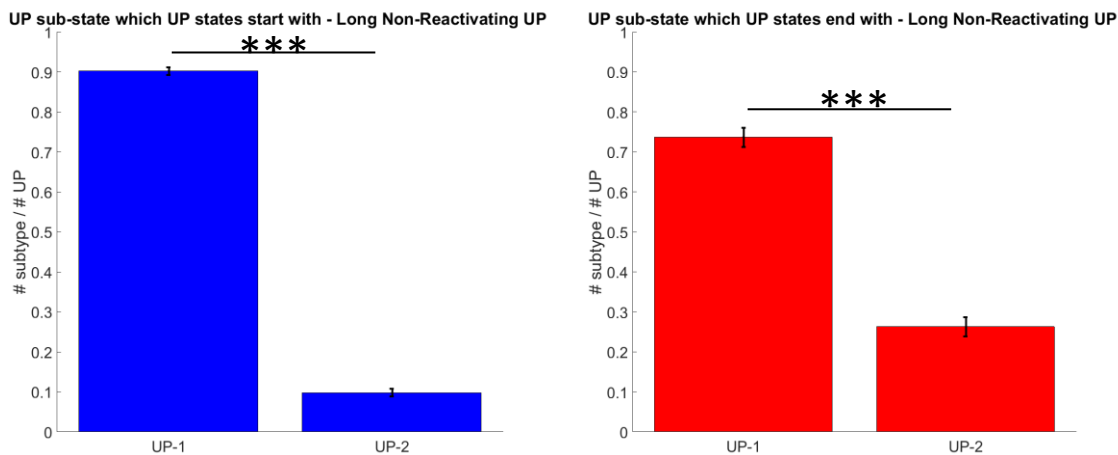


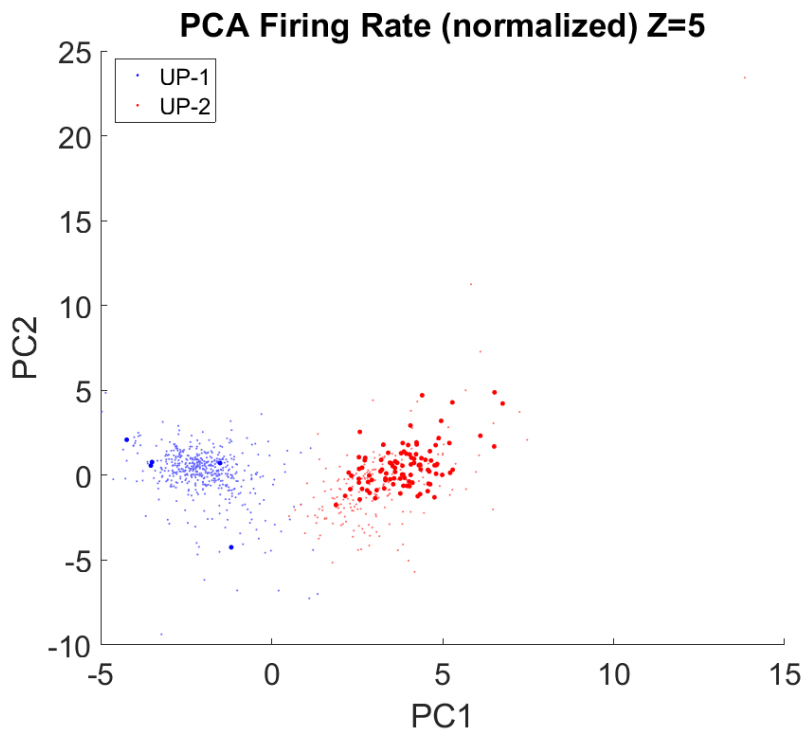
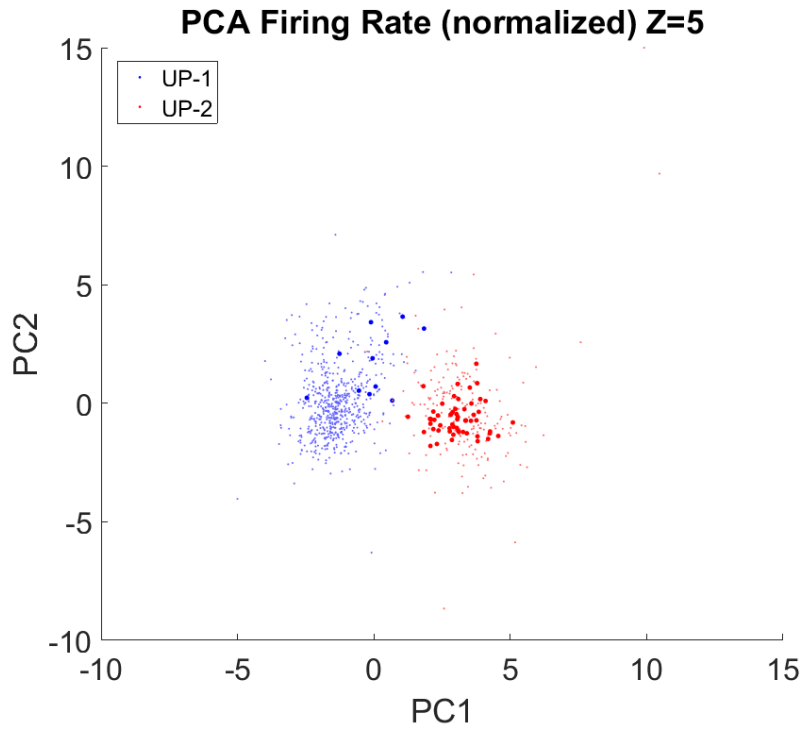
Figure 30. How long non-reactivating UP states start and end. Left: The figure shows that long non-reactivated UP states tend to start with UP-1 than UP-2, which is similar to the case for all UP states. Right: The figure indicates that long reactivating UP states still tend to end with UP-1 than UP-2, again similar to the all UP states.

3.12. UP sub-states were clustered distinctively by PCA and tSNE

Another principal feature that can be investigated regarding UP sub-states characteristics is whether they are distinctively separated or not. In order to explore that, we projected our data points to some dimensional reduction methods amongst which we found PCA and tSNE as the best methods to perform the analysis.

Firstly, we converted the individual sub-state events to the normalized firing rate vectors of neural activity. For the N-dimension vector in firing rates representation, the mean firing rate for each neuron during the sub-state event was found. Subsequently, neuron-wise standardization was performed using the mean and standard deviation of each neuron firing rate. Then, we projected all sub-states event, both UP-1 and UP-2, to the PCA and tSNE representation. Figure 31 shows the PCA results for normalized firing rates of post-task rest for three data sets, 7165_11p, 7165_36, and 8482_15p. These figures suggest that in the first and second principal component analysis, UP-1 and UP-2 were clustered distinctively.

Figure 32 shows the firing rate projection but in the tSNE method. It denotes that UP-1 and UP-2 were distinctly clustered by tSNE as well. These results are consistent for the post-task sleep of all data sets.



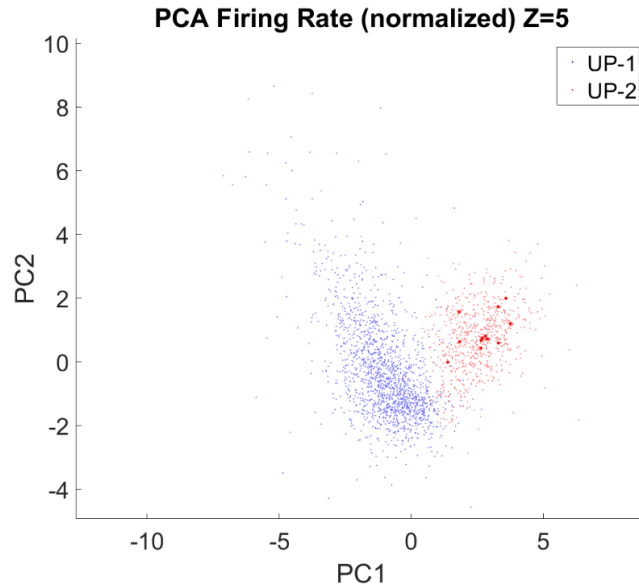


Figure 31. PCA analysis for UP sub-states, UP-1 and UP-2, for post-task sleep. Here we used normalized firing rate vector representation, in which each neuron was represented by its normalized firing rate during the UP state event. For these three examples of three different data sets, it can be seen that UP-1 and UP-2 were clustered distinctly by PCA.

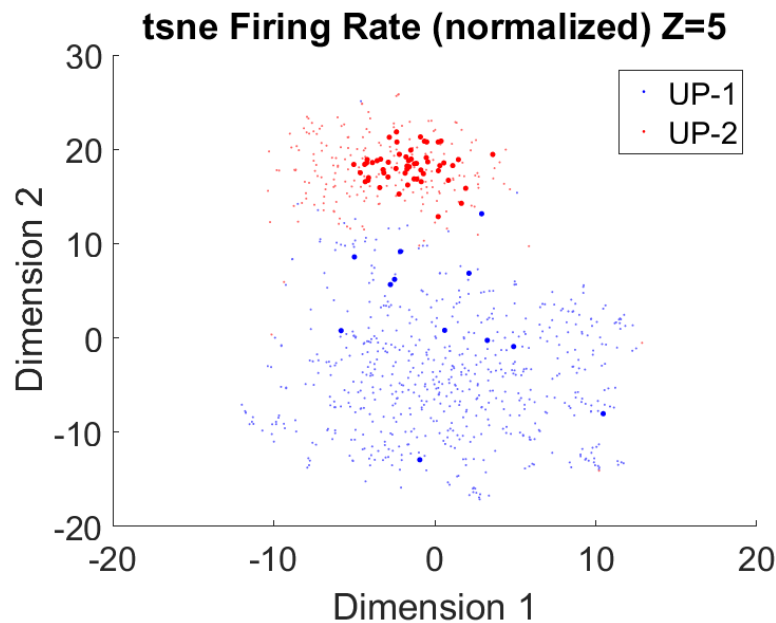


Figure 32. tSNE firing rate analysis for UP sub-states, UP-1 and UP-2, for post-task sleep. Here we used firing rate vector representation, in which each neuron was represented by its firing rate during the UP state event. It demonstrates that UP-1 and UP-2 were clustered distinctly by tSNE. It is the equivalent tSNE analysis for the first PCA result (Last page, top Figure)

3.13. Pre-task sleep analysis in comparison to post-task sleep

A three-state HMM was also applied to the pre-task sleep. We used 10 data sets in this project and analyzed the post-task sleep for all of them in detail. But, we only found 5 pre-task sleep data sets having good quality motionless sleep and were usable in the pre-task sleep analysis. By doing the same procedure for the pre-task sleep, we can distinguish the differences between UP sub-states before and after the task. Consequently, the effect of the task experience on the UP sub-states can be studied. The results suggest that the three-state HMM successfully separated the DOWN and two UP sub-states, as their firing rates and duration are shown in Figure 33 and Figure 34.

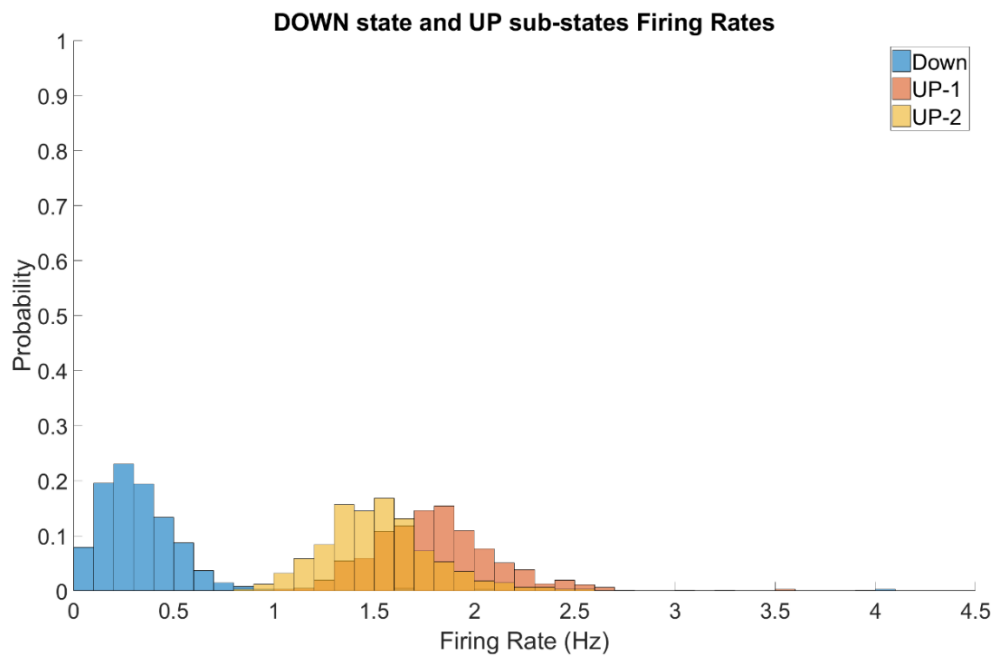


Figure 33. Firing rates distribution of DOWN, UP-1, and UP-2, for pre-task sleep. Using the three-state HMM, three different states were separated, which their firing rates are shown in the figure.

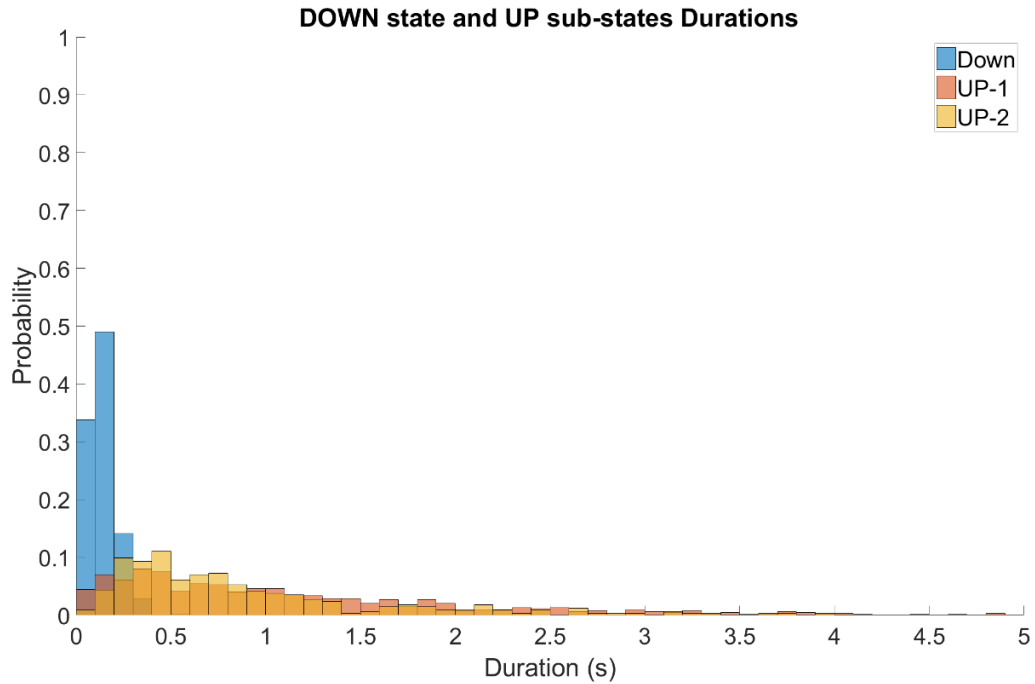


Figure 34. Duration distribution of DOWN, UP-1, and UP-2, for pre-task sleep. Using the three-state HMM, three different states were separated, which their durations are shown in the figure.

For the state vector decorrelation, as Figure 35 suggests there is still a difference between the decorrelation rates for UP-1 and UP-2.

Also, using PCA analysis, the separation between UP-1 and UP-2 is shown for three examples of three data sets (Figure 36, Figure 37, and Figure 38). This figure suggests that the cluster separation is not as distinguished as post-task sleep. Using the same clustering method (Jean-Marc method (Fellous, et al., 2004)), we can measure the cluster strength, which for this data set, the cluster strength is 1.34 and 2.89 for sleep1 and sleep3, respectively. Also, by doing stats for the five data sets that both pre-task and post-task sleeps were used in the analysis, Figure 39 is obtained. (Sleep1_mean = 1.95, Sleep1_sem = 0.54; Sleep3_mean = 2.54, Sleep3_sem = 0.24).

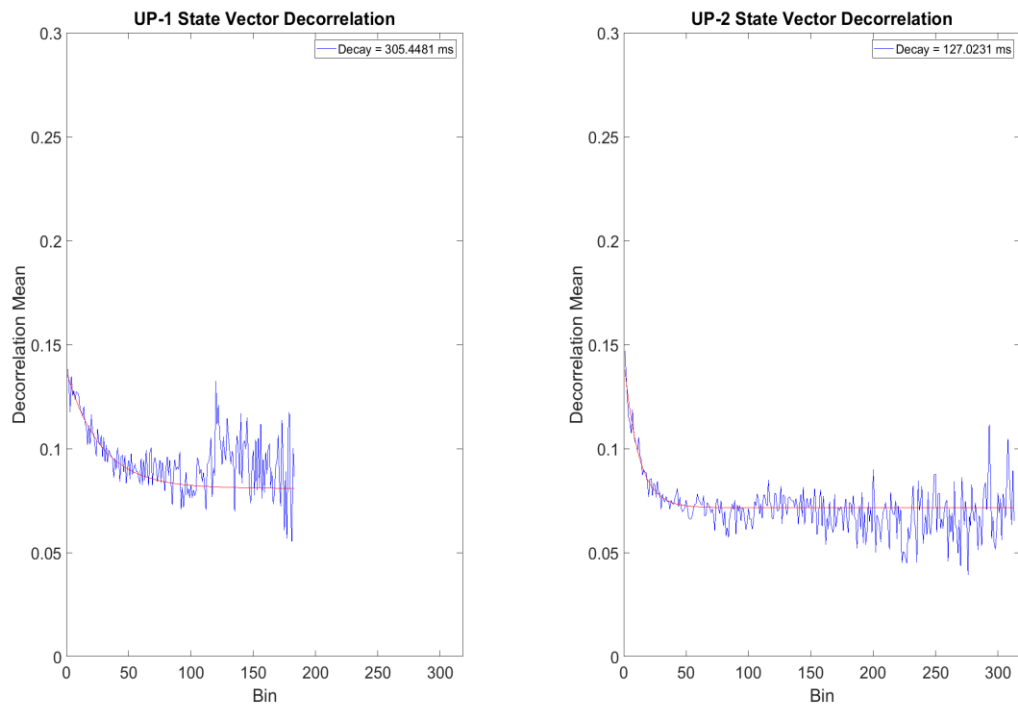


Figure 35. State vector decorrelation of UP-1 and UP-2, for pre-task sleep. Similar to the post-task sleep, one of the UP sub-state has a faster vector decorrelation, which again is called UP-2.

Table 2. The exponential time constant, τ , for UP-1 and UP-2, for pre-task sleep.

Data set	UP-1 Decay Constant (ms)	UP-2 Decay Constant (ms)
1 (Rat1)	305.45	127.02
2 (Rat2)	450.07	250.30
3 (Rat2)	374.10	103.10
4 (Rat3)	289.64	180.73
5 (Rat3)	561.49	384.33

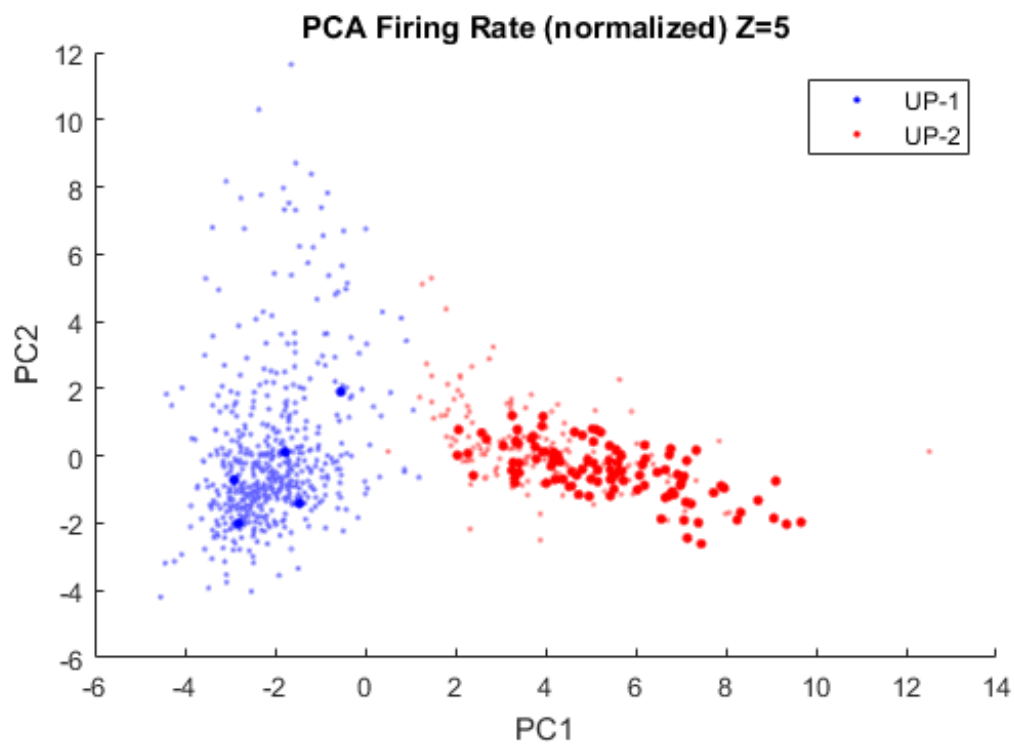
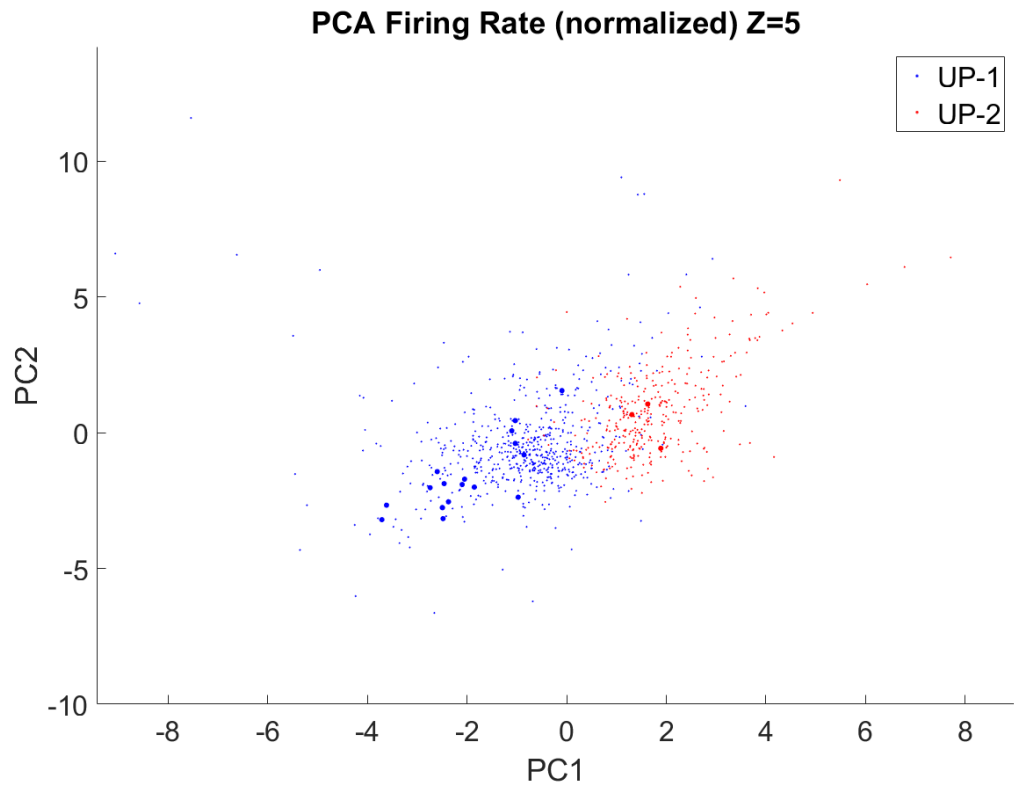


Figure 36. Comparison of PCA analysis for pre-task and post-task sleep. Top: PCA analysis for pre-task sleep showing that UP-1 and UP-2 are not clustered as well as post-task sleep. Bottom: post-task PCA analysis for the same recording.

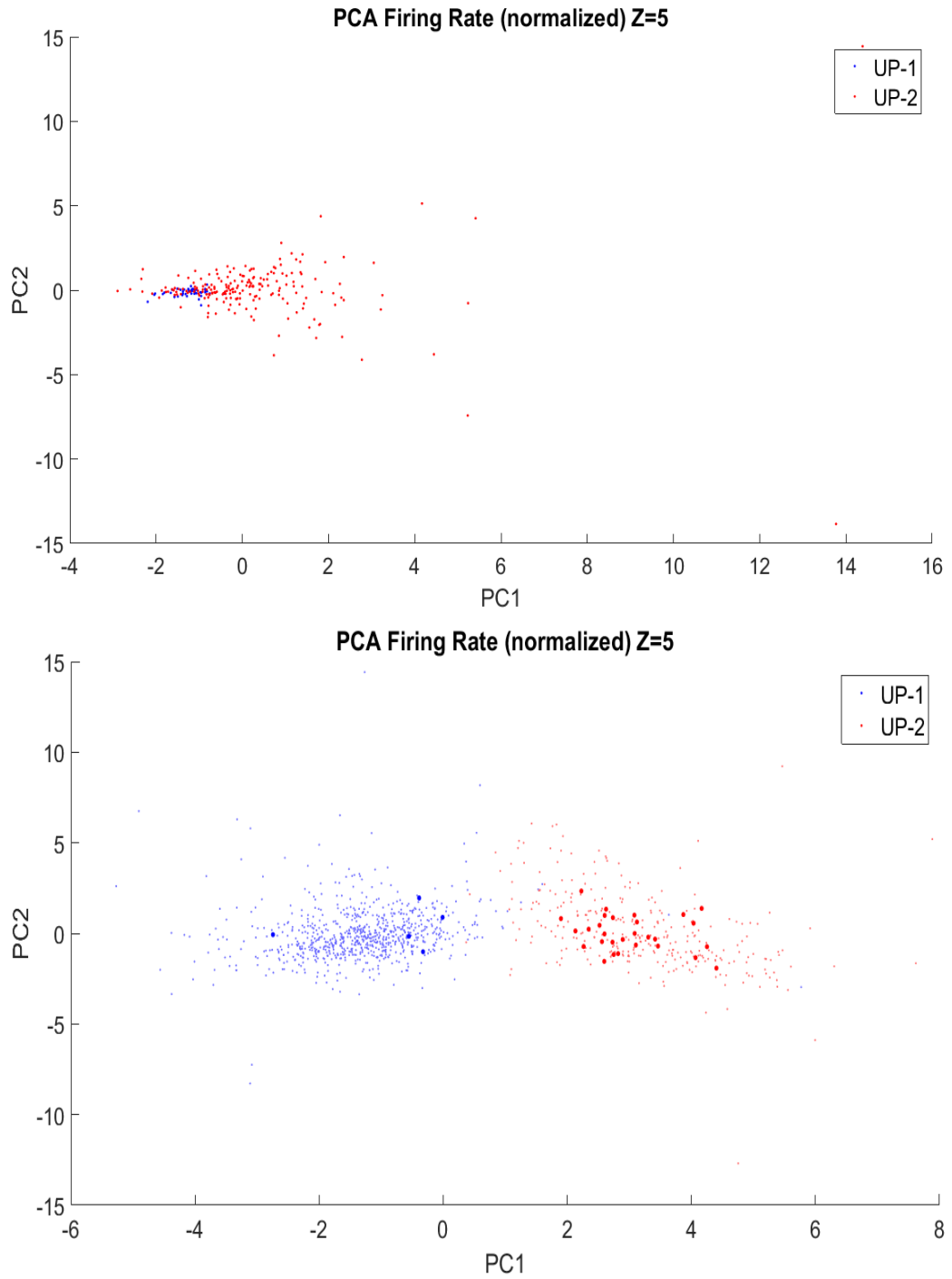


Figure 37. Another example of a comparison of PCA analysis for pre-task and post-task sleep.

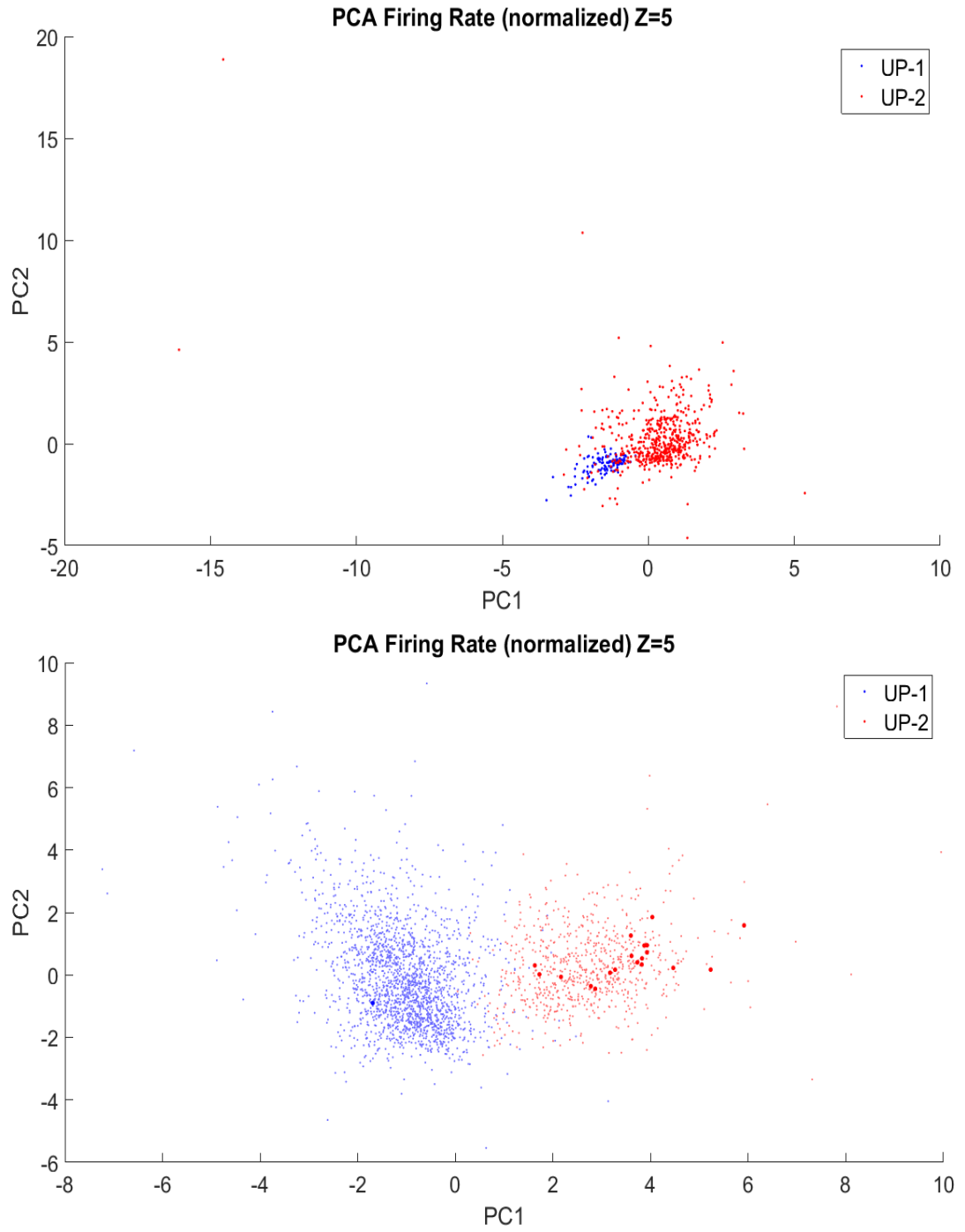


Figure 38. Another example of a comparison of PCA analysis for pre-task and post-task sleep.

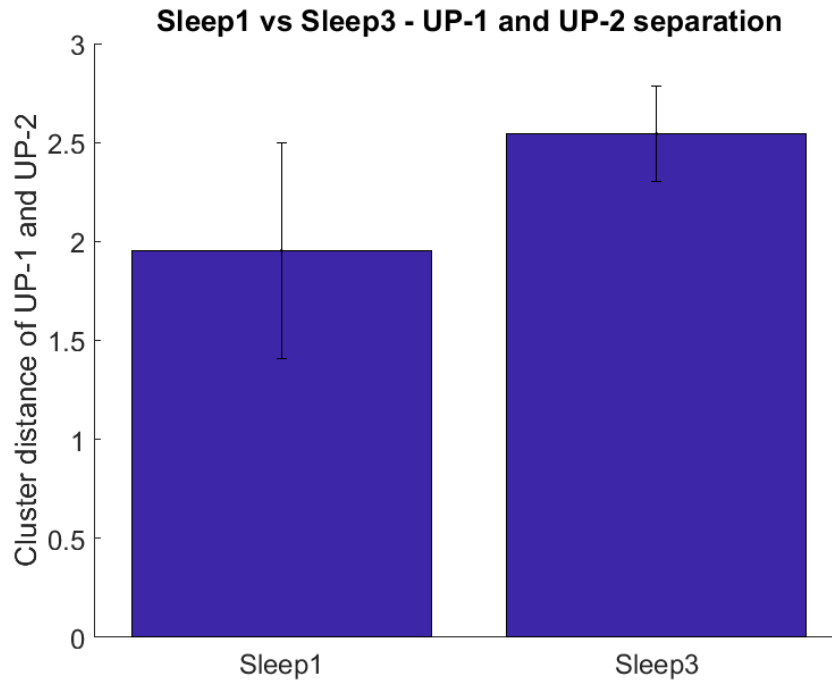


Figure 36. Cluster strength comparison for pre-task and post-task sleep. Two bars show the average cluster strength across all five data sets for pre-task sleep and post-task sleep, respectively.

3.14. Obtaining more than two UP sub-states with higher states of HMM

We showed that UP state can be separated into two subtypes. However, the UP state might be separable to more than two sub-states and the UP state could be classified by those sub-states better. Hence, we are interested to see the results of higher than two UP sub-states, such as three UP sub-states, four UP sub-states, five UP sub-states, and nine UP sub-states. By applying the applications of HMM with more than three states, we would have one DOWN state and more than two UP sub-types. It is expected that the sub-type containing the majority of reactivation, regardless of the number of sub-states would still remain.

Initially, we started with four-states HMM and then doing the exact same procedure for all of the further analysis, except here we have three UP sub-types. Figure 40 and Figure 41 show the distribution of firing rates and duration for all four states, including the three UP sub-states and the DOWN state, for the data set 7165_11p. In these figures, all the states detected by HMM are sorted and then named based on their mean firing rates. The first one, UP-1, has the highest firing rate and the last one with the lowest firing rate is the DOWN state. Figure 42 shows the state vector decorrelation for all three UP sub-states, and similarly, one or some sub-type(s) have a faster rate of decorrelations. The DOWN state is not included in the figure, and clearly, the first and the second UP sub-types have faster vector decorrelation than UP-3. Most importantly, the memory reactivation distribution in Figure 43, for three sub-states shows that still, one of the sub-states, UP-1, contains the majority of reactivation, which is the sub-state with a relatively fast vector decorrelation, not necessarily the fastest vector decorrelation.

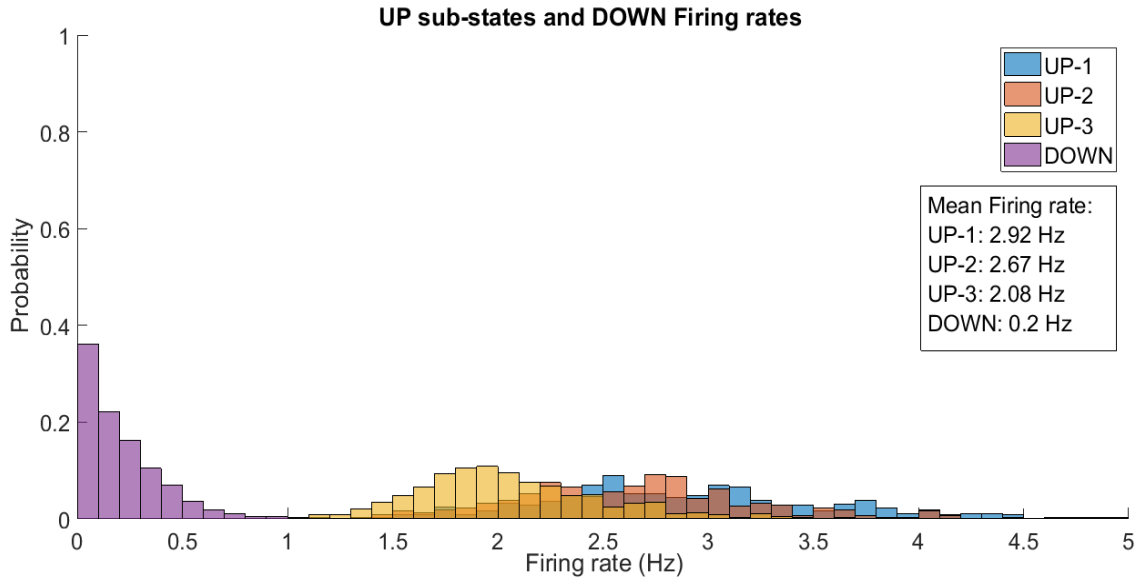


Figure 40. Distribution of firing rates for the four detected states by four-state HMM. Three UP sub-states and the DOWN state were detected by HMM. The three UP sub-types have roughly similar firing rate distributions, but the DOWN state has a different distribution for the firing rate.

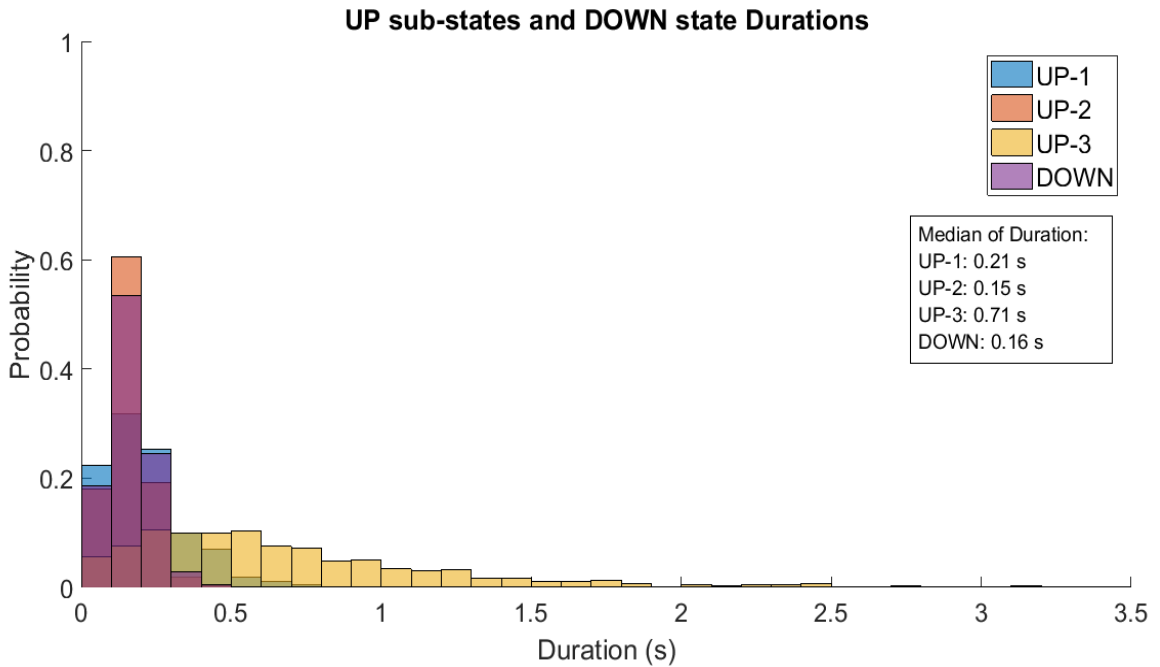


Figure 41. Distribution of duration for the four detected states by four-state HMM. Three UP sub-states and the DOWN state were detected by HMM. The three UP sub-states and the DOWN state have different duration distributions.

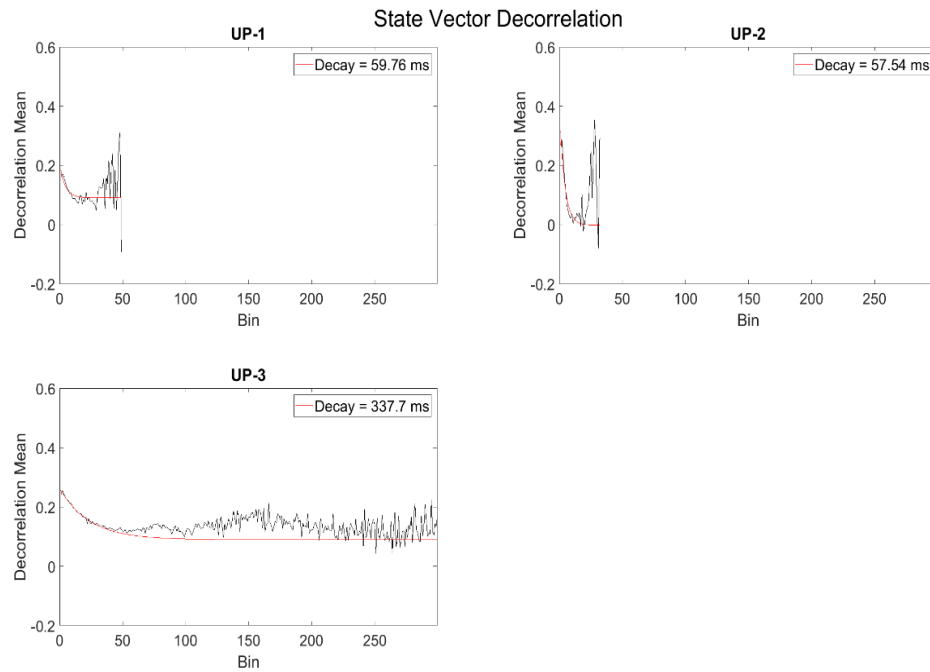
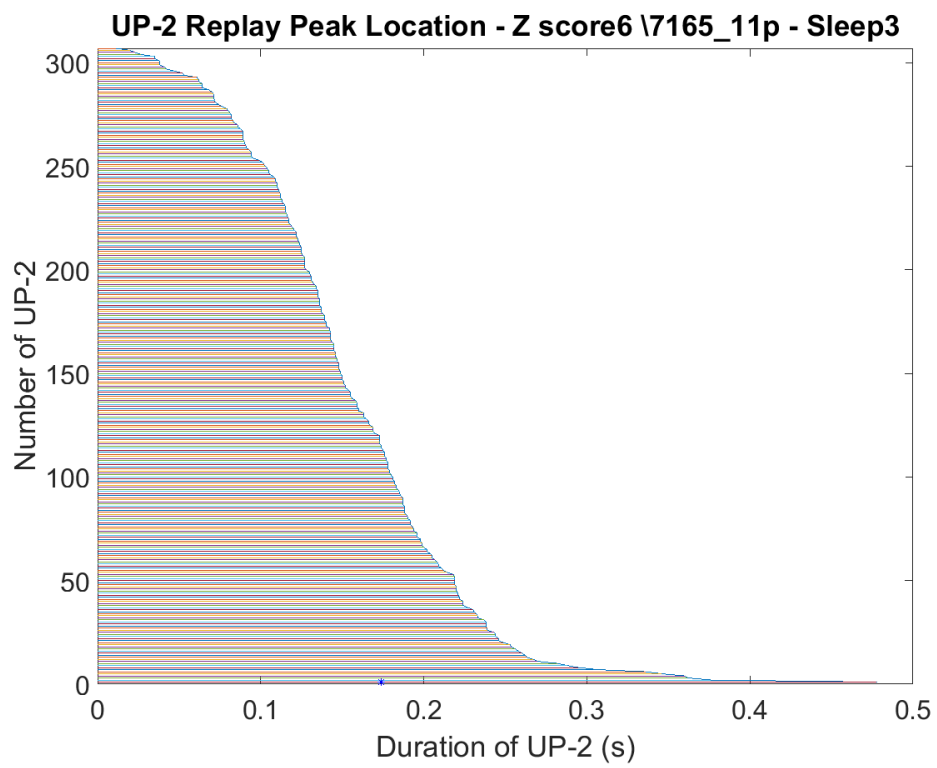
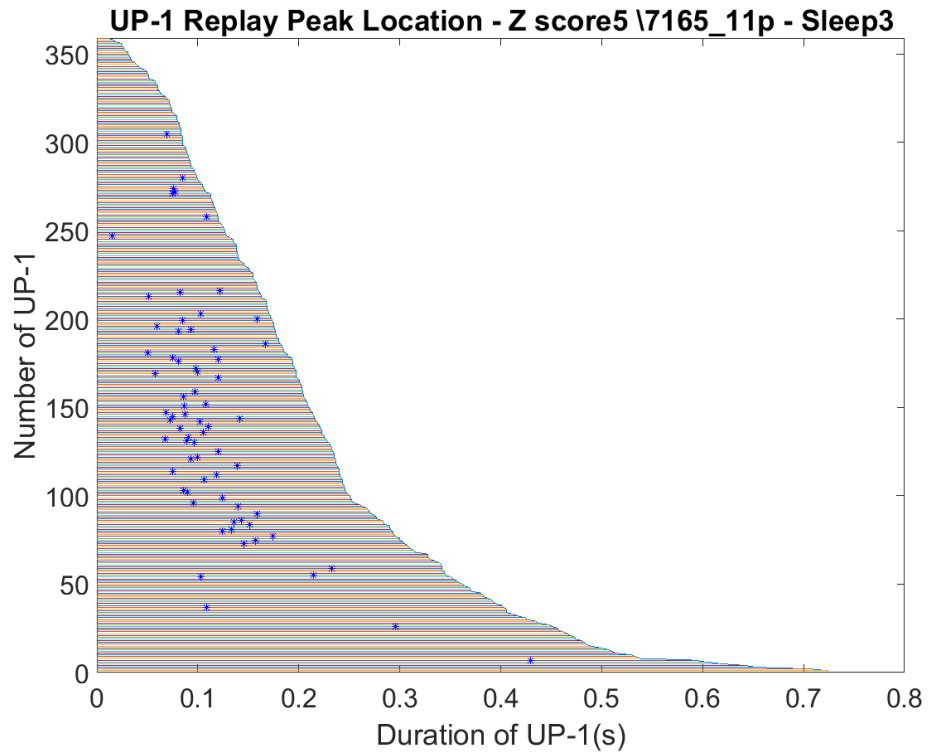


Figure 42. State vector decorrelation for the three detected UP states. UP-1 and UP-2 have much faster decay rates than UP-3.



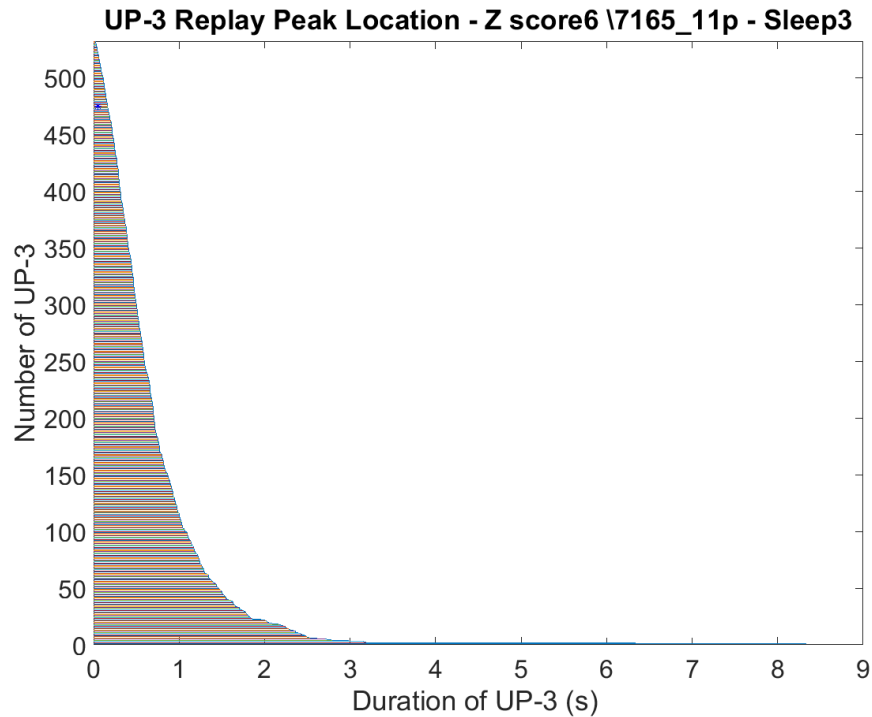


Figure 373. The distribution of reactivation in three UP sub-types. Three figures depict distribution for the three UP sub-states, respectively. It can be seen that still, there is a sub-state, UP-1, containing the majority of reactivation and was distinguished by a fast vector decorrelation and highest firing rate.

These results show that by using four-state HMM, still, there is a UP sub-state that contains the majority of reactivation.

Also, for six-state HMM, the results of firing rates and durations (Figure 44 and Figure 45, respectively), vector decorrelation (Figure 46), and the memory reactivation (Figure 47) are shown. These results again suggest that for these five UP sub-states, still, one of the UP sub-states contains the majority of reactivation.

In addition to four-state and six-state HMMs, which the results have been shown here, we also tried the same analysis for five-state and ten-state HMMs. These results indicate that for five-state HMM, there is one sub-state containing the majority of

reactivation. However, it seems this was not the case when the application of ten-state HMM was used (Figure 48, Figure 49).

Although the reactivating sub-state does not necessarily have the fastest vector decorrelation or the highest firing rate and the lowest variability in the duration similar to the case of two UP sub-states, it seems still state vector decorrelation can be associated with the sub-state containing the majority of reactivation for the most of cases. By more investigation on other data sets, the obtained results for the higher state of HMM, such as four, five, and six, indicate that mostly one of the sub-states contains the majority of reactivation.

Additionally, by using PCA to measure the distinctness of sub-states, it can be shown how the UP sub-states are clustered for different number of UP sub-states (Figure 48).

For more clarification, PCA analysis for four, five, six, and ten-state HMM, for another data set is shown (Figure 49).

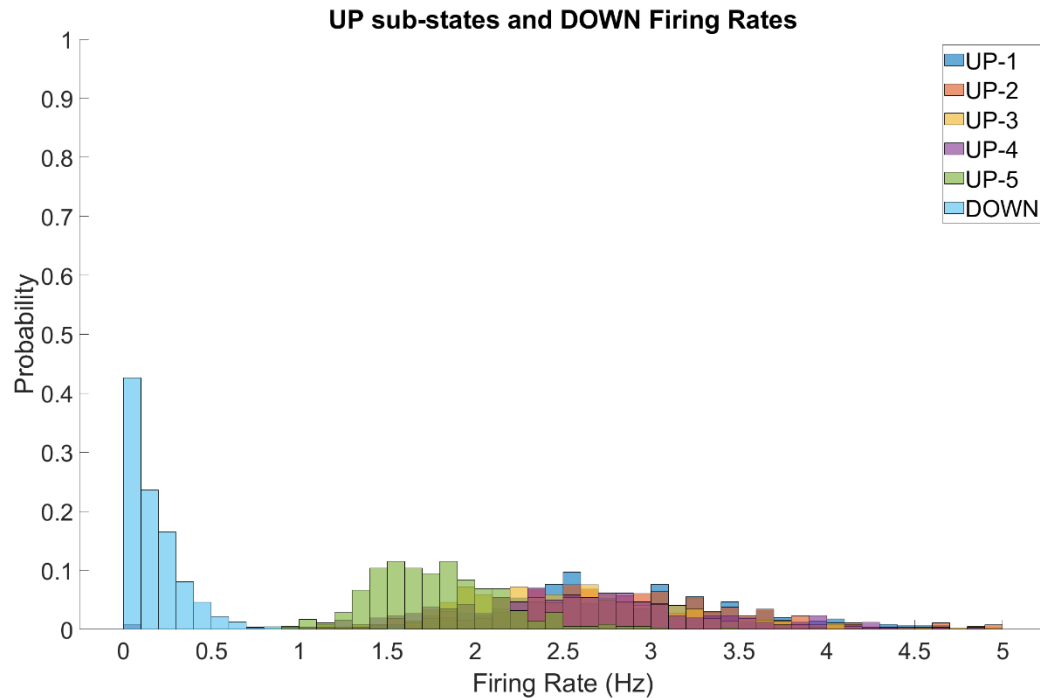


Figure 44. The firing rate distributions for all states detected by a six-state HMM. The figure shows that the firing rates for five UP sub-states and DOWN state, respectively. Here, the UP sub-state has been sorted based on their mean firing rate, where UP-1 has the highest mean firing rate, and UP-5 has the lowest firing rate.

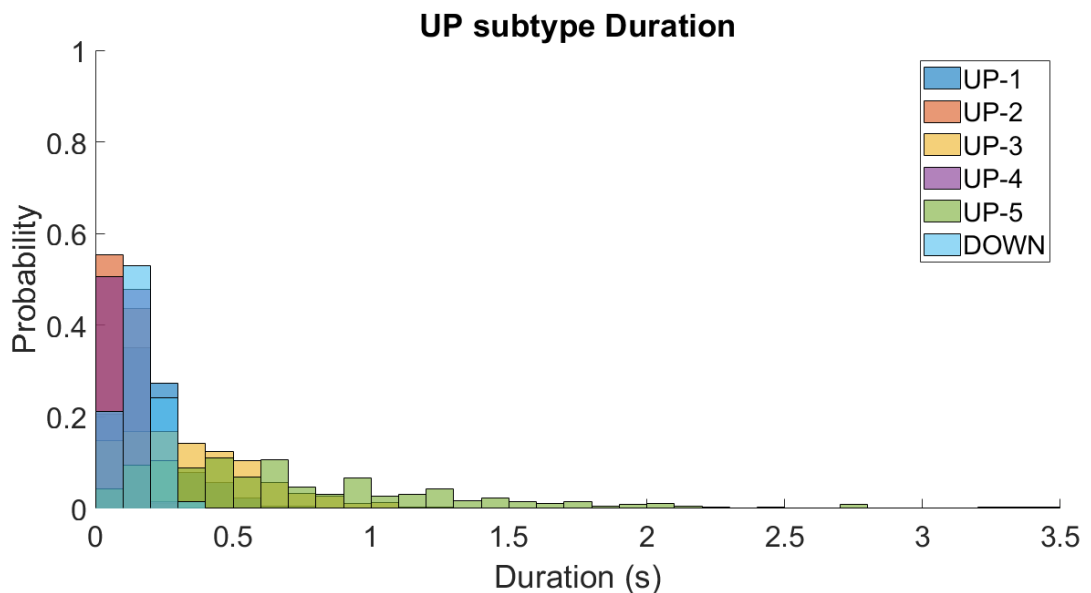


Figure 45. Distribution of duration for the six detected states by six-state HMM. Five UP sub-states and the DOWN state were detected by HMM. The five UP sub-states and the DOWN state have different duration distributions.

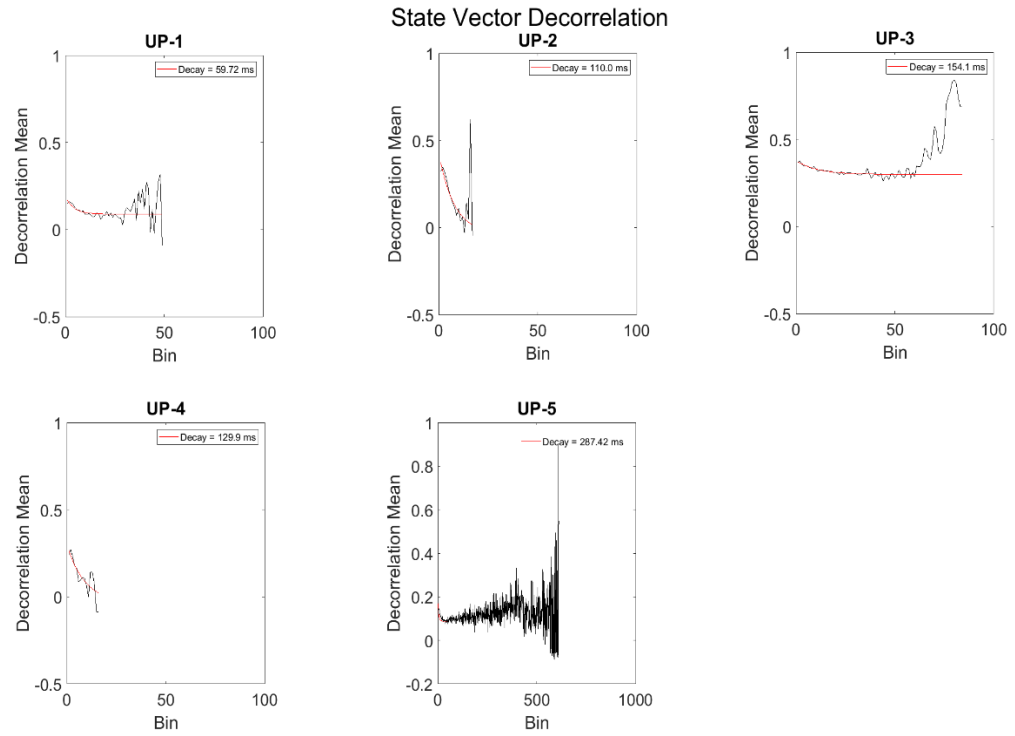
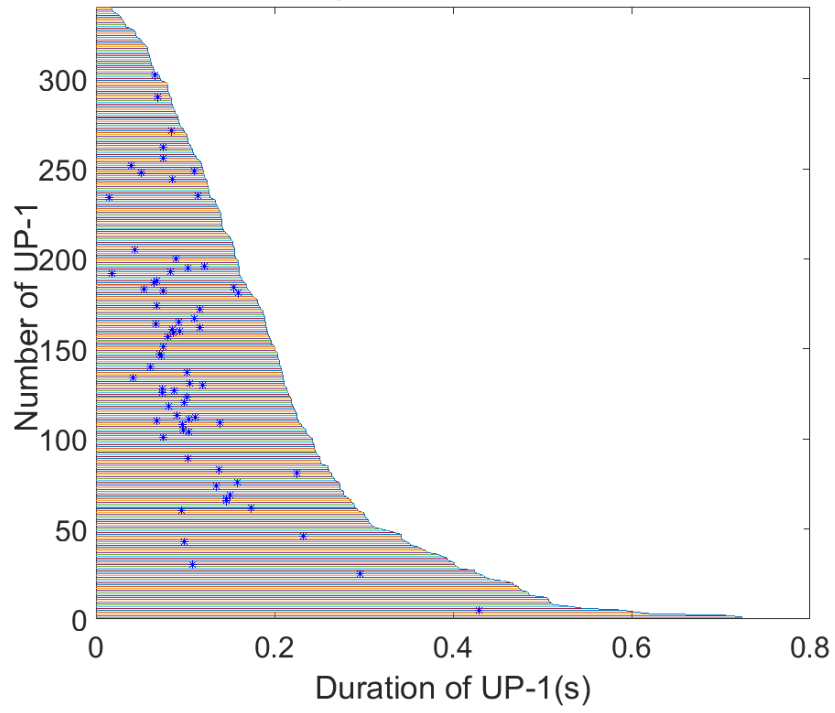
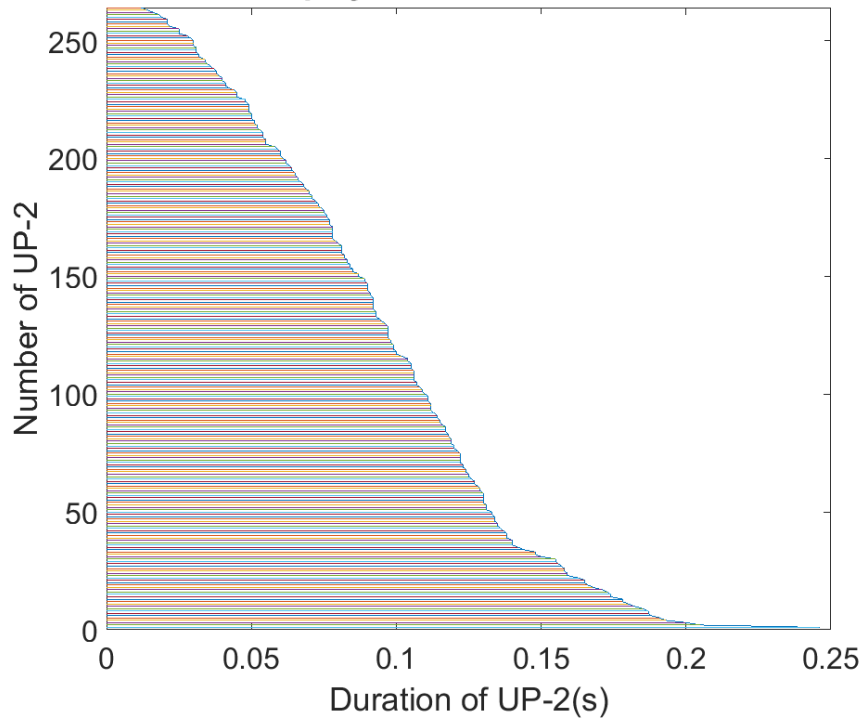


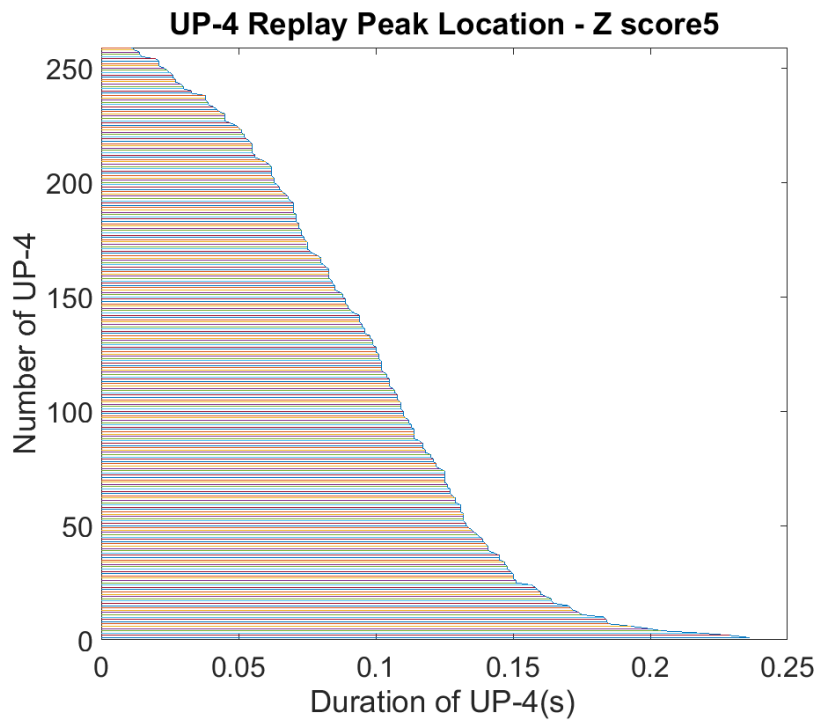
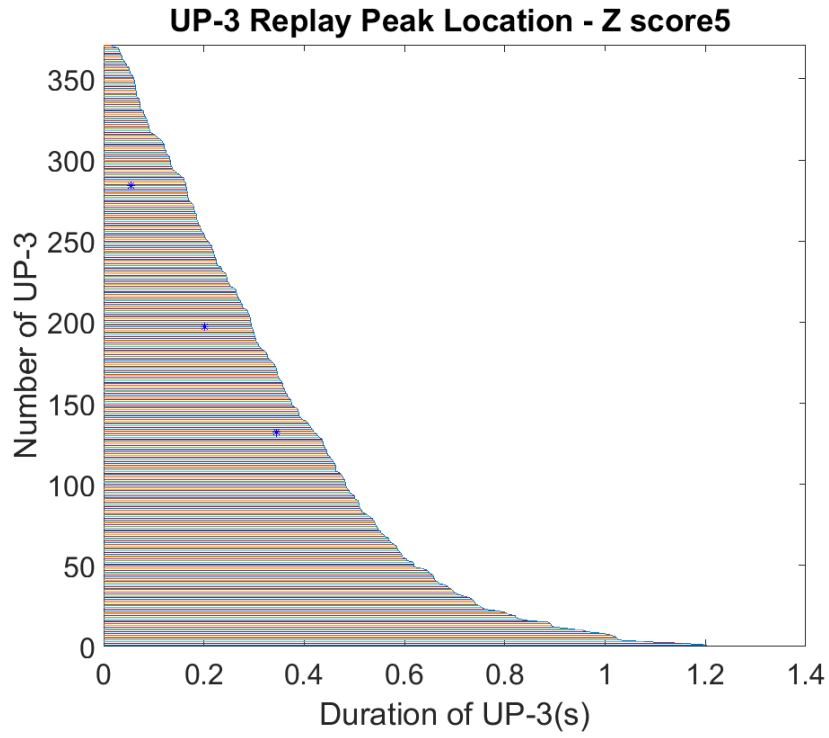
Figure 46. State vector decorrelations for all UP sub-states separated by a five-state HMM. It denotes that UP-1 has the fastest vector decorrelation. This UP sub-state also has the highest firing rate.

UP-1 Replay Peak Location - Z score5



UP-2 Replay Peak Location - Z score5





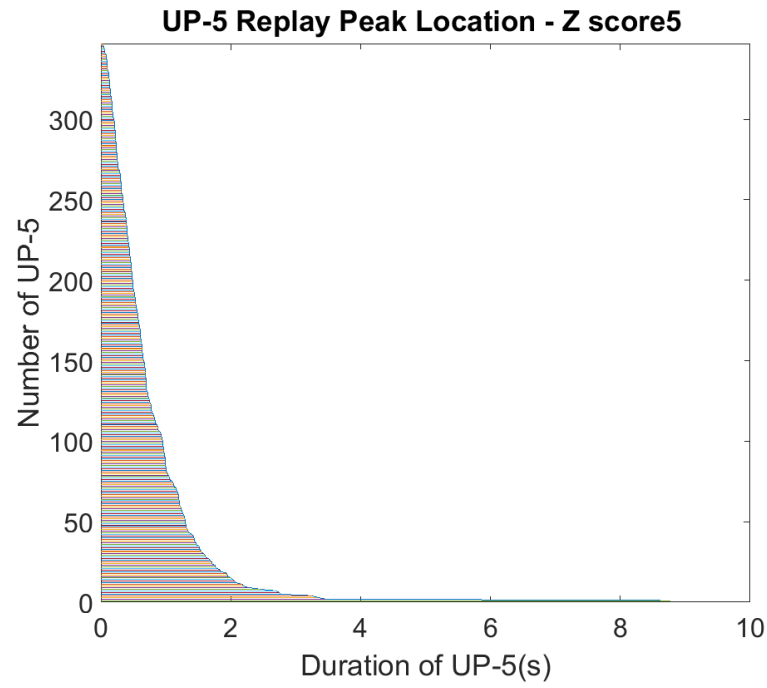
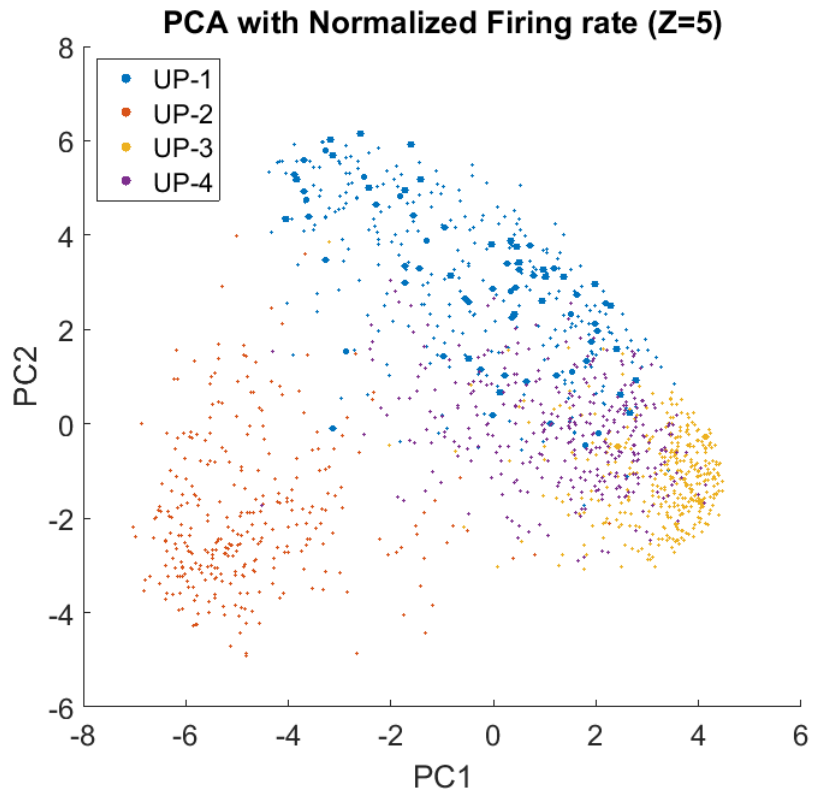
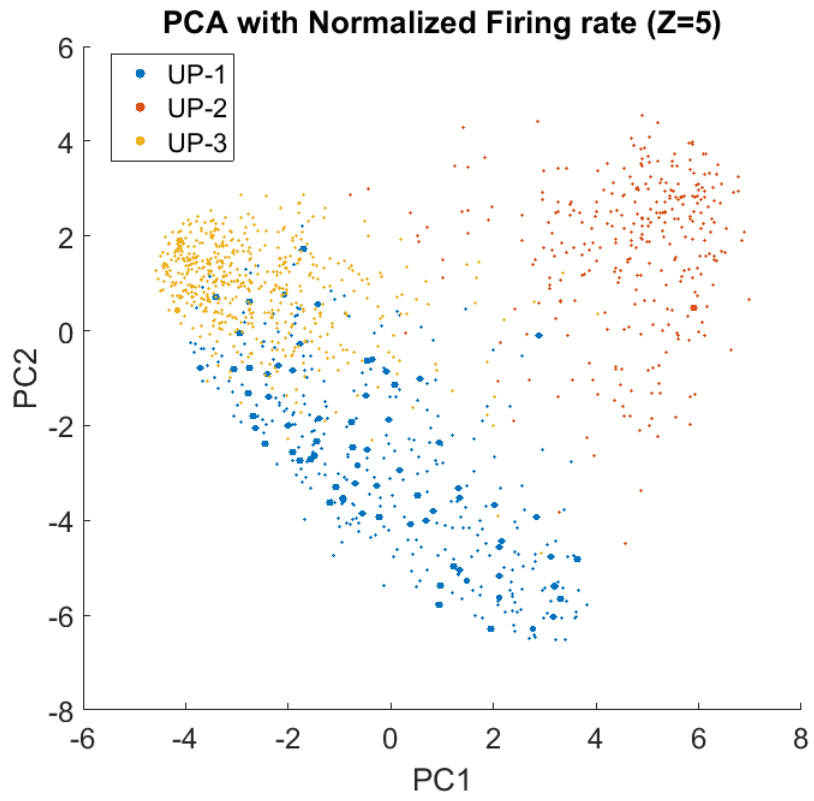


Figure 47. Reactivation distribution for five-state HMM. Five figures depict distribution for the five UP sub-states, respectively. Interestingly, still, one UP sub-state, UP-1, has the majority of reactivation.



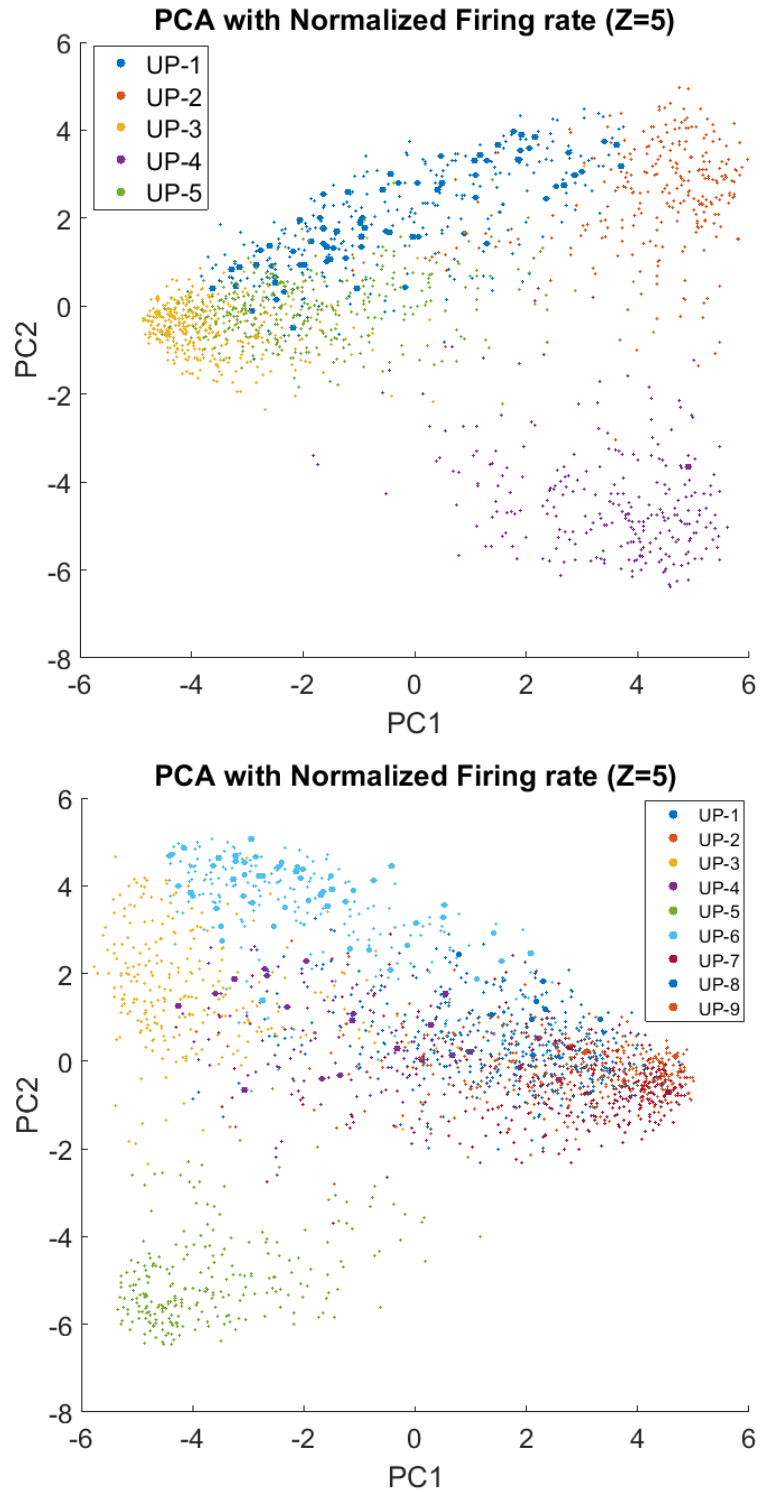
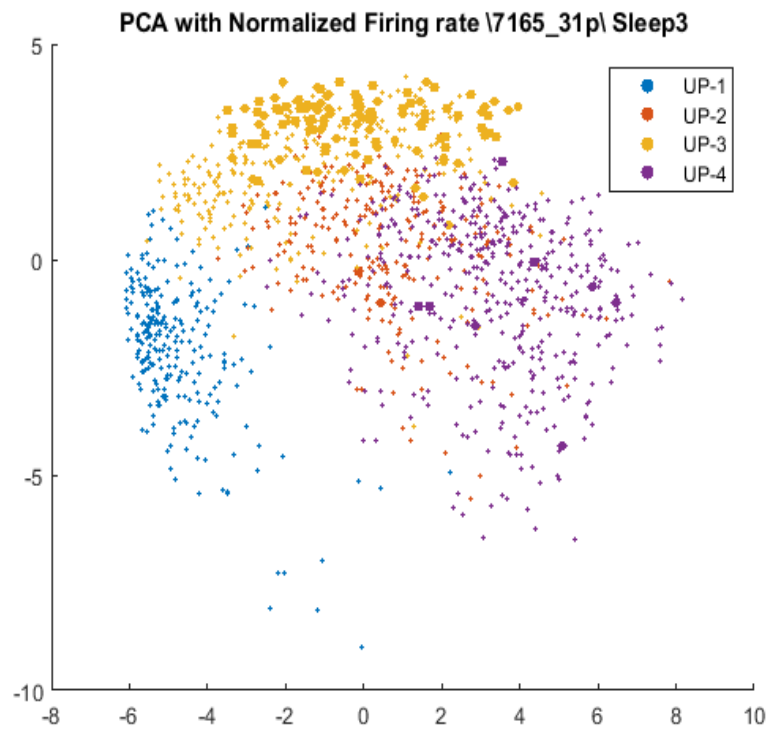
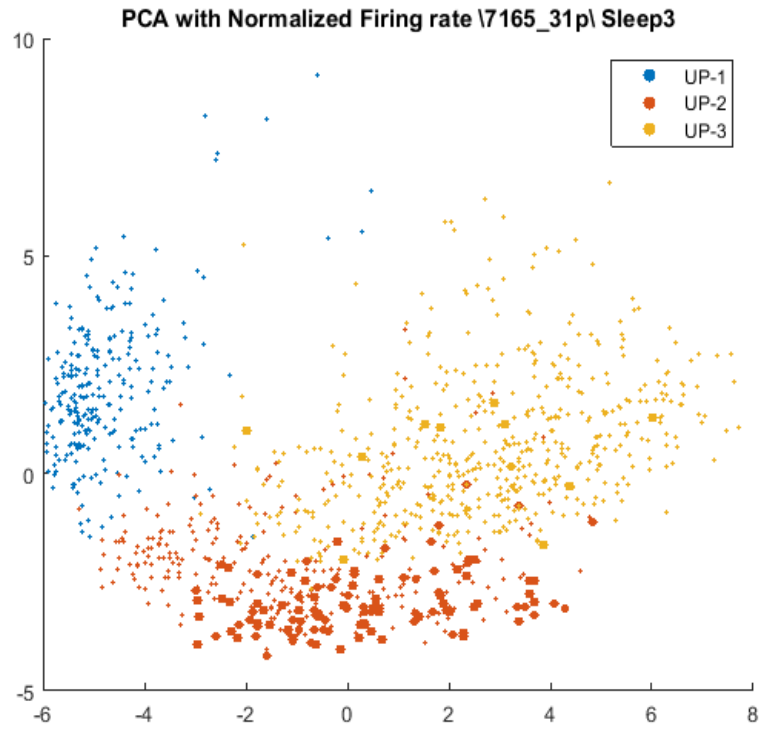


Figure 48. PCA analysis for normalized firing rate for four, five, six-state, and ten-state HMMs (7165-11p). Last page, top: The PCA analysis for the normalized firing rate for four-state HMM. (Only UP sub-states are included in the PCA analysis.) Last page, Bottom: The PCA analysis for five-state HMM. Top: The PCA analysis for six-state HMM. Bottom: The PCA analysis for ten-state HMM.



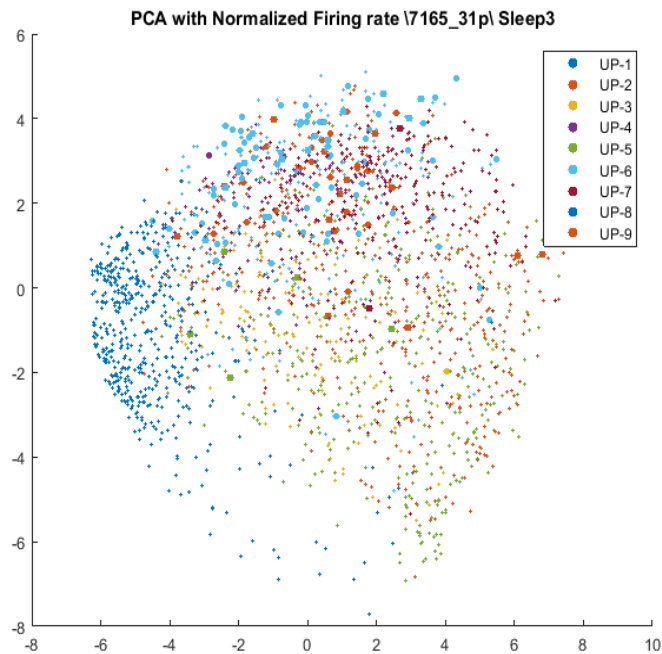
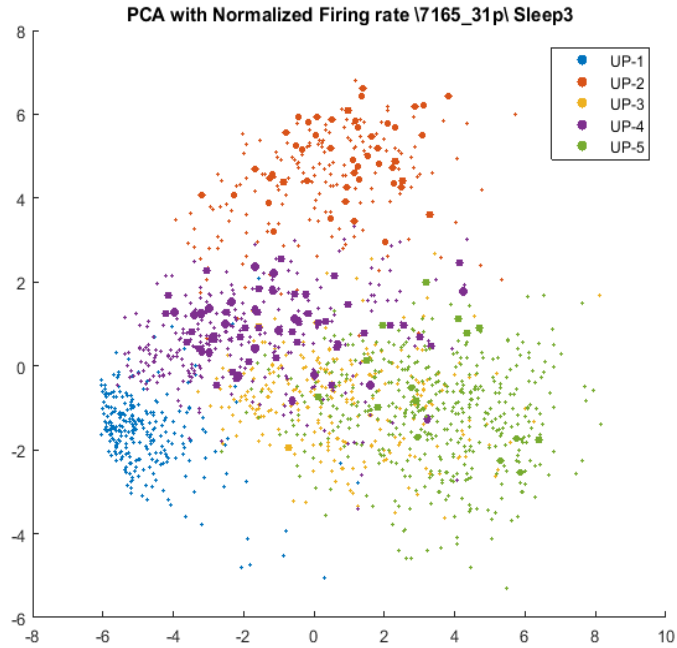


Figure 49. PCA analysis for normalized firing rate for four, five, six-state, and ten-state HMMs (7165-31p). Last page, top: The PCA analysis for the normalized firing rate for four-state HMM. (Only UP sub-states are included in the PCA analysis.) Last page, Bottom: The PCA analysis for five-state HMM. Top: The PCA analysis for six-state HMM. Bottom: The PCA analysis for ten-state HMM.

In order to find which number for UP sub-states is the optimum number of states and also with which we have a better clustering for the UP sub-states, we measured the cluster strength for different states of HMM. Then, we found the cluster strength for each data set and for the different number of states for HMM with Jean-Marc method. Subsequently, we averaged the cluster strength for each number of HMM state across the 10 data sets. The result is shown in Figure 50, suggesting that the HMM three-state has the highest strength in terms of being distinctively clustered. This indicates that the two UP sub-state can be the optimum number to divide the UP state into, and by increasing the number of state for HMM, the obtained sub-states get less and less distinct in comparison to the two UP sub-states.

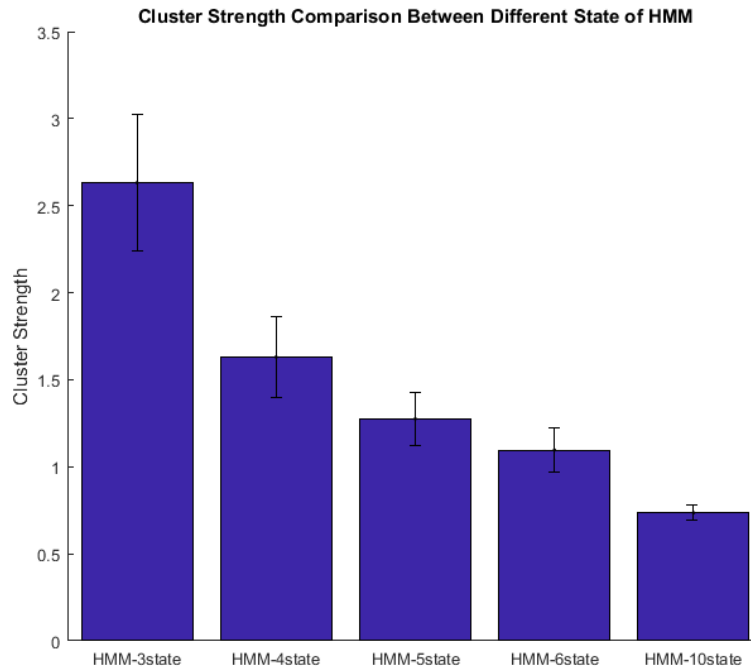


Figure 50. Cluster strength comparison for different states of HMM. Here, the average cluster strength across all data sets and for different states of HMM is shown. It suggests that three-state HMM has the highest cluster strength, and the ten-state HMM has the lowest.

3.15. Correlation of UP sub-states to themselves and to each other

We showed that memory reactivation is predominantly happening in the UP-2 state, which was characterized by faster vector decorrelation and lower mean duration. This observation suggests that there might be more similarities in the UP-2 events, corresponding to the recent memory reactivation. To investigate it, we hypothesized that this might be reflected in the more similarity within the UP-2 pairs than within the UP-1 pairs. To test this hypothesis, first, we made a vector of $[N \times 1]$ regarding each UP-1 event, where N is the number of neurons, and each N element was calculated by a mean firing rate of each neuron during each UP-1 events. Subsequently, for each UP-1 event, we have a vector to represent the event with and calculate the pair-wise correlation of that

event with other UP-1 events. Next, we calculated the pair-wise correlation for all UP-1 pairs, and the histogram of them has obtained as it is in (Figure 51, top) for data set 7165_31.

Then, we repeated the same procedure for UP-2 events, and find the pair-wise correlation of all UP-2 events with each other, and made the same distribution for UP-2 events by considering all the UP-2 pairs (Figure 51, bottom). More specifically, by using the median and the intervals for 50% and 95% range, we tried to characterize the distribution and subsequently performed a statistical test over 10 data sets (Lilliefors test for normality: UP-1: $p = 0.333$, UP-2: $p = 0.20$, two-sample t-test: $p = 0.0204$). The results indicate that the median of UP-2 pairs is significantly higher than the median of UP-1, which suggests that UP-2 pairs are more similar to each other than UP-1 to each other. Although, according to results, some UP-2 states are highly similar to each other, some are not. The latter would contribute to a long tail of the UP-2 distribution in Figure 51, bottom.

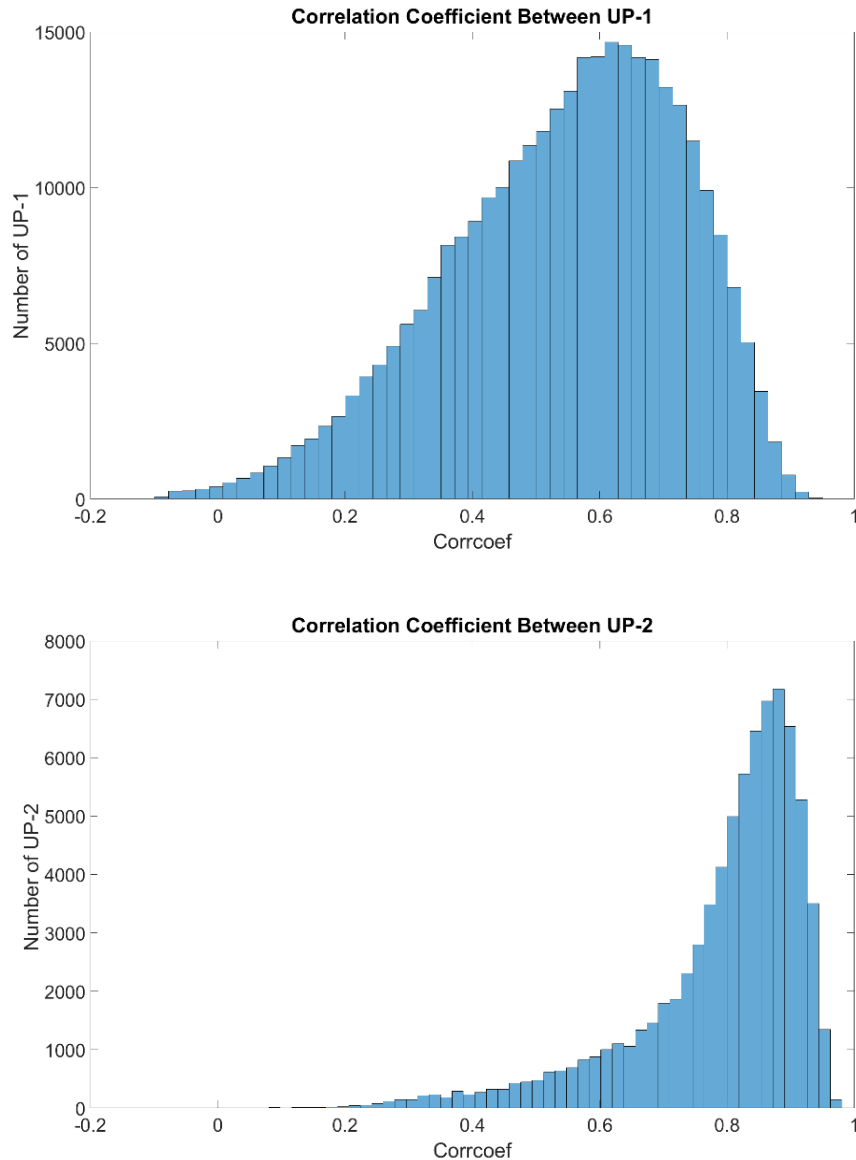


Figure 51. The pair-wise correlation coefficient between each UP sub-state. Top: The pair-wise correlation coefficient between all UP-1. Bottom: The pair-wise correlation coefficient between all UP-2. These figures suggest that UP-2 pairs are more correlated to each other than UP-1 pairs.

3.16. SWRs correlation with DOWN-to-UP transition and UP-1 to UP-2 transition

In order to investigate the relationship between the SWRs and UP state transitions, the detected SWRs were converted to a discrete-time series based on the

location of SWR's peak amplitude. Subsequently, SWRs and UP state transitions were cross-correlated, using the UP state transitions as a reference signal and SWR as a target signal. More specifically, the zero lag in the cross-correlation figure indicates the occurrence of the UP state transition. Consistent with the previous study, showing SWRs are correlated with the DOWN to UP transition (Battaglia et al., 2004), the result for three data sets (one rat) has been shown in (Figure 52), and for two of them, the DOWN to UP transitions precedes the SWRs by 100-200 ms. In this figure, the first and second data sets show that there is an increase in the cross-correlation plot after the DOWN to UP transition (Figure 52, top and middle).

Figure 53 shows the correlation between SWRs and the transition from the UP-1 to UP-2 states for three data sets. This relation is interesting as we showed that UP-2 contains the majority of reactivation. As Figure 53 suggests for two out of three data sets, UP-1 to UP-2 state transitions precede the SWR by 100-200 ms. This indicates that the interaction between the hippocampus and the cortex during SWRs can happen stronger when the cortex exhibits the UP-2 state. Leading the hippocampal by the cortical transitions suggests that cortical reactivation in the UP-2 might trigger the hippocampal reactivation in the SWRs.

In summary, we showed that the SWRs are correlated not only with DOWN to UP transitions but also with the UP-1 to UP-2 transitions. In order to interpret these results, it should be considered that the animal was highly familiarized with the task during the analyzed recording days.

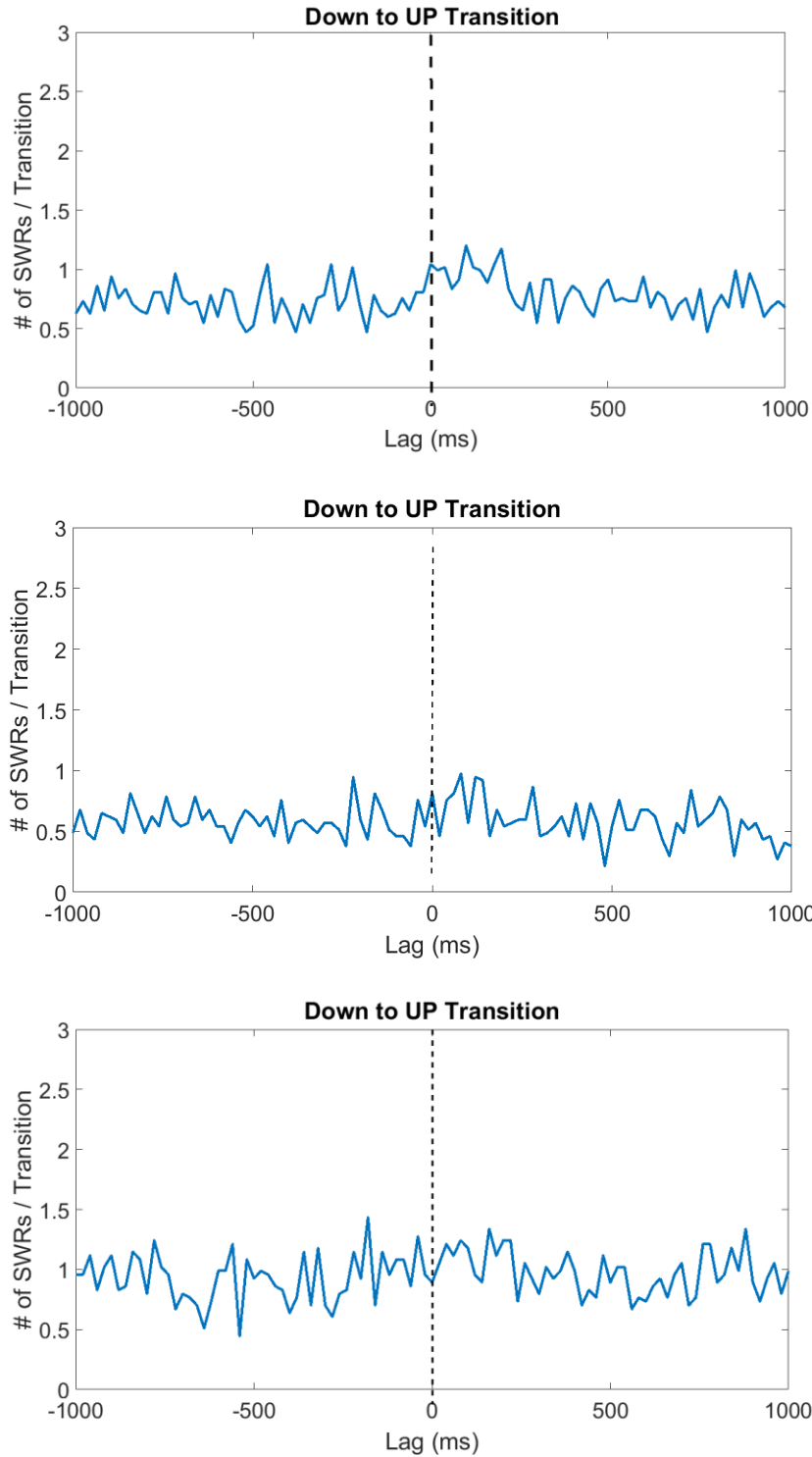


Figure 52. The Cross-correlation of transition between DOWN to UP and Ripple. Here, after finding all the transition points during which DOWN states transit to UP state, we assessed the cross-correlation of these points and Ripple. There are three examples of the three data sets. Two of these examples, top and middle, show the DOWN to UP transitions precedes the SWRs by 100-200 ms.

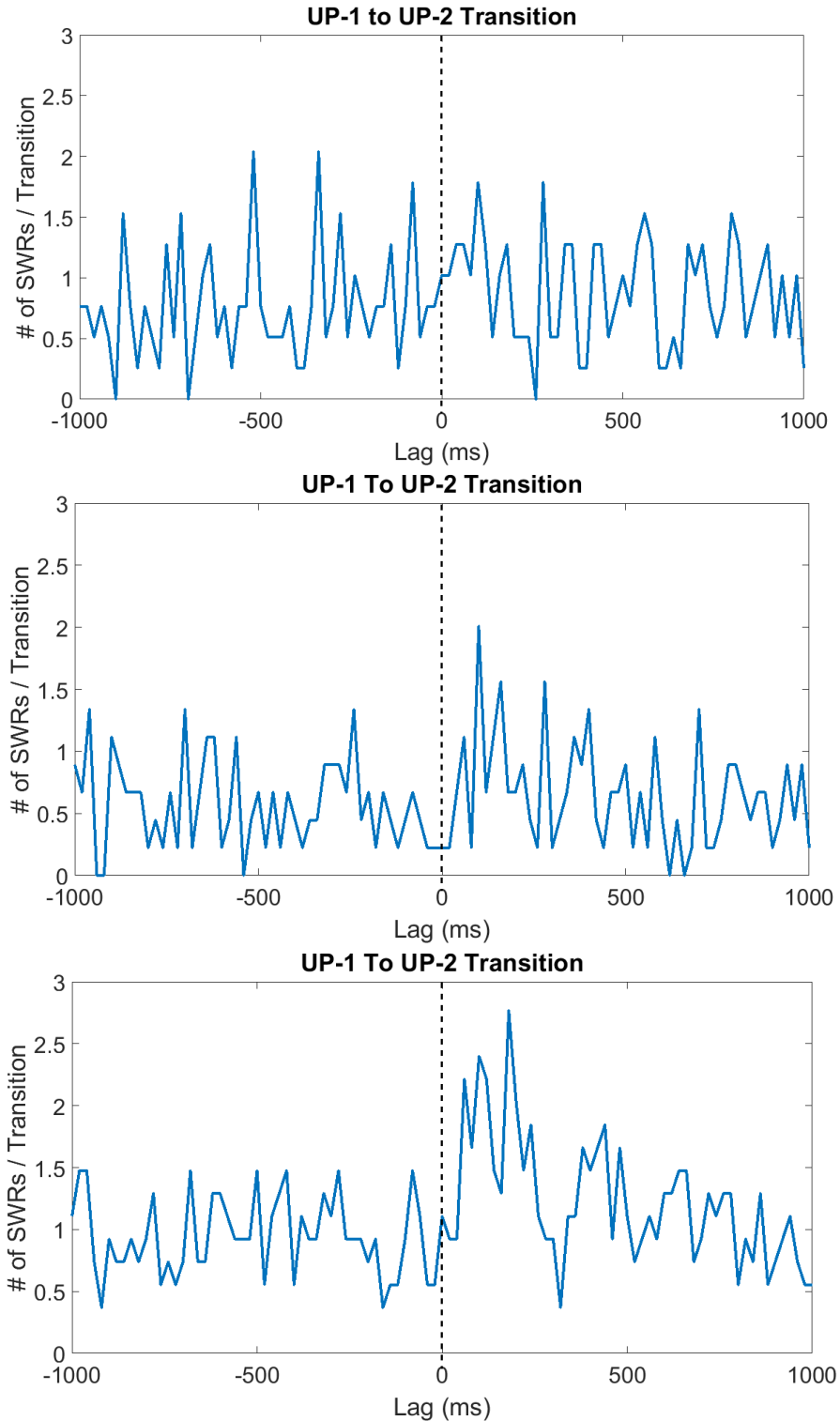


Figure 53. The Cross-correlation of transition between UP-1 to UP-2 and Ripple. Here, after finding all transition points during which UP-1 sub-states transit to UP-2 sub-states, we assessed the cross-correlation of these points and Ripple. There are three examples of the three data sets. Two of these examples, middle and bottom, show the UP-1 to UP-2 transitions precedes the SWRs by 100-200 ms.

3.17. Using two HMM two-states

At the beginning of starting this project, in order to detect the DOWN states and UP sub-states, we used two-state HMM twice; the first time in order to detect the DOWN and UP states, and the second time to detect the UP-1 and UP-2 states. However, as for detecting the UP-1 and UP-2 with this method, we had to concatenate all detected UP states by the first HMM and then use the concatenated UP states as an input to the two-state HMM in the second try. All of the further procedure was pretty similar to what has been explained here. Because of the possible artificial effect of concatenation, which attached one UP state to another UP state where previously was a DOWN state, we decided to continue the project with the three-state HMM instead.

Figure 54 shows the similarity of the detected DOWN, UP, UP-1, and UP-2 states, respectively, by a three-state HMM and two two-state HMM. For finding UP state by a three-state HMM we simply merged the UP-1 and UP-2 detected by three-state HMM. This consistency shows that the results of using two-state HMM twice are pretty much similar, suggesting that even by concatenating UP states, the result are similar. As a result, it might be concluded that the detected UP-1 and UP-2 have a specific dynamic that can be detected by two-state HMM regardless of the concatenating.

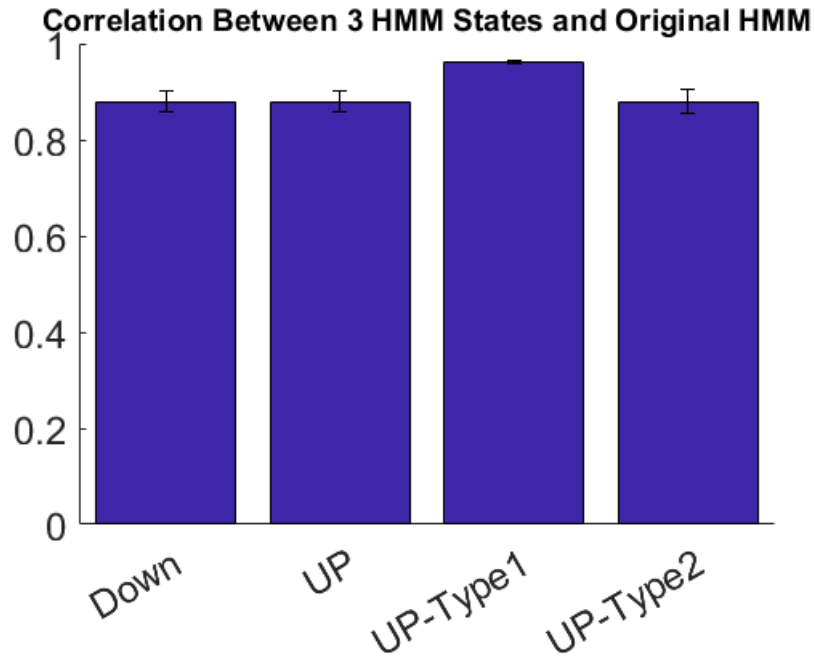


Figure 54. The similarity between states detected by two-state and three-state HMMs. The correlation between the states which were detected by a three-state HMM and two-state HMM used twice was assessed. It shows the correlation for each type of state that was detected by these two methods is significantly high.

3.18. The hippocampus LFP analysis

Additionally, by using local field potential (LFP) from the hippocampus, the power of the signal was obtained by the pwlech function. For this part of the analysis, we had three data sets coming from one rat. Subsequently, we calculated the log of power for each UP sub-state, and then the mean of log power across the all UP sub-types, UP-1 and UP-2, respectively. Therefore, the comparison between the log power happening during UP-1 and UP-2 is shown for one data set, 8482_14p (Figure 55, top). This figure suggests a difference between UP-1 and UP-2 power. Figure 55, bottom, shows the difference between them in the Ripple band frequency. In order to show whether the differences are significant or not, we used the mean of each frequency band.

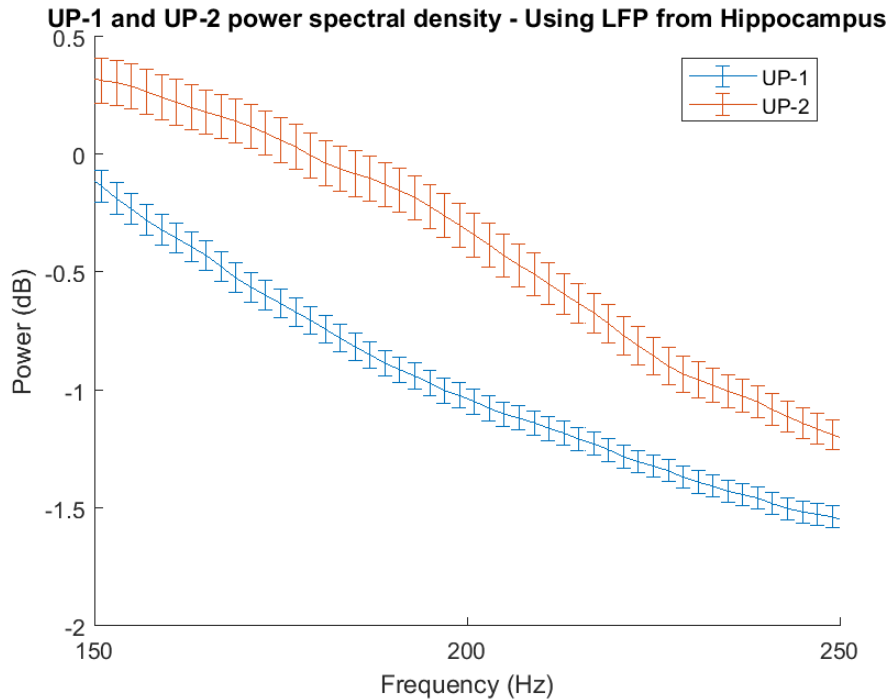
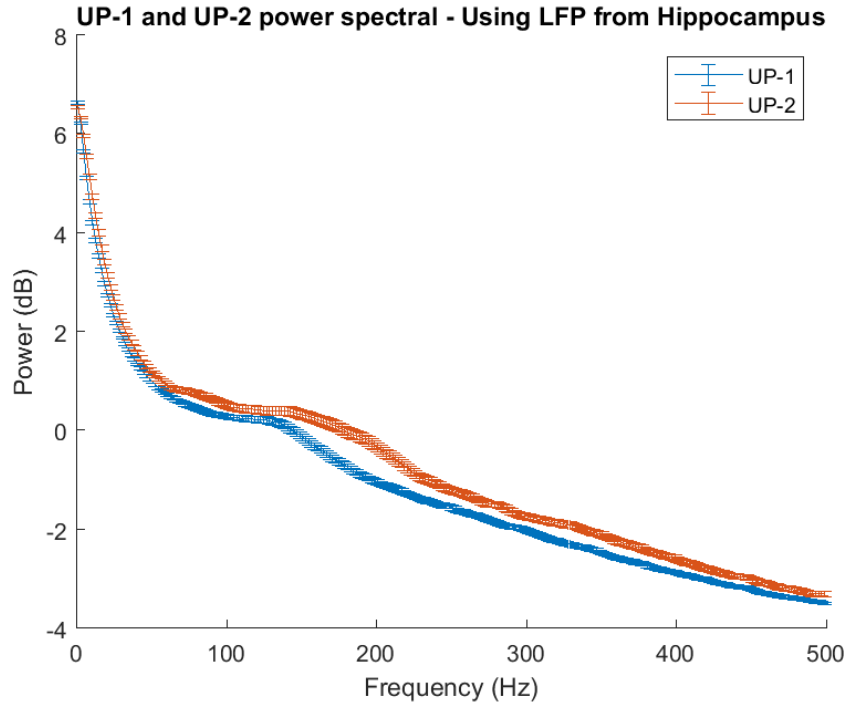


Figure 55. Log power comparison between UP-1 and UP-2 for hippocampus LFP. Top: The comparison between the mean log power of the hippocampus LFP happening during UP-1 and UP-2 events, respectively. It shows that during the UP-2, the power of the hippocampus LFP is stronger than UP-1. Bottom: The same analysis but for the only Ripple frequency band. Again, the power during UP-2 is stronger.

By using the mean power in the (Figure 55) and for the different frequency bands, the difference between the mean power across these frequency bands are shown (Figure 56, top). Also, the difference for the ripple band is shown in (Figure 56, bottom).

These figures suggest that during the UP-2, where the majority of reactivation occurs, there is an increase in the power of the LPF signal from the hippocampus, especially for the Ripple band. However, as it can be seen in (Figure 56) the differences are not significant.

3.19. The cortex LFP analysis

In addition to the hippocampus LFP analysis, cortex LFP also was analyzed. For this part of the analysis, we had the cortex LFP for 10 data sets. Similar to LFP from the hippocampus, the power of the LFP signal from cortex was obtained by pwelch function. Subsequently, we calculated the log of power for each UP sub-state, and then the mean of log power across the all UP sub-types, UP-1 and UP-2, respectively. The comparison between the log power happening during the UP-1 and UP-2 shown here (Figure 57, top). The result shows there is not a considerable difference between these UP sub-states for the log power of the cortex LFP. Also, specifically for the Spindle band, there is no apparent difference between UP-1 and UP-2 in the power of the LFP signal (Figure 57, bottom).

Again, by using the mean power in the (Figure 57) for different frequency bands, the difference between the mean power across these frequency bands has depicted (Figure 58, top). Next, the difference in only the spindle band is shown (Figure 58,

bottom), indicating there is no difference between the power of spindle during UP-1 and UP-2.

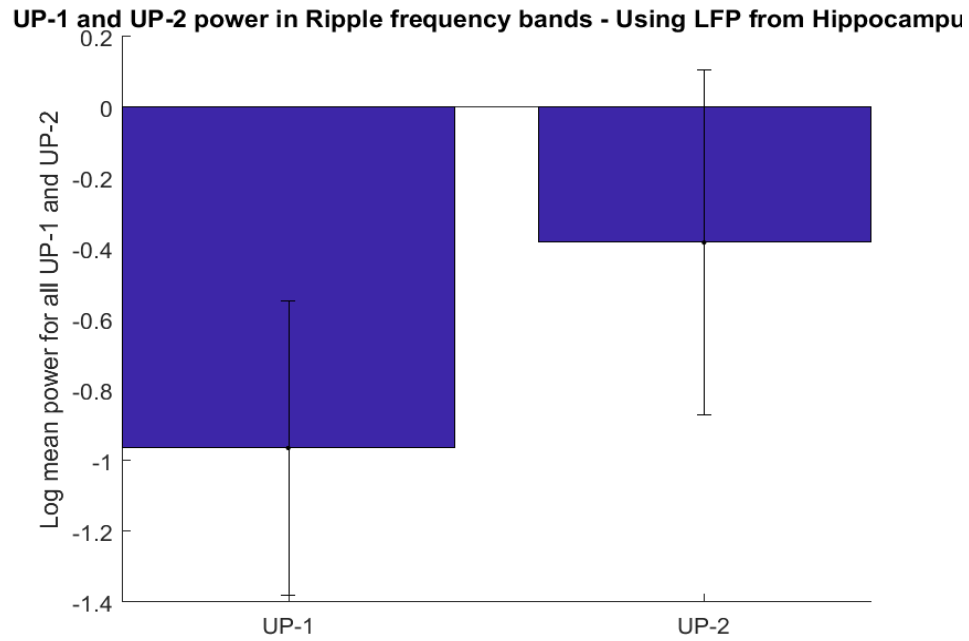
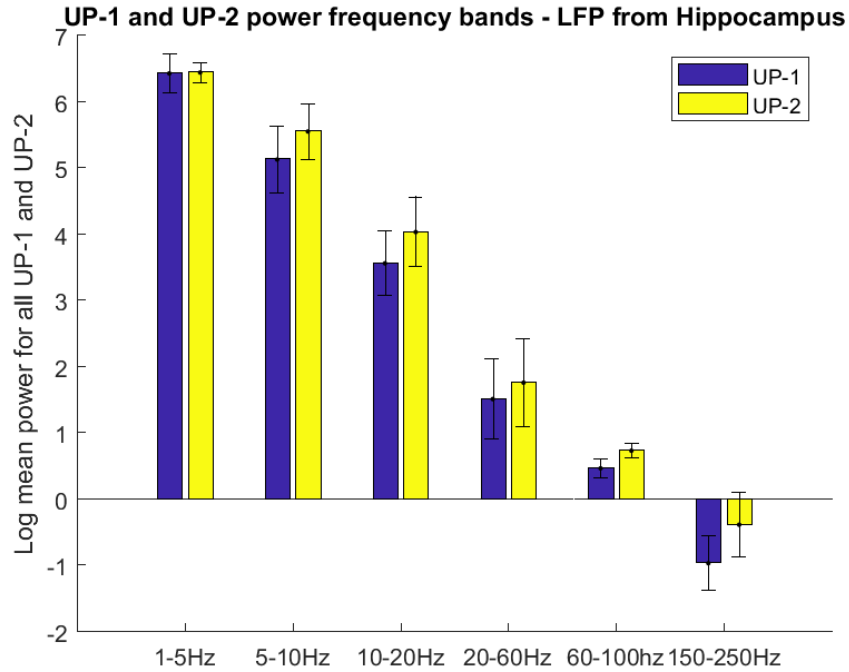


Figure 56. UP-1 and UP-2 power frequency bands comparison (Hippocampus LFP). Top: The comparison between UP-1 and UP-2, log mean power, for all frequency bands, using hippocampus LFP, is shown. For all frequency bands, UP-2 has higher powers than UP-1. Bottom: The comparison between UP-1 and UP-2, for only the Ripple frequency band. UP-2 has a higher power in comparison to UP-1.

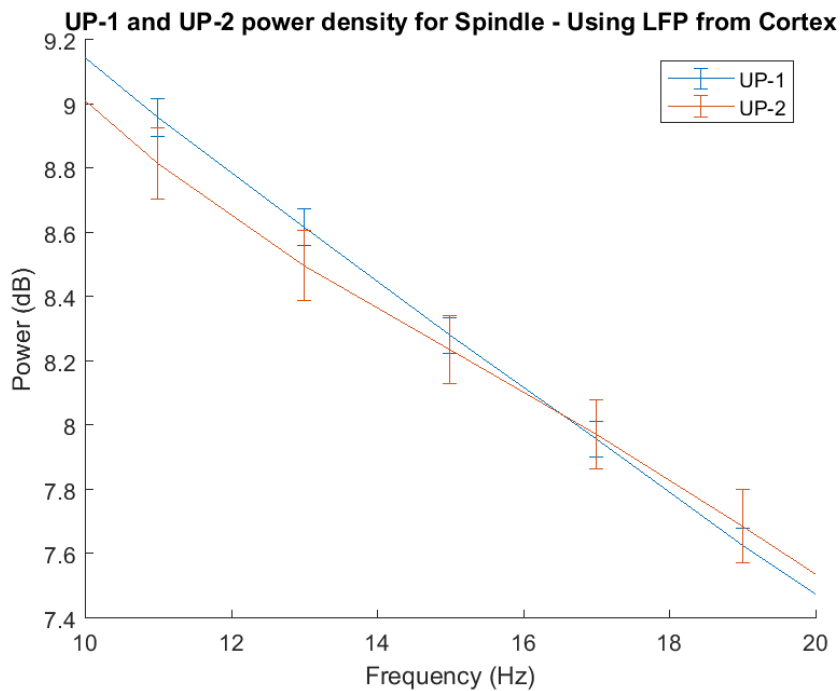
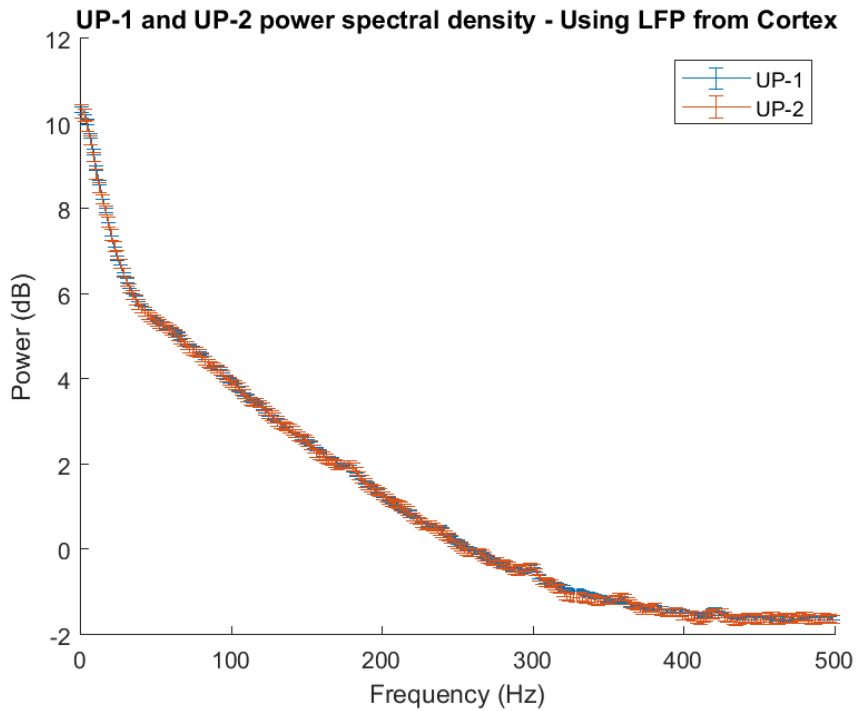


Figure 57. Log power comparison between UP-1 and UP-2 for cortex LFP. Top: The comparison between the mean log power of the cortex LFP happening during UP-1 and UP-2 events, respectively. It does not show a clear difference between UP-1 and UP-2. Bottom: The same analysis but for the only Spindle frequency band. Again, the power of UP-1 and UP-2 are similar.

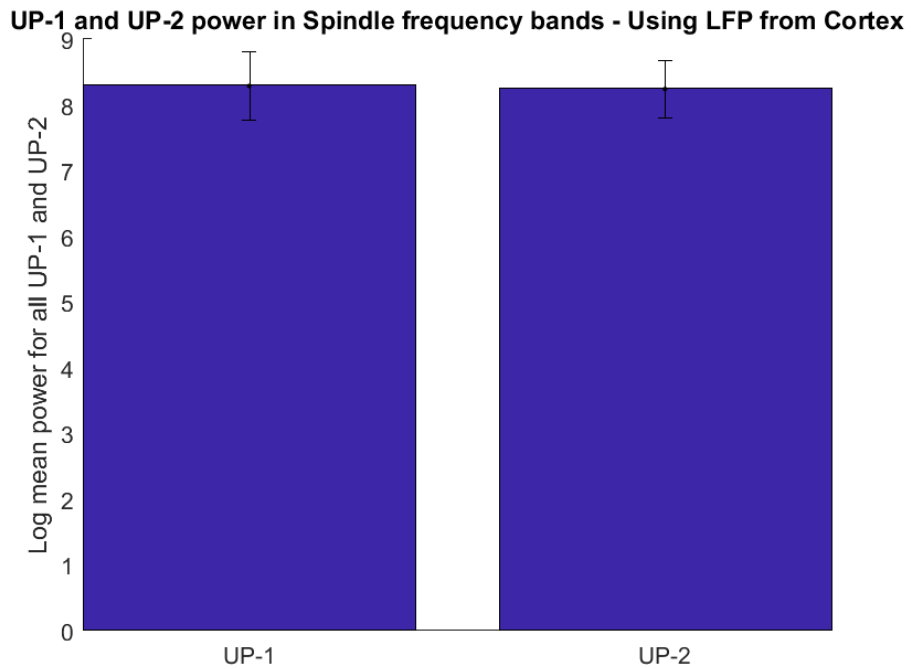
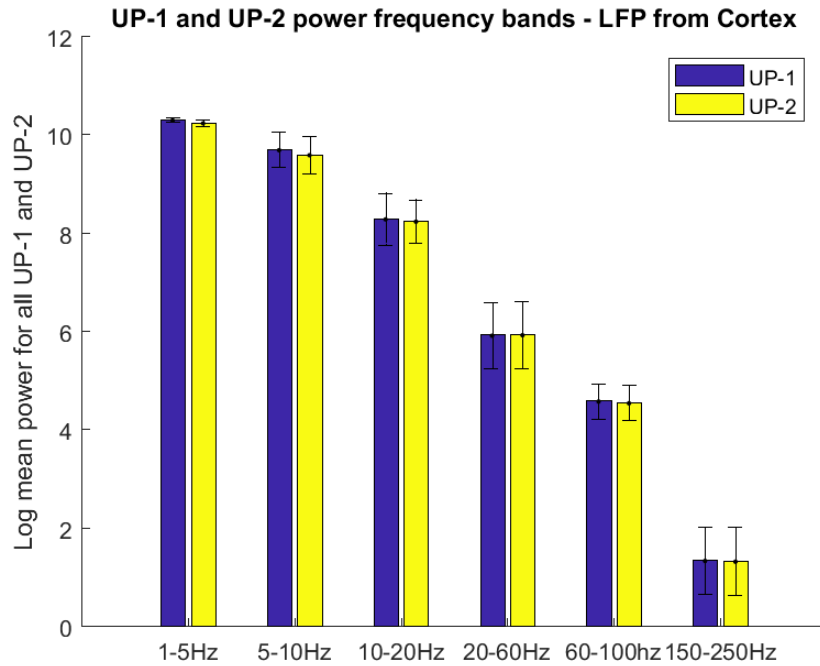


Figure 58. UP-1 and UP-2 power frequency bands comparison (Cortex LFP). Top: The comparison between UP-1 and UP-2 for all frequency bands, using the cortex LFP, is shown. There are no clear differences in frequency bands between UP-1 and UP-2. Bottom: The comparison between UP-1 and UP-2, for only the Spindle frequency band.

4. Discussion

In the present study, we have shown that UP state can be separated into two or more sub-states, one of which with a distinguished dynamic and always contains the majority of reactivation. It has been claimed that hippocampal-cortical interaction happens during SWRs in the hippocampus and around UP states in the cortex (Ego-Stengel & Wilson, 2010; Girardeau et al., 2009; Ji & Wilson, 2007; Lansink et al., 2009; Peyrache et al., 2009; Ji & Wilson, 2007). Based on the standard memory consolidation theory (Dudai, 2004), it is hypothesized that the information from the distributed cortical modules can be integrated from the hippocampus and be merged quickly into a coherent memory trace. Knowing from the recent study that SWRs can be decomposed into subtypes (Ramirez-Villegas et al., 2015), we were interested in investigating whether UP states are separable to several sub-types or not. It has been suggested that during sleep, reactivation of the hippocampal-cortical network can be beneficial to rearrange the cortico-cortical connections and gradually may let new memories to get independent of the hippocampus (Bontempi et al., 1999; Maviel et al., 2004; Frankland et al., 2004; Frankland & Bontempi, 2005). Consequently, as it is assumed that reactivation in cortex dominantly happens during UP state (Ji & Wilson, 2007; Euston et al., 2007; Peyrache et al., 2009), we were focusing on its characteristics to show they also can be decomposed to at least two sub-states. These sub-states are characterized by their population vector decorrelation rates and mean durations, and the sub-state with a faster decorrelation contains the majority of reactivation. Using PCA, we also showed that these sub-states are distinctively separated.

Our study suggests that instead of being a single state, UP state has different dynamics and is composed of several sub-states, each of which can be associated with different functions. The results suggest that the function of the sub-state with a faster decorrelation population is to consolidate the recent memory experience, while a slower decorrelation sub-state has other functions such as remote memory experiences.

Additionally, we have shown that the UP state dynamic is affected by the presence of reactivation and also the duration of UP state. The general tendency for the UP state is they usually start and end with UP-1; however, for short reactivating UP states, they tend to start with UP-1 but end with UP-2. This might indicate that the key function of short reactivating UP state, which is almost only composed of UP-2, is only to consolidate recent experiences. The long reactivating UP states, on the other hand, may initially associate with reactivating other experience such as remote experiences, and then transit to the recent experience during the UP-2.

Also, one of the goals of this research was to find the optimum number of sub-states for HMM, which can bring the highest strength for clustering distant. The results suggest the three-state HMM, generating DOWN state and two UP sub-states, has the optimum strength for cluster distance. As a result, however, there is usually a sub-state containing the majority of reactivation, regardless of the number of sub-states, clustering the UP state to two UP sub-states seems to be the best clustering approach. This postulates that there are two major distinct dynamics in the UP state. It is also consistent with the idea that one UP sub-state is mainly associated with the recent memory and the other related to the remote memories.

Studying the differences between UP state happening in the pre-task sleep and post-task sleep, it can be claimed that the task-experience may change the dynamic of UP state to mediate the presence of reactivation. Even though there are two UP sub-states in the pre-task sleep, and one of them has a relatively faster vector decorrelation, they cannot be distinguished by the reactivation distribution, in contrast to the post-task sleep. This may indicate that the task effect can induce a similar neural activity pattern, which the animal had experienced during the task, in the post-task sleep. This could change one of the sub-dynamics of UP state more, the one with a relatively faster vector decorrelation, which is more susceptible to be induced by new patterns, and this would lead to predominant reactivation distribution across this UP sub-state.

The PCA analysis results for pre-task and post-task sleeps together proposed that for the post-task sleep UP sub-states have a higher cluster distance, may claim that the experience of task can increase the differences in the dynamics of UP sub-state in the post-task sleep in comparison to pre-task sleep.

Even though there is no significant difference in the cortex LFP power, and especially spindle power, during UP-1 and UP-2, the results showed that during UP-2, SWRs in the hippocampus have a relatively stronger power, proposing the cortex is led by SWRs more during UP-2 (Mean and std of log mean power for UP-1 and UP-2, for three data sets we have, are -1.79 ± 0.72 dB and -1.47 ± 0.96 dB, respectively). This is consistent with the previous finding of the memory consolidation theory (Frankland & Bontempi, 2005).

4.1. Future work

This study shows that in addition to the SWRs (Ramirez-Villegas et al., 2015), also UP states are separable to sub-states. As it is shown that memory reactivation mainly occurs during SWRs in the hippocampus and this study found memory reactivation is dominant in one of the UP sub-states in the cortex, the relation between SWRs sub-types and UP sub-states is interesting. By designing the behavioural task during which the animal multi-unit activities can be recorded from both the hippocampus and the cortex, first, it can be investigated that is there any sub-state in SWRs to contain the reactivation happening in the hippocampus dominantly? If that is the case, the relationship between their sub-states, the hippocampus and the cortex, would be interesting. The expectation might be that there is a higher correlation between the sub-types of the hippocampus and the cortex during which the reactivation predominantly occurs in them.

By having enough days of recording to be matched with the learning curves of the mentioned experimental task, another interesting question is how the occurrence of reactivation in both the hippocampal and the cortex would change during the different days of the learning curve. More specifically, we are interested to see how the UP state dynamics, and UP-1 and UP-2 features will change undergoing learning days. The prediction might be as the animal undergoes to days with the highest number of reactivation, UP state dynamic experiences the most changes. Also, we can study the relationship of sub-states, UP-1 and UP-2, with those reactivation happening during the SWRs in the hippocampus, for different days of recording. Additionally, investigating the changes in some features of UP sub-states such as state vector decorrelation and reactivation distribution in these sub-states in different recording days could be

interesting. Again, the prediction could be UP-1 and UP-2 would have the most different values for those features when the animal experience the highest number of template matching.

In this study, we found that the UP state tends to start and end with different dynamics in the presence of the reactivation. As a result, the more detailed study of the changes in the UP state dynamic, for different days of recording, can be interesting.

Further studies on pre-task sleep can show whether UP state dynamics are different from the post-task ones.

4.2. Conclusion

In this thesis, we were interested to see whether the UP states similar to SWRs can be separated into different subs-states or not. Applying a three-state HMM on the epochs of high UP and DOWN oscillations, the DOWN state was detected and then distinguished by a significantly lower firing rate and duration. Also, two UP sub-states were detected and then distinguished by their state vector decorrelations and durations. We called the UP sub-state with a faster decaying rate and the lower mean duration UP-2, and the slower decaying rate and the higher mean duration UP-1. Additionally, UP-2 has a comparatively higher mean firing rate than UP-1; also, UP-2 has much less variety in its duration distribution in comparison to UP-1, and the mean duration of UP-2 is significantly lower than UP-1. Most importantly, although the UP-1 is the dominant UP sub-state and the UP states were mainly composed of it, we have shown that the other UP sub-state, UP-2, contains the majority of reactivation. By using PCA to cluster the

normalized firing rate events of UP sub-states, the result asserted that the two UP sub-states are distinctly clustered.

Different ways of visualization have been used to show how precisely the reactivation of recent experience was distributed. By depicting the UP sub-states based on their durations, we showed how the reactivation distributed across UP states with different durations. The results claimed that there are no preferences for reactivation to happen more in longer UP state or the shorter one. Then, by using chronologically sorting, we tried to find whether the reactivation happens mostly within a specific time of sleep. But, again, we could not find any particular time of sleep during which the reactivation happens the most.

Our results asserted that the presence of the reactivation in the UP state could change the firing rate within the UP state. UP state firing rate is usually the highest at the start and the end of the UP state and decreases in the middle, but for the reactivating UP states the firing rate increases at the middle where there is relatively more reactivation.

The presence of reactivation can change the composition of the UP state as well. UP state usually starts and ends with UP-1, but for long reactivating UP states, they mainly start with UP-1 but mostly end with UP-2. Also, for short reactivating UP states, they dominantly consist of UP-2, start and end with it mainly. Also, by comparing these results to the non-activating long and short UP states, we concluded that the composition of the UP states for them is similar to the general tendency for all UP states and in contrast with reactivating UP states. Both the short and long non-activating UP states start and end with UP-1 mostly.

For the pre-task sleep also the same analysis was performed. Similar to post-task sleep, one sub-state had a faster vector decorrelation, and then the UP sub-states were distinguished based on that. On the other hand, by using PCA analysis, the cluster distance was compared to the post-task sleep, indicating for pre-task sleep, the sub-states are not as clearly clustered as the post-task sleep.

Our results suggest that regardless of the number of state for HMM, there is one UP sub-state contains the majority of reactivation (That is always true for six-state HMM or less). This UP sub-state usually accompanied by a very fast vector decorrelation, not necessarily the fastest and a high mean firing rate, not necessarily the highest. We also showed that the strength of cluster distance decreases by the increase in the state of HMM application. As a result, three-state HMM generates the most distinct clusters for sub-states of UP state.

Reference

- Ambrose, R. E., Brad E. Pfeiffer, B. E., & Foster D. J. Reverse replay of hippocampal place cells is uniquely modulated by changing reward. *Neuron*. 91(5): p 1124–1136. 2016.
- Amzica, F., & Steriade, M. The K-complex: Its slow (< 1-Hz) rhythmicity and relation to delta waves. *Neurology*, 49(4), p 952–959. 1997.
- Barrett TR, Ekstrand BR. Effect of sleep on memory. 3. Controlling for time-of-day effects. *J Exp Psychol* 93: 321-327, 1972.
- Battaglia, F. P., Benchenane, K., Sirota, A., Pennartz, C. M., & Wiener, S. I. The hippocampus: Hub of brain network communication for memory. *Trends in Cognitive Sciences*, 15(7), p 310–318. 2011.
- Battaglia, F. P., Sutherland, G. R., & McNaughton, B. L. Hippocampal sharp wave bursts coincide with neocortical “up-state” transitions. *Learning & Memory*, 11(6), p 697–704. 2004.
- Bazhenov M Timofeev I Steriade M Sejnowski TJ. Model of thalamocortical slow-wave sleep oscillations and transitions to activated states. *J. Neurosci*. 22: p 8691-8704. 2002.
- Bontempi, B., Laurent-Demir, C., Destrade, C., and Jaffard, R. Time dependent reorganization of brain circuitry underlying long-term memory storage. *Nature* 400: p 671 -674. 1999.
- Bramham, C. R.; Messaoudi, E. BDNF function in adult synaptic plasticity: The synaptic consolidation hypothesis. *Progress in Neurobiology*. 76 (2): 99–125, 2005.
- Brown, E. N., Frank, L., And Wilson, M. Statistical approaches to place field estimation and neuronal population decoding. *Soc. Neurosci. Abstr.* 22: 910, 1996.
- Brown, E.N., Frank, L.M., Tang, D., Quirk, M.C., and Wilson, M.A. A statistical paradigm for neural spike train decoding applied to position prediction from ensemble firing patterns of rat hippocampal place cells. *J. Neurosci*. 18, 7411-7425. 1988.
- Buzsaki, G. Hippocampal sharp waves - their origin and significance. *Brain Res*, 398: p 242–252, 1986.
- Buzsaki, G. Two-stage model of memory trace formation: A role for “noisy” brain states. *Neuroscience*, 31(3), p 551–570. 1989.

- Buzsaki, G., Hippocampal sharp wave-ripple: A cognitive biomarker for episodic memory and planning. *Hippocampus* 25: p 1073-1183, 2015.
- Buzsaki, G., Horvath, Z., Urioste, R., Hetke, J. & Wise, K. High-frequency network oscillation in the hippocampus. *Science* 256: p 1025–1027, 1992.
- Buzsaki, G., Leung, L. W. & Vanderwolf, C. H. Cellular bases of hippocampal EEG in the behaving rat. *Brain Res*, 287: p 139–171, 1983.
- Carlson, Neil R. (2012). *Physiology of Behavior*. Pearson. p. 291,293.
- Carr, M. F., Jadhav, Sh. P. & Frank, L. M. Hippocampal replay in the awake state: a potential physiological substrate of memory consolidation and retrieval. *Nat Neurosci*, 14: p 147-153, 2011.
- Compte A Sanchez-Vives MV McCormick DA and Wang X-J. Cellular and network mechanisms of slow oscillatory activity (<1 Hz) and wave propagations in a cortical network model. *J. Neurophysiol.* 89: p 2707-2725. 2003
- Cossart, R., Aronov, D., and Yuste, R. Attractor dynamics of network UP states in the neocortex. *Nature* 423, p 283–288. 2003.
- Cowan, R. L., and Wilson, C. J. Spontaneous firing patterns and axonal projections of single corticostriatal neurons in the rat medial agranular cortex. *J. Neurophysiol.* 71, p 17–32. 1994.
- Dave AS, Margoliash D. Song replay during sleep and computational rules for sensorimotor vocal learning. *Science*; 290: p 812–816. 2000.
- Davidson, T. J Kloosterman, F. & Wilson, M. A. Hippocampal replay of extended experience. *Neuron*, 63(4): p 497–507, 2009.
- Dempster, A., Laird, N., Rubin, D. Maximum likelihood from incomplete data via the EM algorithm. *J R Stat Soc Ser B* 39: p 1–38. 1977.
- Destexhe A, Rudolph M and Pare D. the high-conductance state of neocortical neurons in vivo. *Nat. Rev. Neurosci.* 4: p 739-751. 2003.
- Destexhe, A. & Sejnowski, T. J. Interactions between membrane conductances underlying thalamocortical slow-wave oscillations. *Physiol. Rev.* 83: p 1401-1453. 2003.
- Dudai, Y. The Neurobiology of Consolidations, Or, How Stable is the Engram? *Annual Review of Psychology.* 55: 51–86, 2004.
- Ego-Stengel, V., Wilson, M. A. Disruption of ripple-associated hippocampal activity during rest impairs spatial learning in the rat. *Hippocampus*, 20: p 1–10, 2010.

- English, D. F., Peyrache, A., Stark, E., Roux, L., Vallentin, D., Long, M. A. & Buzsaki, G. Excitation and inhibition compete to control spiking during hippocampal ripples: intracellular study in behaving mice. *J Neurosci*, 34: p 16509–16517, 2014.
- Euston, D. R., Tatsuno, M. & McNaughton, B. L. Fast-forward playback of recent memory sequences in prefrontal cortex during sleep. *Science* 318: p 1147-1150, 2007.
- Fellous, J., Tiesinga, P. H. E., Thomas, P. J., Sejnowski, T. J. Discovering Spike Patterns in Neuronal Responses. *J Neurosci* 24, p 2989-3001. 2004.
- Fenn K. M., Hambrick D. Z. Individual differences in working memory capacity predict sleep-dependent memory consolidation. *J Exp Psychol Gen.* 2011.
- Fishbein W. Disruptive effects of rapid eye movement sleep deprivation on long-term memory. *Physiol Behav* 6: p 279–282, 1971.
- Foldiak P. The “ideal humunculus”: statistical inference from neural population responses. In: *Computation and Neural Systems 1992*, edited by F. Eeckman and J. Bower. Norwell, MA: Kluwer, 1993.
- Foster, D. J. & Wilson, M. A. 2006 Reverse replay of behavioural sequences in hippocampal place cells during the awake state. *Nature* 440, 680-683.
- Frankland, P. W., Bontempi, B. The organization of recent and remote memories. *Nature Reviews Neuroscience*. 6 (2): 119–130. 2005.
- Frankland, P.W., Bontempi, B., Talton, L.E., Kaczmarek, L., and Silva, A.J. The involvement of the anterior cingulate cortex in remote contextual fear memory. *Science* 304: p 881-883. 2004.
- Genzel, L., Kroes, MC., Dresler, M. & Battaglia, FP. Light sleep versus slow wave sleep in memory consolidation: a question of global versus local processes? *Trends in Neurosciences*, vol 37, No.1, 2014.
- Gerrard, J. L., Ginzburg, I., Barnes, C. A., Sejnowski, T. J., And McNaughton, B. L. Accuracy of hippocampal place fields in predicting location is enhanced in the presence of theta rhythm. *Soc. Neurosci. Abstr.* 21: 942, 1995.
- Ghorbani, M., Mehta, M., Bruinsma, R. & Levine, A. J. Nonlinear-dynamics theory of up-down transitions in neocortical neural networks. *Phys Rev E Stat Nonlin Soft Matter Phys* 85, 021908, 2012.
- Girardeau, G., Benchenane, K., Wiener, S. I., Buzsaki, G., Zugaro, M. B. Selective suppression of hippocampal ripples impairs spatial memory. *Nature Neuroscience*. 12: p 1222–1223, 2009.
- Giri, B., Miyawaki, H., Mizuseki, K., Cheng, S. & Diba, K. Hippocampal Reactivation Extends for Several Hours Following Novel Experience. *J Neurosci* 39, p 866-875. 2019. (DOI:10.1523/JNEUROSCI.1950-18.2018).

- Gothard, K. M., Skaggs, W. E., Moore, K. M. & McNaughton, B. L. Binding of hippocampal CA1 neural activity to multiple reference frames in a landmark-based navigation task. *J Neurosci* 16, p 823-835. 1996.
- Gutwein BM , Fishbein W. Paradoxical sleep and memory (I): selective alterations following enriched and impoverished environmental rearing. *Brain Res Bull* 5: p 9–12, 1980.
- Haider B, Duque A, Hasenstaub AR and McCormick DA. Neocortical network activity in vivo is generated through a dynamic balance of excitation and inhibition. *J. Neurosci.* 26: p 4535-4545. 2006.
- Harris, K, D. & Thiele, A. Cortical State and Attention. *Nat Rev Neurosci* 12: p 509-523, 2012.
- Hebb, D. 1949 *The Organization of Behavior*. New York, Wiley.
- Hoffman, K. L. & McNaughton, B. L. 2002 Coordinated reactivation of distributed memory traces in primate neocortex. *Science* 297, 2070-2073.
- Holcman D and Tsodyks M. The emergence of up and down states in cortical networks. *PLOS Computational Biology* 2: p 174-181. 2006.
- Isomura, Y., Sirota, A., Özen, S., Montgomery, S., Mizuseki, K., Henze, D. A., & Buzsáki, G. Integration and segregation of activity in entorhinal-hippocampal subregions by neocortical slow oscillations. *Neuron*, 52(5), p 871–882. 2003.
- Jenkins JG, Dallenbach KM. Obliviscence during sleep and waking. *Am J Psychol* 35: p 605-612, 1924.
- Ji, D. & Wilson, M. A. Coordinated memory replay in the visual cortex and hippocampus during sleep. *Nat Neurosci* 10, p 100-107. 2007.
- Johnson, L. A., Euston, D. R., Tatsuno, M., & McNaughton, B. L. Stored-trace reactivation in rat prefrontal cortex is correlated with down-to-up state fluctuation density. *J Neurosci*, 30(7), p 2650-2661. 2010.
- Joo H. R. & Frank L. M., The hippocampal sharp wave–ripple in memory retrieval for immediate use and consolidation. *Nature Reviews Neuroscience*, 19: p 744-757, 2018.
- Joshua E. Brinkman; Sandeep Sharma, *Physiology, Sleep*, StatPearls Publishing, Jan. 2018.
- Karni A, Tanne D, Rubenstein BS , Askenasy JJ , Sagi D. Dependence on REM sleep. *Science*: p 679–682, 1994.

Korman, M., Doyon, J., Doljansky, J., Carrier, J., Dagan Y. & Avi Karni. Daytime sleep condenses the time course of motor memory consolidation. *Nat Neurosci* 10: p 1206-1213, 2007.

Kudrimoti, H. S., Barnes, C. A. & McNaughton, B. L. Reactivation of hippocampal cell assemblies: effects of behavioral state, experience, and EEG dynamics. *J Neurosci* 19, p 4090-4101. 1999.

Lansink, C. S., Goltstein, P. M., Lankelma, J. V., Joosten, R. N., McNaughton, B. L., & Pennartz, C. M. Preferential reactivation of motivationally relevant information in the ventral striatum. *J Neurosci*, 28(25), p 6372-6382. 2008.

Laureys S , Peigneux P , Phillips C , Fuchs S , Degueldre C , Aerts J , Del Fiore G , Petiau C , Luxen A , van der Linden M , Cleeremans A , Smith C , Maquet P. Experience-dependent changes in cerebral functional connectivity during human rapid eye movement sleep. *Neuroscience* 105: p 521–525, 2001.

Lee, A. K. & Wilson, M. A. Memory of sequential experience in the hippocampus during slow wave sleep. *Neuron* 36, p 1183-1194. 2002.

Luczak, A., Bartho, P., Marguet, S. L., Buzsaki, G. & Harris, K. D., Sequential structure of neocortical spontaneous activity in vivo. *Proc Natl Acad Sci U S A* 104, p 347-352. 2007.

Maquet P, Laureys S, Peigneux P, Fuchs S, Petiau C, et al. Experience-dependent changes in cerebral activation during human REM sleep. *Nat Neurosci.* ;3: p 831–836. 2000.

Marr D., Willshaw D., McNaughton B. (1991) Simple Memory: A Theory for Archicortex. In: Vaina L. (eds) *From the Retina to the Neocortex*. Birkhäuser Boston

Marr, D. Simple memory: A theory for archicortex. *Philosophical Transactions of the Royal Society of London*, 262, p 23–81. 1971.

Maviel, T., Durkin, T.P., Menzaghi, F., and Bontempi, B. Sites of neocortical reorganization critical for remote memory. *Science* 305: p 96 -99. 2004.

McClelland, J. L., McNaughton, B. L., & O'reilly, R. C. Why there are complementary learning systems in the hippocampus and neocortex: Insights from the successes and failures of connectionist models of learning and memory. *Psychological Review*, 102(3), 419. 1995.

McFarland, J. M., Hahn, T. T. & Mehta, M. R. Explicit-duration hidden Markov model inference of UP-DOWN states from continuous signals. *PLoS One* 6, e21606. 2011. (DOI:10.1371/journal.pone.0021606).

McNaughton, B. L. Cortical hierarchies, sleep, and the extraction of knowledge from memory. *Artificial Intelligence*, 174(2), p 205–214. 2010.

- Nadasdy, Z., Hirase, H., Czurko, A., Csicsvari, J. & Buzsáki, G. Replay and time compression of recurring spike sequences in the hippocampus. *J Neurosci* 19, p 9497-9507. 1999.
- Nadasdy, Z., Hirase, H., Czurkó, A., Csicsvari, J., & Buzsáki, G. Replay and time compression of recurring spike sequences in the hippocampus. *Josilvaurnal of Neuroscience*, 19(21), p 9497–9507. 1999.
- Nadel, L., Moscovitch, M. Memory consolidation, retrograde amnesia and the hippocampal complex. 1997.
- Navarro-Lobato, I. & Genzel, L. The up and down of sleep: From molecules to electrophysiology. *Neurobiology of Learning and Memory* 160: p 3-10, 2019.
- O’Keefe, J. & Nadel, L. *The Hippocampus as a Cognitive Map*. Oxford Univ. Press, 1978.
- P. W. Frankland, B. Bontempi, L. E. Talton, L. Kaczmarek, A. J. Silva. The involvement of the anterior cingulate cortex in remote contextual fear memory. *Science* 304, 881, 2004.
- Pare D Shink E Gaudreau H Destexhe A and Lang E. Impact of spontaneous synaptic activity on the resting properties of cat neocortical pyramidal neurons in vivo. *J. Neurophysiol.* 79: p 1450-1460. 1998.
- Pavlidis, C. & Winson, J. Influences of hippocampal place cell firing in the awake state on the activity of these cells during subsequent sleep episodes. *J Neurosci* 9, p 2907-2918. 1989.
- Pearlman C, Becker M. REM sleep deprivation impairs bar-press acquisition in rats. *Physiol Behav* 13: p 813–817, 1974.
- Peyrache, A., Battaglia, F. P. & Destexhe, A. Inhibition recruitment in prefrontal cortex during sleep spindles and gating of hippocampal inputs. *Proc Natl Acad Sci USA* 108, p 17207-17212. 2011.
- Peyrache, A., Benchenane, K., Khamassi, M., Wiener, S. I. & Battaglia, F. P. Sequential Reinstatement of Neocortical Activity during Slow Oscillations Depends on Cells' Global Activity. *Front Syst Neurosci* 3, 18. 2010.
- Peyrache, A., Khamassi, M., Benchenane, K., Wiener, S. I. & Battaglia, F. P. Replay of rule-learning related neural patterns in the prefrontal cortex during sleep. *Nature Neuroscience* volume 12, p 919–926. 2009.
- Plihal W, Born J. Effects of early and late nocturnal sleep on declarative and procedural memory. *J Cogn Neurosci* 9: 534-547, 1997.

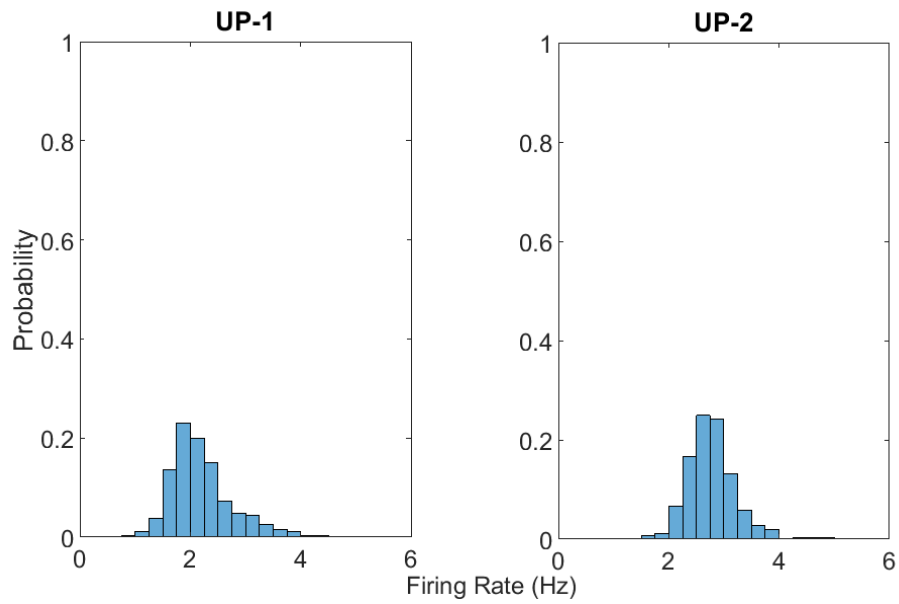
- Ponce-Alvarez, A., Nacher, V., Luna, R., Riehle, A. & Romo, R. 2012 Dynamics of cortical neuronal ensembles transit from decision making to storage for later report. *J Neurosci* 32, 11956-11969. (DOI:10.1523/JNEUROSCI.6176-11.2012).
- Psychophysiology*, 21(3), p 279-289, 1984.
- Qin, Y. L., McNaughton, B. L., Skaggs, W. E. & Barnes, C. A. Memory reprocessing in corticocortical and hippocampocortical neuronal ensembles. *Philos Trans R Soc Lond B Biol Sci* 352, p 1525-1533. 1997.
- R. Brunelli, *Template Matching Techniques in Computer Vision: Theory and Practice*, Wiley, 2009.
- Rabiner, L. R. A Tutorial on Hidden Markov-Models and Selected Applications in Speech Recognition. *P Ieee* 77, p 257-286. 1989. (DOI:Doi 10.1109/5.18626).
- Ramirez-Villegas, J. F., Logothetis, N. K. & Besserve, M. Diversity of sharp-wave-ripple LFP signatures reveals differentiated brain-wide dynamical events. *Proc Natl Acad Sci U S A* 112, E: p 6379-6387. 2015. (DOI:10.1073/pnas.1518257112).
- Rasch B, Born J. About sleep's role in memory. *Physiol Rev* 93: p 681-766, 2013.
- Ribeiro S , Gervasoni D , Soares ES , Zhou Y , Lin S , Pantoja J , Lavine M , Nicolelis MAL. Long-lasting novelty-induced neuronal reverberation during slow-wave sleep in multiple forebrain areas. *PLoS Biol* 2: E24, 2004.
- Ribeiro S , Goyal V , Mello CV , Pavlides C. Brain gene expression during REM sleep depends on prior waking experience. *Learn Mem* 6: p 500–508, 1999.
- Rigas P and Castro-Alamancos MA Thalamocortical up states: Differential effects of intrinsic and extrinsic cortical inputs on persistent activity. *J. Neurosci.* 27: p 4261-4272. 2007.
- Robinson, T. E., Kramis, R. C., & Vanderwolf, C. H. Two types of cerebral activation during active sleep: relations to behavior. *Brain Res*, 124(3), p 544-549. 1977
- Rothschild, G., Eban, E. & Frank, L. M. A cortical-hippocampal-cortical loop of information processing during memory consolidation. *Nat Neurosci* 20, p 251-259. 2017. (DOI:10.1038/nn.4457).
- Rudolph M, Pospischil M, Timofeev I, and Destexhe A. Inhibition determines membrane potential dynamics and controls action potential generation in awake and sleeping cat cortex. *J. Neurosci.* 16: p 5280-5290. 2007.
- Sanger, T. D. Probability density estimation for the interpretation of neural population codes. *J. Neurophysiol.* 76: p 2790–2793, 1996.

- Scarpetta, S. & Candia, A. D. Alternation of up and down states at a dynamical phase-transition of a neural network with spatiotemporal attractors. *Front. Syst. Neurosci.*, 19. 2014.
- Shore, E. T., Millman, R. P., Silage, D. A., Chung, D. C., & Pack, A. I. Ventilatory and arousal patterns during sleep in normal young and elderly subjects. *J Appl Physiol*, 59(5), p 1607-1615, 1985
- Shu, Y., Hasenstaub, A., and McCormick, D. A. Turning on and off recurrent balanced cortical activity. *Nature* 423, p 288–293. 2003.
- Siapas, A. G., & Wilson, M. A. Coordinated interactions between hippocampal ripples and cortical spindles during slow-wave sleep. *Neuron*, 21(5), p 1123–1128. 1998.
- Sirota, A., Csicsvari, J., Buhl, D., & Buzsáki, G. Communication between neocortex and hippocampus during sleep in rodents. *Proceedings of the National Academy of Sciences*, 100(4), p 2065–2069. 2003.
- Skaggs, W. E. & McNaughton, B. L. Replay of neuronal firing sequences in rat hippocampus during sleep following spatial experience. *Science* 271, p 1870-1873. 1996.
- Skelin, I., Kilianski, S., McNaughton, B. L. Hippocampal coupling with cortical and subcortical structures in the context of memory consolidation. *Neurobiology of Learning and Memory* 160, p 21–31. 2019.
- Smith C, Butler S. Paradoxical sleep at selective times following training is necessary for learning. *Physiol Behav.* 29(3): p 469-73. 1982.
- Smith C, Kelly G. Paradoxical sleep deprivation applied two days after end of training retards learning. *Physiol Behav* 43: p 213–216, 1988.
- Squire, L. R., Alvarez, P. Retrograde amnesia and memory consolidation: A neurobiological perspective. *Current Opinion in Neurobiology.* 5 (2): p 169–177. 1995.
- Staresina, B. P., Bergmann, T. O., Bonnefond, M., Van Der Meij, R., Jensen, O., Deuker, L., ... Fell, J. Hierarchical nesting of slow oscillations, spindles and ripples in the human hippocampus during sleep. *Nature Neuroscience*, 18(11), p 1679–1686. 2015.
- Stark, E., Roux, L., Eichler, R., Senzari, Y., Royer, S., Buzsaki, G. Pyramidal cell-interneuron interactions underlie hippocampal ripple oscillations. *Neuron* 83: p 467–480, 2014.
- Steriade, M. & McCarley, R. W. *Brainstem control of wakefulness and sleep.* Second edition. Springer, 2005.

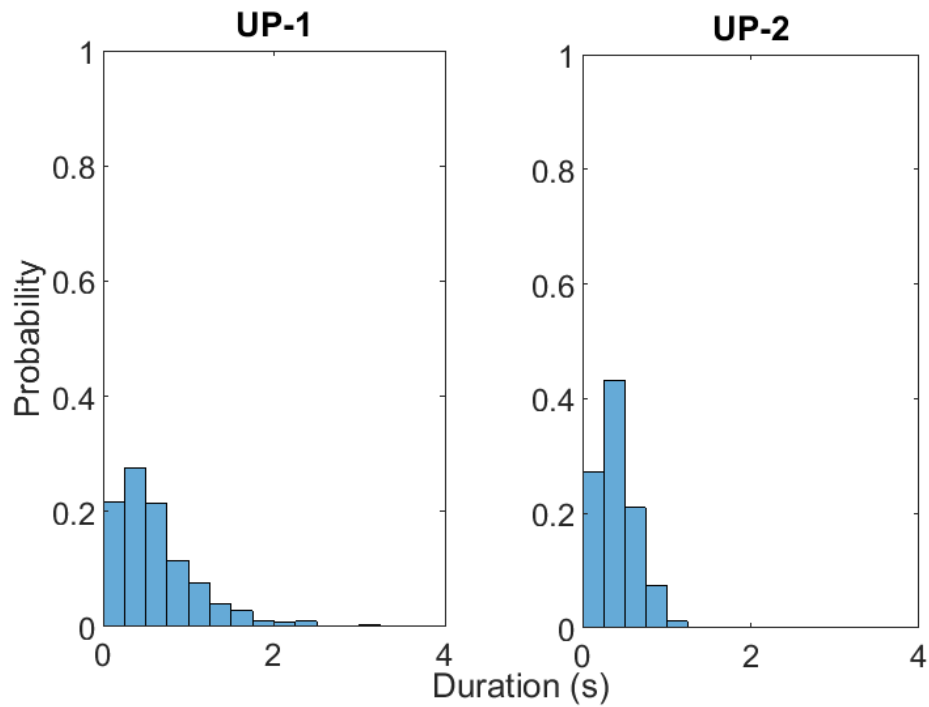
- Steriade, M., McCormick, D. A., & Sejnowski, T. J. Thalamocortical oscillations in the sleeping and aroused brain. *Science*, 262(5134), p 679-685, 1993.
- Steriade, M., Timofeev, I., & Grenier, F. Natural waking and sleep states: a view from inside neocortical neurons. *J Neurophysiol*, 85(5), p 1969-1985, 2001.
- Stickgold R , James L , Hobson JA. Visual discrimination learning requires sleep after training. *Nat Neurosci* 3: p 1237–1238, 2000.
- Stickgold R, James L, Hobson JA. Visual discrimination learning requires sleep after training. *Nat Neurosci* 3: p 1237-1238, 2000.
- Sullivan, D., Csicsvari, J., Mizuseki, K., Montgomery, S., Diba, K., & Buzsaki, G., Relationships between hippocampal sharp waves, ripples, and fast gamma oscillation: influence of dentate and entorhinal cortical activity. *J Neurosci*, 31: p 8605–8616, 2011.
- Suzuki, S. S. & Smith, G. K., Spontaneous EEG spikes in the normal hippocampus. V. Effects of ether, urethane, pentobarbital, atropine, diazepam and bicuculline. *Electroencephalogr. Clin. Neurophysiol.* 70: p 84–95, 1988.
- Suzuki, S. S. & Smith, G. K., Spontaneous EEG spikes in the normal hippocampus. I. Behavioral correlates, laminar profiles and bilateral synchrony. *Electroencephalogr. Clin. Neurophysiol*, 67: p 348–359, 1987.
- T. Maviel, T. P. Durkin, F. Menzaghi, B. Bontempi, Sites of neocortical reorganization critical for remote spatial memory. *Science* 305, 96, 2004.
- Takashima A, Petersson KM, Rutters F, Tendolkar I, Jensen O, Zwarts MJ, McNaughton BL, Fernández G. Declarative memory consolidation in humans: a prospective functional magnetic resonance imaging study. *Proc. Natl. Acad. Sci. U.S.A.* 103,756, 2006.
- Tatsuno, M., Lipa, P. & McNaughton, B. L. Methodological considerations on the use of template matching to study long-lasting memory trace replay. *J Neurosci* 26, p 10727-10742. 2006.
- Teyler, T. J., & DiScenna, P. The hippocampal memory indexing theory. *Behavioral Neuroscience*, 100(2), 147. 1986.
- Timofeev, I., Contreras, D. & Steriade, M. Synaptic responsiveness of cortical and thalamic neurons during various phases of slow sleep oscillation in cat. *J. Physiol.* 494: p 265-278. 1996.
- Timofeev, I., Grenier, F. & Steriade, M. Disfacilitation and active inhibition in the neocortex during the natural sleep-wake cycle: an intracellular study. *PNAS* 98: p 1924-1929. 2001.

- Timofeev, I., Grenier, F., Bazhenov, M., Sejnowski, T. J. & Steriade, M. Origin of slow cortical oscillations in deafferented cortical slabs. *Cereb. Cortex* 10: p 1185-1199. 2000.
- Tononi, G. & Cirelli, C. Sleep and the price of plasticity: from synaptic and cellular homeostasis to memory consolidation and integration. *Neuron*, 8;81(1): p12-34, 2014 Jan.
- Vanderwolf, C. H., Hippocampal electrical activity and voluntary movement in the rat. *Electroencephalogr. Clin. Neurophysiol.* 26, p 407–418, 1969.
- Waters J and Helmchen F. Background synaptic activity is sparse in neocortex. *J.Neurosci.* 26: p 8267-8277. 2006.
- Wilson, C.J. and Kawaguchi, Y. The origins of two-state spontaneous membrane potential fluctuations of neostriatal spiny neurons. *J. Neurosci.* 16: p 2397-2410. 1996.
- Wilson, M. A. & McNaughton, B. L. Reactivation of hippocampal ensemble memories during sleep. *Science* 265: p 676-679, 1994.
- Wu. X & Foster D. J. Hippocampal Replay Captures the Unique Topological Structure of a Novel Environment. *J Neurosci.* 34(19): p 6459–6469. 2014.
- Yuste R, MacLean JN, Smith, J. and Lasner A. The cortex as a central pattern generator. *Nature Reviews Neuroscience* 6: p 477-483. 2005.
- Zemaityte, D., Varoneckas, G., & Sokolov, E. Heart rhythm control during sleep. *Psychophysiology.* Pages 279-289. 1984.
- Zhang, K., Ginzburg, I., McNaughton, B. L., and Sejnowski, T. J. Interpreting Neuronal Population Activity by Reconstruction: Unified Framework With Application to Hippocampal Place Cells. *Journal of Neurophysiology*, 79(2): p 1017-1044. 1998.
- Zoubin Ghahramani. An Introduction to Hidden Markov Models and Bayesian Networks. *International Journal of Pattern Recognition and Artificial Intelligence* 15: p 9-42. 2001.

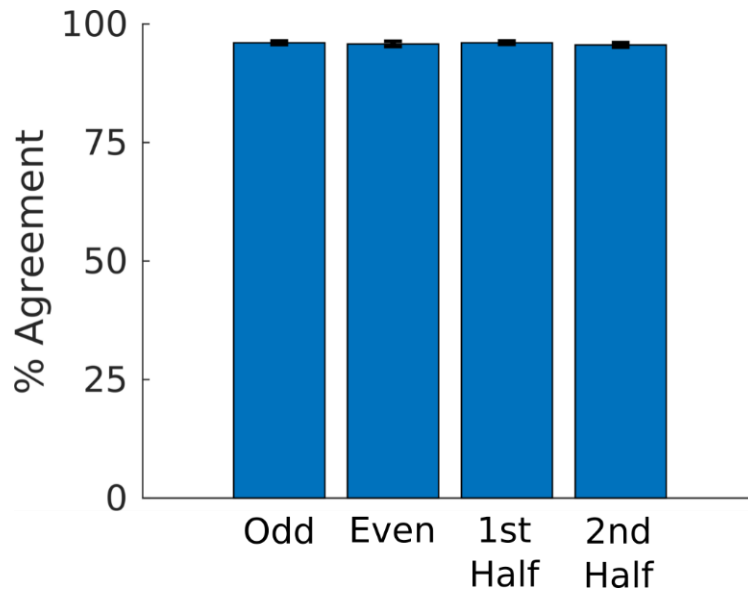
Appendix



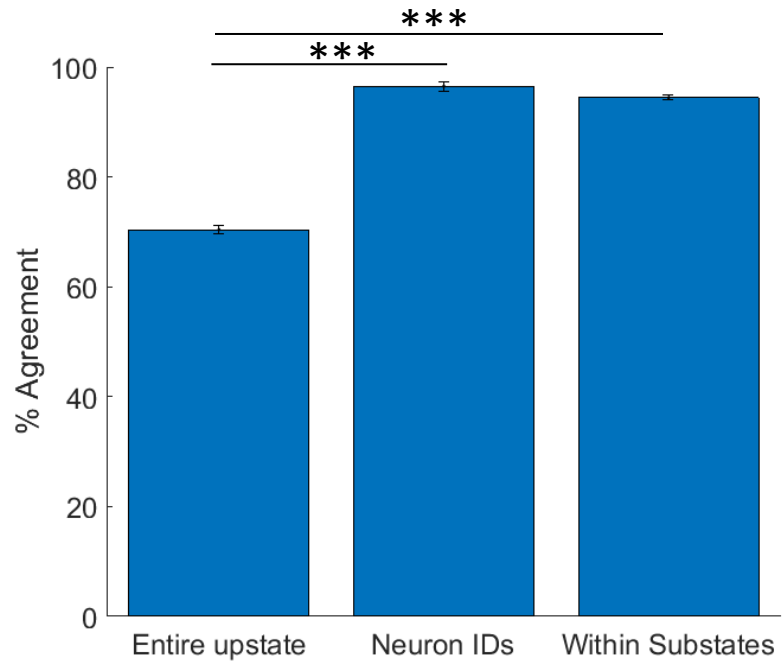
Supplementary Figure 1. Firing rate distribution for UP-1 and UP-2, in two different panels, for a representative case.



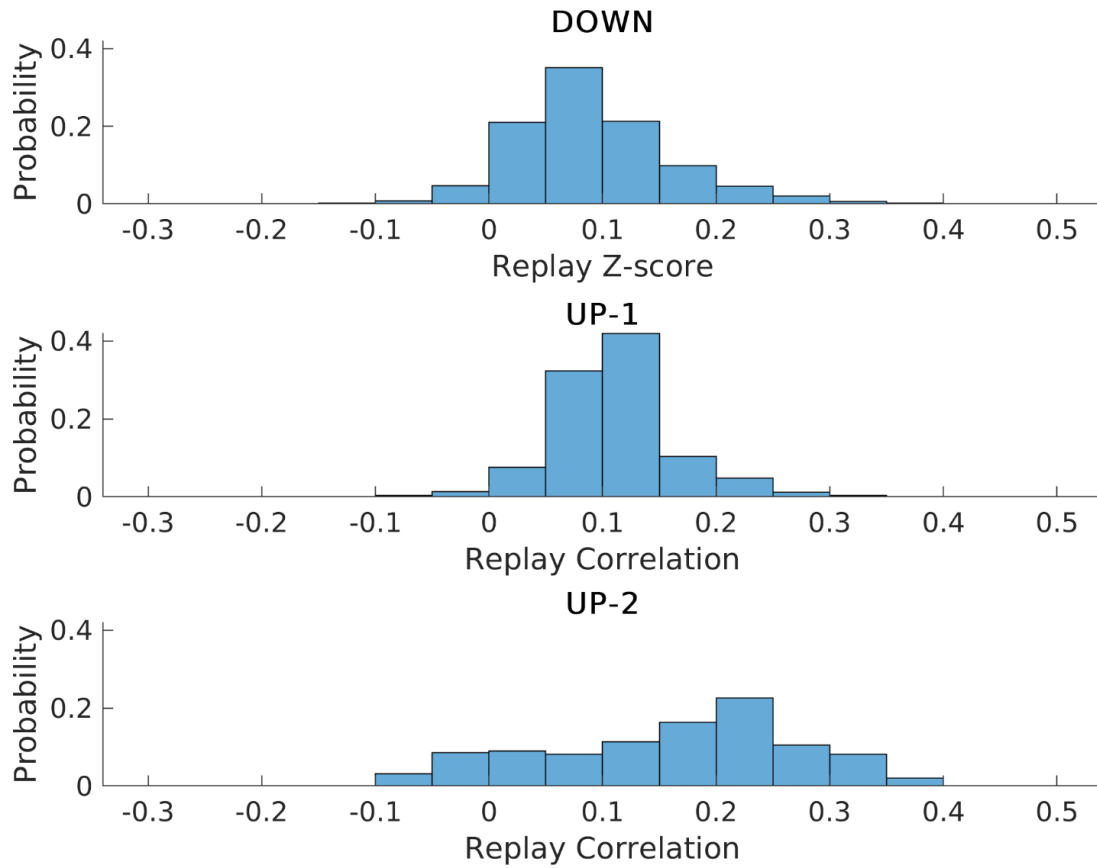
Supplementary Figure 2. Duration distribution for UP-1 and UP-2, in two different panels, for a representative case.



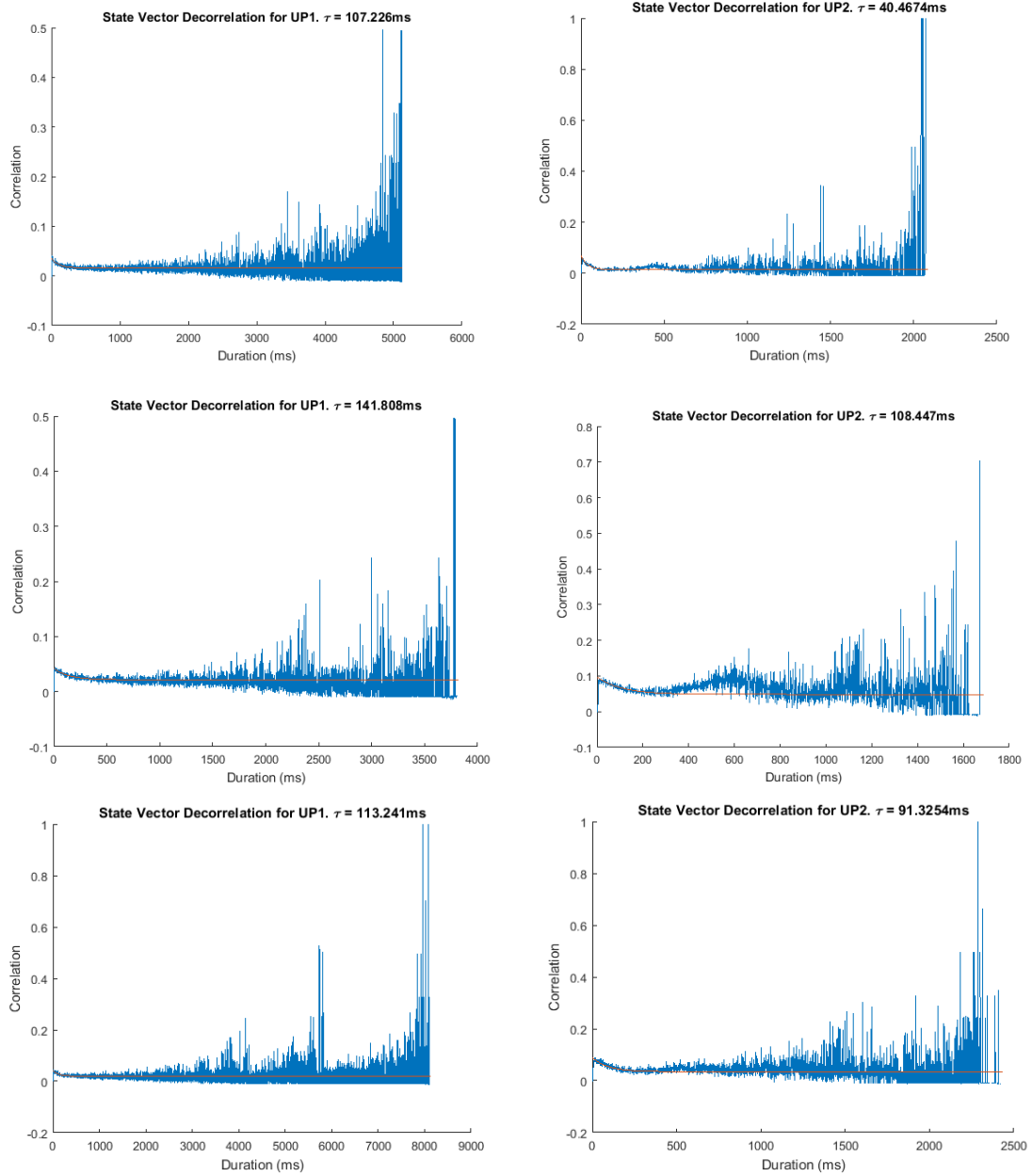
Supplementary Figure 3. Consistency of HMM Using Partial Data.



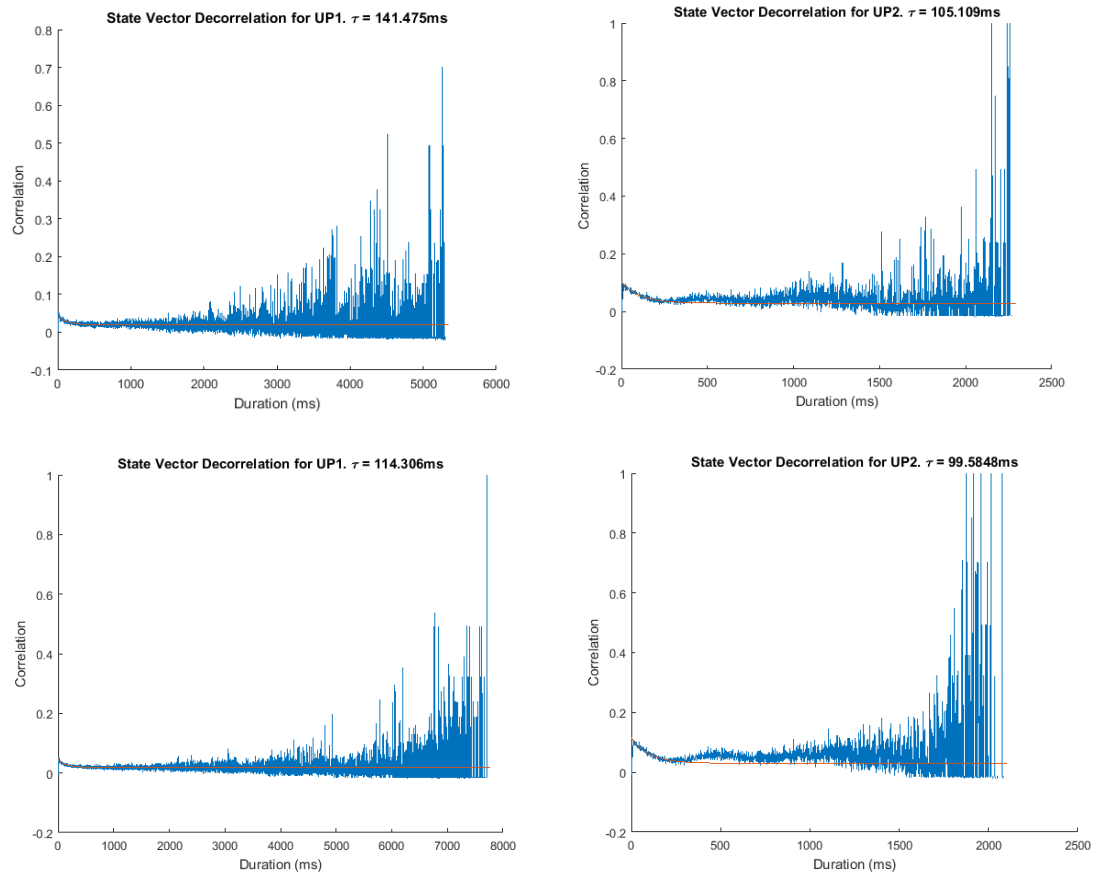
Supplementary Figure 4. Percent Agreement for Shuffled HMM.



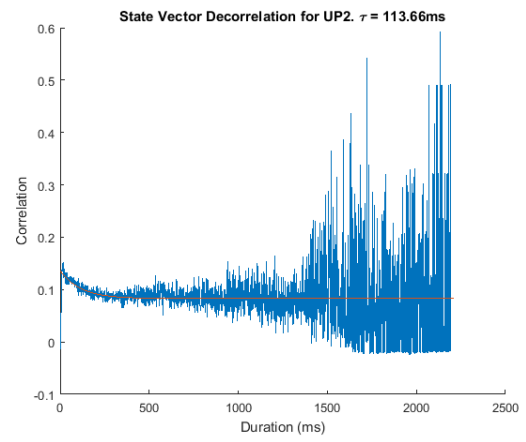
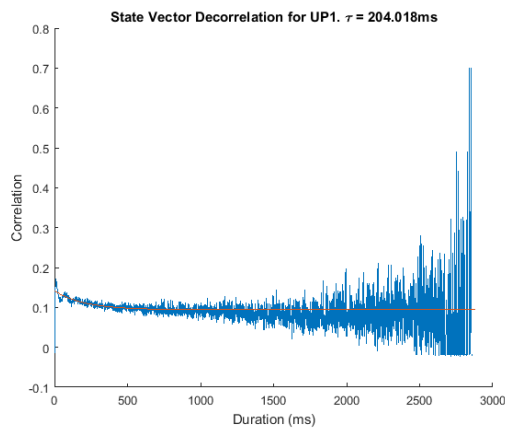
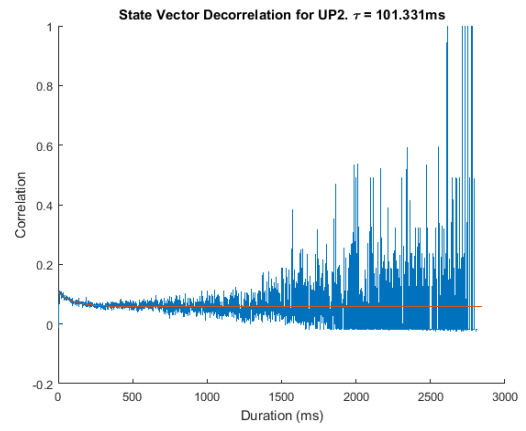
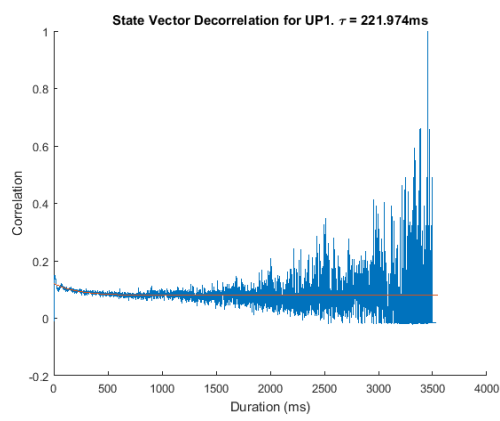
Supplementary Figure 5. The result of template matching correlation distribution.



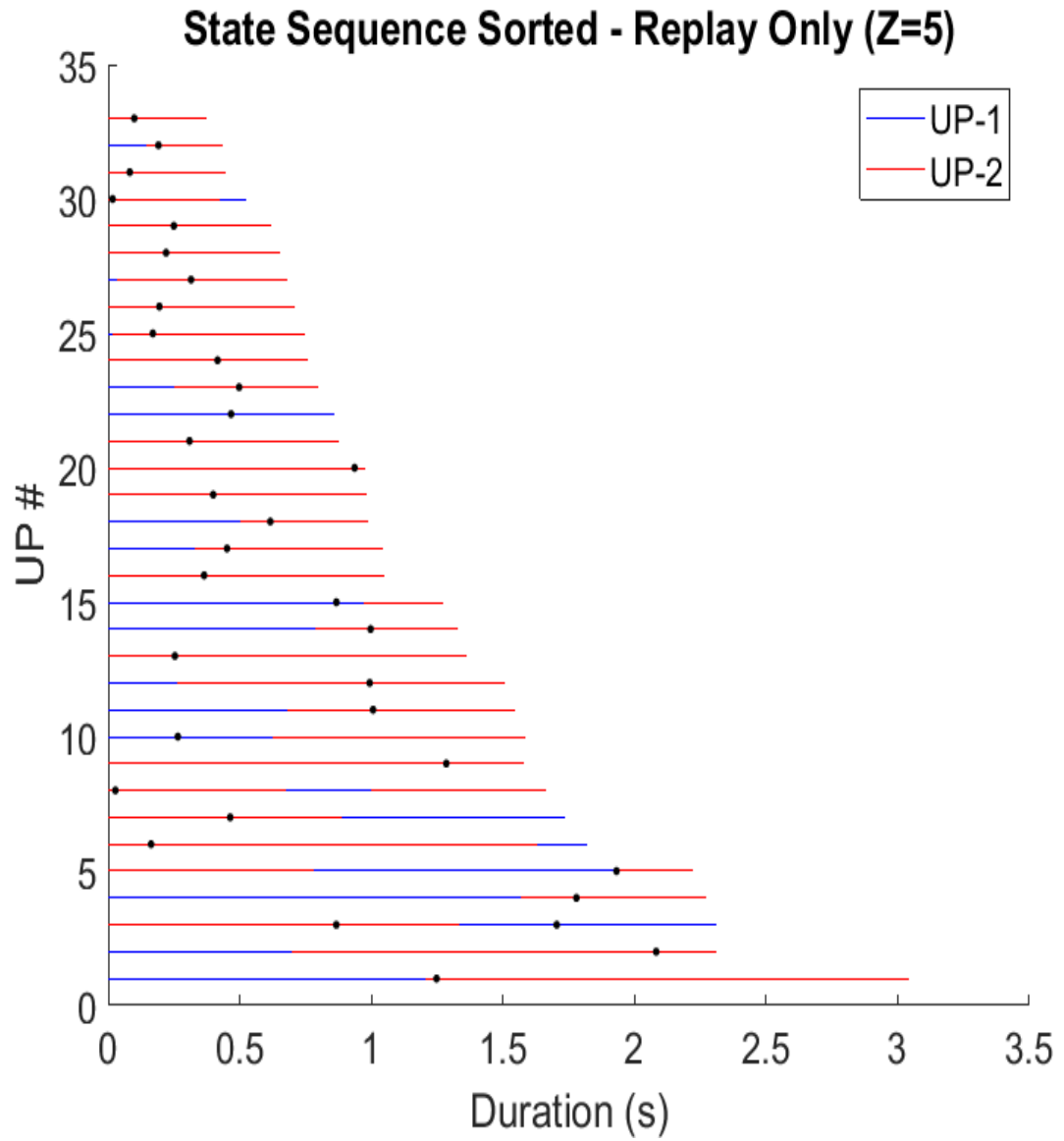
Supplementary Figure 6. State Vector Decorrelation. (Rat1)



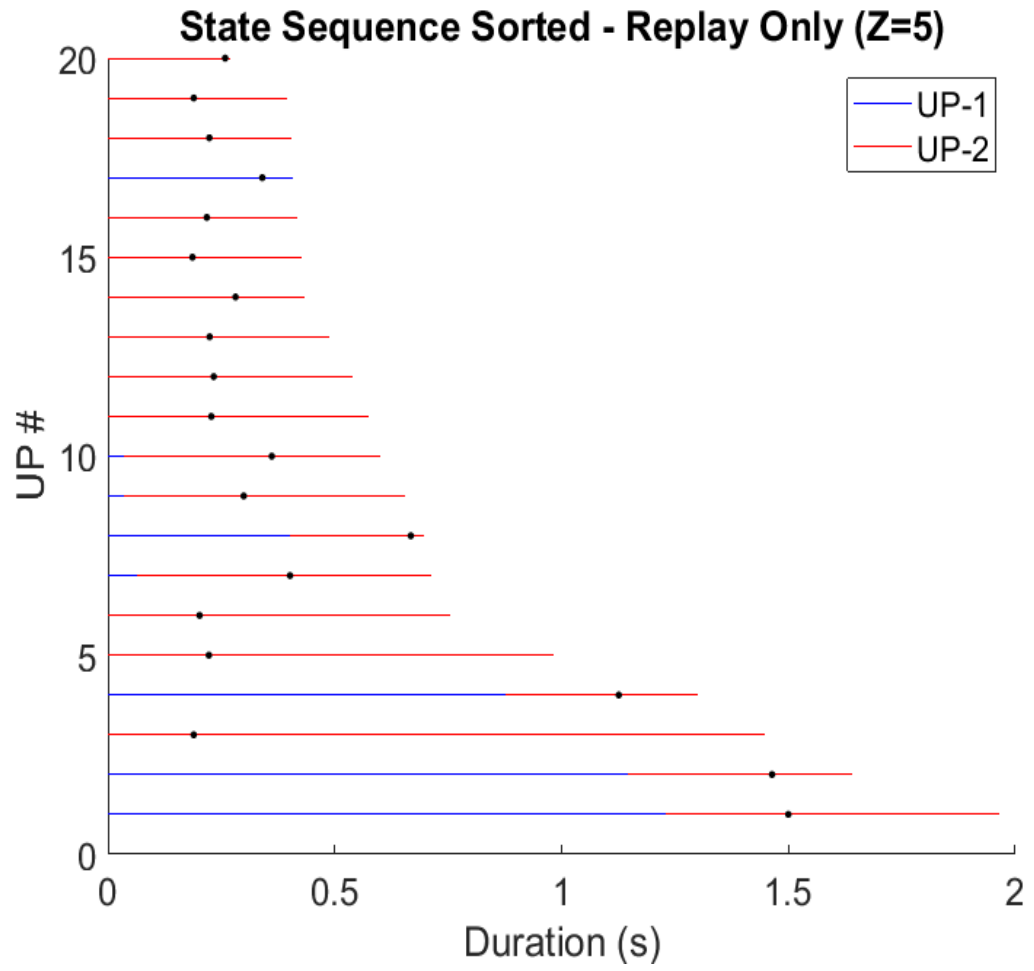
Supplementary Figure 7. State Vector Decorrelation. (Rat2)



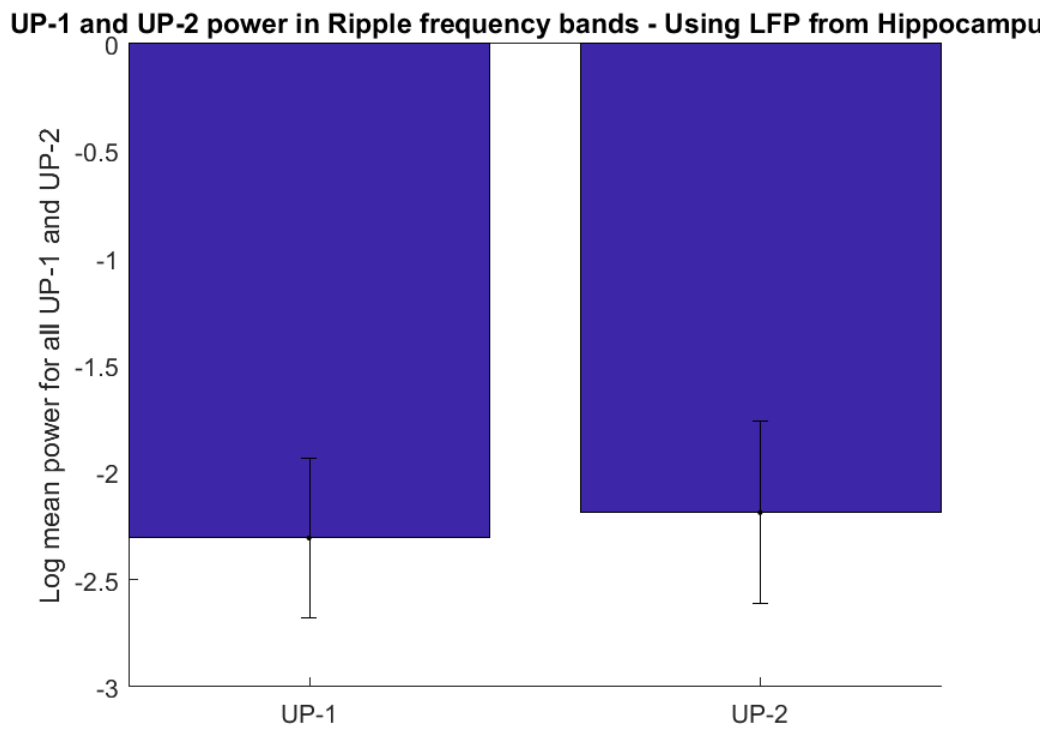
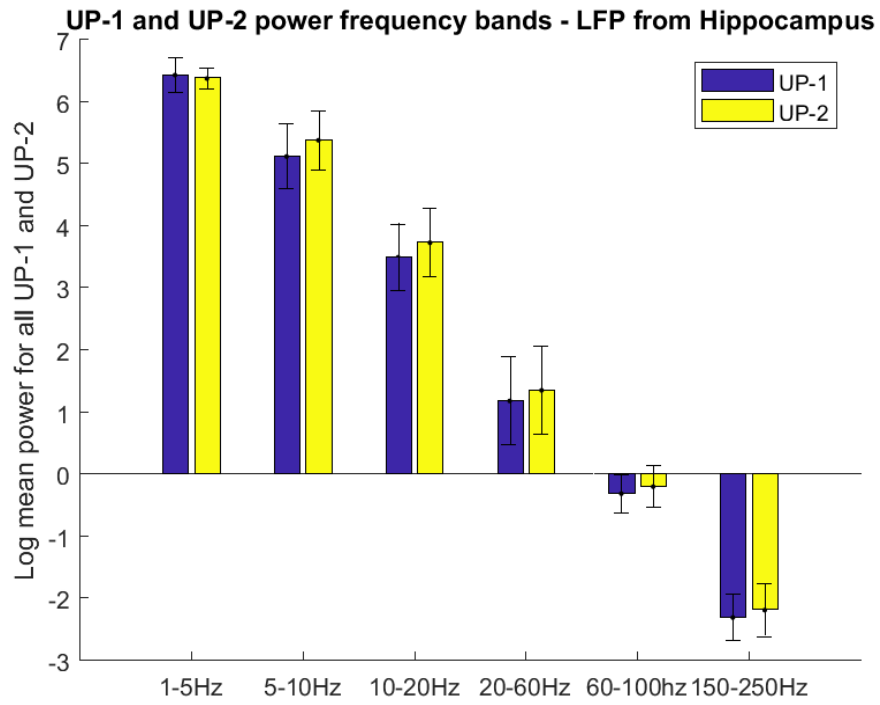
Supplementary Figure 8. State Vector Decorrelation. (Rat3)



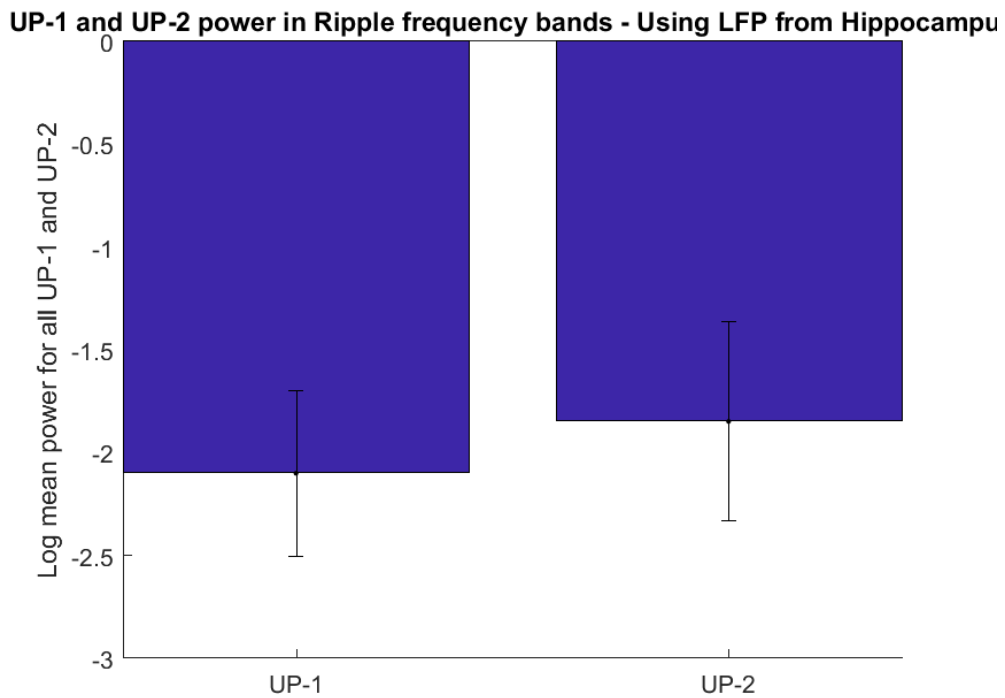
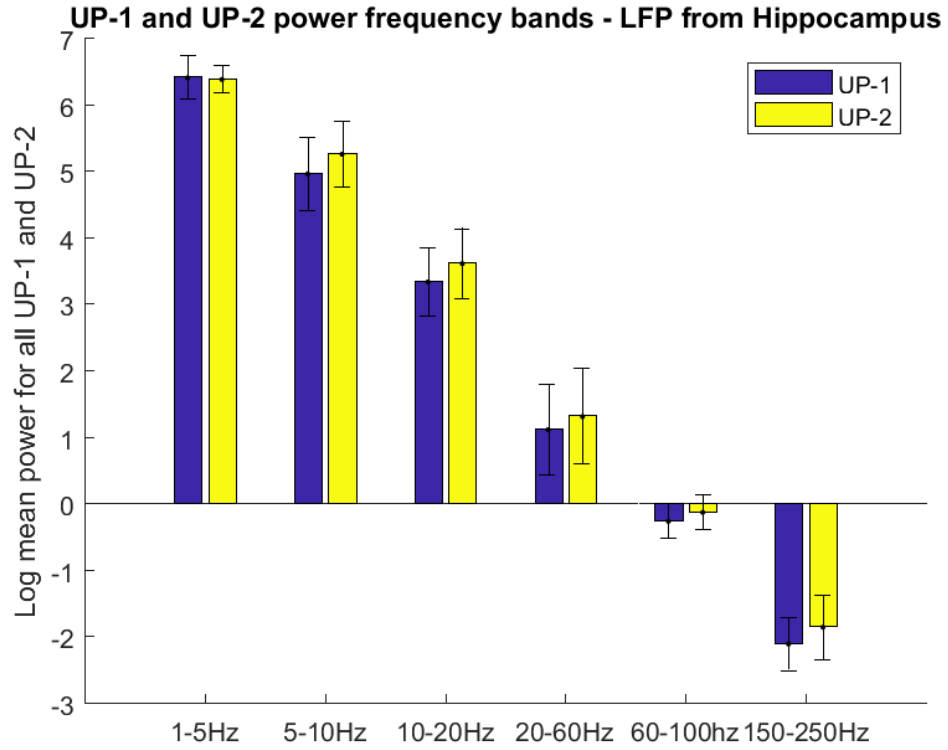
Supplementary Figure 9. Reactivating UP states with z-score 5. (Rat2)



Supplementary Figure 10. Reactivating UP states with z-score 5. (Rat3)



Supplementary Figure 11. UP-1 and UP-2 power frequency bands comparison (Hippocampus LFP). (8482_15p)



Supplementary Figure 12. UP-1 and UP-2 power frequency bands comparison (Hippocampus LFP). (8482_16p)

Supplementary table 1. Firing rate and duration for UP-1 and UP-2 (mean \pm SEM).

Dataset	UP-1 Firing Rate (Hz)	UP-2 Firing Rate (Hz)	UP-1 Duration (s)	UP-2 Duration (s)
1	2.21 \pm 0.023	2.85 \pm 0.047	0.63 \pm 0.020	0.40 \pm 0.014
2	1.99 \pm 0.021	2.41 \pm 0.033	0.78 \pm 0.029	0.41 \pm 0.018
3	1.91 \pm 0.017	2.43 \pm 0.027	0.68 \pm 0.024	0.43 \pm 0.017
4	1.29 \pm 0.011	1.54 \pm 0.021	0.99 \pm 0.040	0.55 \pm 0.022
5	2.16 \pm 0.023	2.59 \pm 0.024	0.82 \pm 0.024	0.55 \pm 0.020
6	2.64 \pm 0.015	2.64 \pm 0.026	0.70 \pm 0.017	0.56 \pm 0.016
7	2.23 \pm 0.013	2.55 \pm 0.023	0.93 \pm 0.025	0.53 \pm 0.018
8	3.28 \pm 0.020	3.66 \pm 0.029	0.56 \pm 0.011	0.47 \pm 0.011
9	2.97 \pm 0.019	3.11 \pm 0.025	0.56 \pm 0.011	0.51 \pm 0.013
10	3.00 \pm 0.023	3.41 \pm 0.027	0.59 \pm 0.014	0.55 \pm 0.015